The evolution of Ultra Diffuse Galaxies in nearby galaxy clusters

Msc Thesis by

PAVEL ENRIQUE MANCERA PIÑA

ADVISOR: prof. dr. REYNIER F. PELETIER

KAPTEYN ASTRONOMICAL INSTITUTE
FACULTY OF SCIENCE AND ENGINEERING
UNIVERSITY OF GRONINGEN

A dissertation to obtain the Degree of Master of Science
in Astronomy by the University of Groningen.

JUNE 2018

Abstract

In this work we carried out a study on the evolution of Ultra Diffuse Galaxies (UDGs) in a set of nearby ($0.02 < z < 0.04$) galaxy clusters, with the aim of understanding more about the evolution of such galaxy population in clusters.

We chose a set of eight X-ray selected clusters with different masses, but reasonable well virialized, that are part of the WEAVE-Clusters Project sample; and we observed them using deep photometric observations with the Isaac Newton Telescope in the SDSS g– and r–bands. The images were reduced using the Astro-WISE facilities. Using the software SExtractor, we detected all the potential UDG candidates, based on their effective radius and surface brightness, and got preliminary photometry of them. Then, with the model decomposition software GALFIT we obtained the final photometric parameters and were able to find out which objects fulfilled the definition of UDG (under the assumption that they lie at the distance of each cluster), finding a total number of 442 new UDGs in the eight observed field of views.

We studied the properties (color, effective radius, axis ratio, Sérsic index, magnitude and surface brightness) of UDGs compared with other types of galaxies in different scaling relations, finding that they fit very well in a continuous giant-dwarf relation; only differing from other dwarfs for being the faint tail of the surface brightness distribution, and the large end of the sizes of dwarf galaxies. From these scaling relations we find no evidence to support UDGs inhabiting non-dwarf-sized halos, but of course the ultimate parameter to see this is the total mass, that remains highly undetermined. When studying only the scaling relations for UDGs, we find that the axis ratio distribution is flatter for relatively isolated UDGs, than for the innermost. There is also evidence that the size of UDGs does not depend on their stellar populations.

Also presented here is the first homogeneous study of the abundance of UDGs as a function of the host cluster mass, finding that UDGs are more abundant, per unit host cluster mass, in low-mass systems, following a relation $N(\mathrm{UDGs}) \propto M_{200}^{0.82\pm0.07}$. This slope is different than the last slope reported in the literature and has important consequences on how do we think UDGs form and evolve. In general, our finding points to a scenario of UDGs being formed more easily in low-mass systems, or being destroyed in high-mass systems (or to the subhalo mass function depending on the environment). The slope and the derived structural parameters are in agreement with a scenario where UDGs are field (or are in groups) galaxies accreted into clusters, where they follow a passive evolution being quenched and some of they destroyed due to cluster interactions. There

are also signs of UDGs being destroyed in the center of massive systems, in agreement with the statement above.

To further study the effect of the environment in the evolution of UDGs, we investigated their spatial distribution as well as the behavior of their structural parameters as a function of the local (projected clustercentric distance) and global (cluster mass) environment. As previous works about UDGs and dwarfs, we found that the properties of UDGs do not significantly change as a function of the projected clustercentric distance, at least up to 1 R_{200}. The structural properties do change a bit as a function of the host cluster mass, but there is no clear trend on the variations.

Acknowledgements

Antes que nada quiero agradecer a mi familia por todo su apoyo y constantes muestras de afecto y ánimo. Principalmente a mi papá, mi mamá y mi hermana por haberme ayudado a cumplir todas mis metas y sueños, y ser mi motivación para intentar ser mejor cada día. Siempre dicen estar orgullosos de mí, pero soy yo quien está orgulloso de ustedes y les agradezco todo lo que han hecho por mí.

Gracias a mis abuelitos, tías, tíos, y al resto de mi familia por tener tan buena opinión de mí que me obligan a dar lo mejor de mí. También aprovecho este párrafo para agradecer a Samantha, por el apoyo, cariño, comprensión, los ánimos todos los días, y en pocas palabras ser algo esencial en mi vida durante los últimos dos años.

Quiero también agradecer a personas cercanas que me ayudaron a estar hoy en día estudiando en Países Bajos: maestros, amigos, y todos los que de una u otra forma me impulsaron y motivaron. Particularmente mencionar a mi asesor de licenciatura, el Dr. Armando Arellano Ferro, por introducirme al mundo de la investigación, apoyar mi idea de estudiar en el extranjero, y proveerme con cartas de recomendación y opiniones sobre distintas universidades y países. Seguir con la maestría y pronto con el doctorado tiene que ver en gran medida a lo mucho que disfruté trabajando con usted en el Insitituto de Astronomía.

After thank to my family and people very close to me, I want to say thanks to all the people who helped me in some way during the process of getting my Msc degree.

First of all to my advisor, Prof. Reynier Peletier, for his willingness proposing me this very nice topic and the helpful and instructive discussions during the research; for his directness helping me in becoming a more critic and independent scientist, and for always supporting me getting new enriching scientific experiences. Also for all his help in my search for PhD programs and for introducing me to very interesting people. I will be always in debt and thankful for how extremely good person are you with me, and for how much do you concern about my preparation. I really admire your deep knowledge in astrophysics and the humbleness and empathy you keep.

To Dr. José Alfonso López Aguerri for all the help in this research, basically co-supervising my thesis and for all his patience, clarifications, ideas and goodwill. Thank you for the Skype calls discussing my results and giving me advices, and of course for inviting me to spend some very nice time at the IAC in Tenerife; I really enjoyed working with you and I hope to keep collaborating in the future.

And also to Aku Venhola, for helping me a lot during the project with his pipeline

and all the explanations and clarifications about it; for seating during hours with me solving problems, and also with interesting discussions and ideas that for sure helped me to improve this thesis; I really admire your deep knowledge on each topic I asked you and your willingness to help.

To the good friends I made here in the Netherlands, specially the Mexican and the Kapteyn Community; thanks to you all I always feel happy of being in Groningen.

I am of course also grateful with the University of Groningen and the Kapteyn Astronimical Institute for two amazing years and a excellent academic quality. Getting a diploma from the university of J. Kapteyn, J. Oort, W. de Sitter or F. Zernike is such a big honor.

Last but no least, I want to thank the Consejo Nacional de Ciencia y Tecnología de México (CONACyT) and the Netherlands Research School for Astronomy (NOVA) for supporting my studies with their respective grants.

Table of Contents

List of Figures

Figure **Page**

List of Tables

CHAPTER 1

INTRODUCTION

In this Introduction we briefly introduce some basic concepts that will be used throughout this work. We do not attempt to give an extensive revision on these topics, but just mentioning some key facts that are important in the context of the upcoming Chapters. The rest of the thesis is organized as follows: in Chapter 2 we describe the observations on which our analysis is based, the data reduction process, and the selection of our final cluster sample; while in Chapter 3 we delve into the search of Ultra Diffuse Galaxies in our sample, describing in detail our searching methods and criteria for classifying them. The properties and scaling relations of the found galaxies are studied in Chapter 4, together with the analysis of their abundance in galaxy clusters. In Chapter 5 we discuss the spatial distribution of the Ultra Diffuse Galaxies in our sample, and the effect that the environment could have on them. Finally in Chapter 6 the main conclusions and remarks found in this work are pointed summarised.

During the preparation of this work, we actively participated in proposals for getting telescope time for studying UDGs. Specifically, in proposals for doing deep imaging (as a part of the photometric survey lead by Prof. Peletier) of galaxy clusters, and also to obtain spectra of UDGs. Regarding the spectroscopic proposals, they were three: one for taking slit-spectroscopy of UDGs, discovered by us, in the cluster Abell 2152 using the instrument OSIRIS in its MOS mode, at the Grantecan telescope; another for using MUSE to take integral field spectroscopy of UDGs from the sample of Venhola et al. (2017); and the last one also for integral field spectroscopy, using the new instrument MEGARA at Grantecan, again for a set of UDGs discovered in this work, in the cluster

Abell 2634. The photometric proposals where approved, as well as the ORISIS one, and the data is being collected. Very recently we were informed that the MEGARA proposal has been also granted with the time and data will be observed next semester. We are still waiting for the decision on the other proposal. These proposals are not included here, but the reader can contact us if wants to know more about them.

1.1 Low Surface Brightness and Ultra Diffuse Galaxies

The population of galaxies in the nearby Universe is very diverse, ranging from massive galaxies, like our Milky Way, to tiny ultra faint galaxies like those in our Local Group. Dwarf and low surface brightness (LSBs) galaxies are very interesting in the ΛCDM paradigm, because they dominate by number densities, their high-z counterparts are likely the progenitors of more massive galaxies at lower redshifts; and given their extreme properties are key evidence to study and constrain our models of galaxy formation an evolution, for instance investigating the roll of the environment, the feedback processes that control the star formation in galaxies, or tracing the dark matter profiles in the diversity of galaxies.

In the recent couple of years a special class of galaxies, the so-called Ultra Diffuse Galaxies (UDGs), have drawn a lot of attention. van Dokkum et al. (2015a), using the Dragonfly Telephoto Array (Abraham & van Dokkum 2014), discovered 47 extremely low surface brightness ($\mu(g,0)$ = 24–26 mag arcsec^{-2}) galaxies in the Coma cluster. To distinguish these galaxies from other galaxy populations, they arbitrarily introduced the term UDG for galaxies with effective radius $R_e \gtrsim 1.5$ kpc and central surface brightness $\mu(g,0) \gtrsim 24$ mag arcsec^{-2}.
With time it is becoming clearer that these galaxies with very low, dwarf-like, surface brightness, but with sizes comparable to the Milky Way or other normal spiral galaxies (see Fig. 1.1), could also be very abundant. Although this special class of LSB was discovered and studied in the 1980's (e.g. Sandage & Binggeli 1984, Impey et al. 1988), only now, with better and larger detectors, has it become possible to systematically observe such objects in various nearby clusters (e.g., van Dokkum et al. 2015a; van der Burg et al. 2016; Román & Trujillo 2017a), groups (e.g. Makarov et al. 2015; Trujillo et al. 2017) and in the field (e.g. Martínez-Delgado et al. 2016; Bellazzini et al. 2017). An analogous field HI-rich population has been also identified (Leisman et al. 2017) and moreover, from

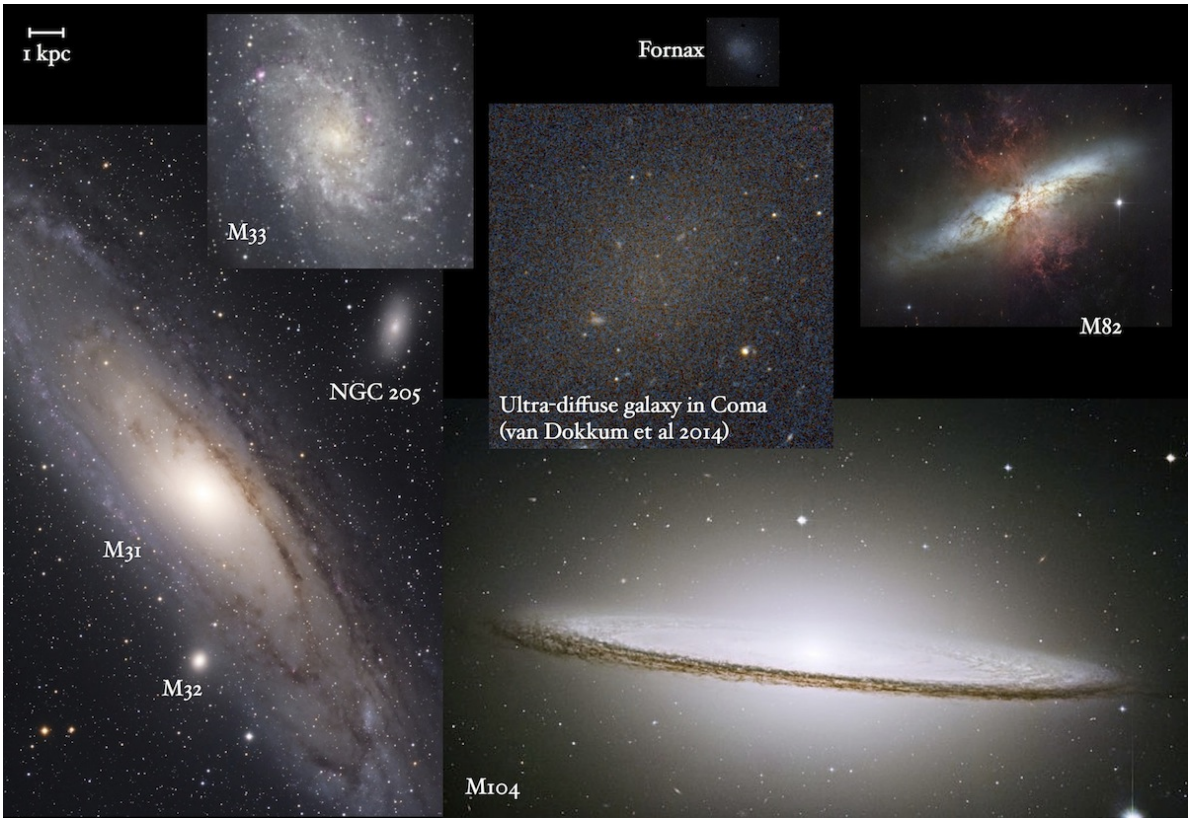

Figure 1.1: Comparison of sizes between a UDG, normal $L_\star$ galaxies and dwarfs. Credits: Pieter van Dokkum.

simulations it seems that UDGs can form in isolation (Di Cintio et al. 2017).

From several studies in recent years, we know some general properties of such faint population, for instance that: i) their stellar content ($M_\star \sim 10^{6-8} M_\odot$) is very poor for their mass (although constraining the total mass is hard and not very accurate, as we will later discuss), and its star formation had to be quenched very early during their infall into clusters (although they are found to have associated globular cluster systems, with most, *but not all*, of the UDGs following the same relation between globular clusters richness and stellar mass as dwarf galaxies Amorisco et al. 2018), ii) most of UDGs in clusters follow the red sequence (RS), meaning that they are a passively evolving stellar population; but some UDGs in isolation could host ongoing star formation, presenting bluer colors, iii) they follow exponential-like light profiles, with a peak in the Sérsic index (Sérsic 1963) distribution at $n \approx 0.7$, and iv) axis ratios around 0.7.

Although UDGs appear to be very abundant in clusters, and we know some general

properties about them, we know very little about the way they form and evolve. Some scenarios to explain their appearance and mass have been proposed, as we briefly explain below.

1.1.1 Formation mechanisms of UDGs: failed MW-like or extended dwarf galaxies?

Given the large size but low surface brightness characteristic of UDGs, the question arises: are they failed $L_\star$ galaxies that quenched most of their star formation, failing in building up stellar mass, or are actually dwarf galaxies than became larger?.

About the former idea, van Dokkum et al. (2016) suggested that at least a fraction of UDGs are failed giant galaxies with very massive halos (M_h ~10^{12} $M_\odot$). In principle, halos of that size should be conducive to star formation given the known stellar mass/halo mass–halo mass relation (Behroozi et al. 2013); however, van Dokkum et al. (2016) proposed that due to cluster infall, feedback, reionization or other yet-undetermined processes, the star formation was quenched and UDGs were not capable to build a stellar population typical for Milky Way- like galaxies (although, at least some of them, had enough time to form globular clusters). The observational support for this idea comes from van Dokkum et al. (2016), who, via globular cluster kinematics presumably associated with the UDG "DF44", found that it has a velocity dispersion σ ~47 km/s. That velocity dispersion implies a dynamical mass of ~$0.7\times10^{10}M_\odot$ and neglecting the gas content, the authors reported a dark matter fraction of 98%. Finally, using NFW models and an extrapolation from effective radius to virial radius, they report a total halo mass of 8×10^{11} $M_\odot$. Nevertheless the same group (van Dokkum et al. 2018) recently found, also via the kinematics of some globular clusters in the UDG "NGC1052–DF2", that apparently that UDG could be "laking dark matter" (with M_{DM}/M_{stars} ~1). In our opinion that kind of results show how uncertain is the mass determination based on globular cluster kinematics more than enlightening in the mass-to-light ratios (M/L) and in the (total) mass of UDGs, and more detailed studies are needed. For instance Laporte et al. (2018) and Martin et al. (2018) discuss in detail how uncertain are the methods used for estimating the velocity dispersion and the mass so far and how sensitive are the results to how one takes into account the uncertainties; as well as showing how a conclusion of DM-dominated or DM-free is strongly dependent on the statistical method employed. Moreover, Trujillo et al. (in prep) actually found that the distance determination by van

Dokkum et al. (2018) is wrong and the galaxy is closer, meaning that its stellar mass is smaller, and not it does not lack dark matter anymore. The recent measurements by Toloba et al. (2018) (with uncertainties in the inferred mass of the order 100–300% of the mass estimation by itself) also emphasize how uncertain is measuring the dynamical mass.

Rough mass estimations can also be inferred form the observed absence of UDGs towards the center of very massive systems (e.g. Koda et al. 2015; Merritt et al. 2016; van der Burg et al. 2016; van Dokkum et al. 2015a; Venhola et al. 2017; Wittmann et al. 2017). van Dokkum et al. (2015a) and van der Burg et al. (2016) concluded that UDGs should be centrally dark matter to survive at distances $\sim$ 300 kpc of the center of Coma-like clusters. However, super massive halos should be also rejected since they should be able to survive those high density environments without being disrupted. Recently (although based on some not necessarily 100% correct assumptions, as we will discuss), Amorisco (2018) estimated the fractions of dwarf-sized and MW-sized (10^{12}M$_\odot$) halos for UDGs to be $\sim$ 10%. Given all the literature on UDGs, it is evident that while maybe some UDGs reside in MW-sized halos, most of the discovered UDGs should inhabit dwarf-like ones.

About the second idea, of UDGs being dwarfs, some other authors posit that UDGs originate in dwarf galaxy-like dark matter (DM) halos ($\sim 10^{10-11}$ M$_\odot$) and have low baryonic content accordingly, and somehow they become large and diffuse. For instance, from and observational point of view, Beasley et al. (2016) found that the UDG VCC 1287 has a halo mass of $\sim 8\times10^{10}$ M$_\odot$; while Beasley & Trujillo (2016) deduced a virial mass of $\sim 9\times10^{10}$M$_\odot$ for "DF17". Also, from globular cluster counts, Amorisco et al. (2018) found more similarity between UDGs and dwarfs than for UDGs and L$_\star$ galaxies. But how do they become large?

Amorisco & Loeb (2016) showed, working with pure dark matter simulations, that the size of UDGs can be the result of them living in high-spin halos (see their Figure 4). Even without taking into account the baryonic content, they were able to reproduce the observed sizes of UDGs, as well as the relation between the number of UDGs inhabiting a galaxy cluster and the mass of that cluster (e.g. Román & Trujillo 2017b; van der Burg et al. 2016).

On the other hand, using UDG-like galaxies from the NIHAO simulations sample, Di Cintio et al. (2017) demonstrated that under certain feedback implementation, UDGs can form in isolation due to internal processes: the dark matter and the gas contents

may expand from strong feedback generated by moderated and episodic star formation bursts, leaving traces in the dark matter profile slope and star formation history (SFH). This scenario also implies that isolated UDGs should have high gas fractions, meaning that there should be a relation between the size and the location of the galaxies in the clusters, in a way that the size should increase with the distance, because galaxies in the outskirts should have been able to grow more than galaxies near the cluster' center. This also implies that the sizes of the UDGs is dependent on their SFHs. Something not yet clear from these simulations is what exactly makes some dwarfs have this SFHs, while others do not.

Finally it is worth mentioning that some authors have proposed that some fraction of UDGs may also be formed via galaxy collisions (Baushev 2018) or that they are tidally disrupted dwarfs (Mihos et al. 2015), dynamically stirred upon accretion in a cluster or group environment (Beasley & Trujillo 2016). As pointed out by Venhola et al. (2017), the tidal interactions in clusters could originate the largest UDGs and the interactions in clusters should be studied in more detail.

With this evidence supporting different kinds of UDGs, a multiple-channels formation mechanism cannot be rejected. For example, one of the predictions of the isolation forming UDGs of Di Cintio et al. (2017) is that the largest UDGs should have a higher gas fraction than more compact UDGs; however, Papastergis et al. (2017), studying the HI content of UDGs in the field, have shown that while the prediction is correct for some UDGs, there are also large UDGs that are gas-poor and whose locations in the plane gas fraction ($M_{HI}/M_\star$) – stellar mass are not matched by the `NIHAO` UDGs. Furthermore Leisman et al. (2017) found, also from HI observations, that while some of the field HI-bearing UDGs from the ALFALFA survey, reside in high spin parameter halos, as proposed in the model by Amorisco & Loeb (2016), there are also several that have a low spin parameter (although the authors mentioned the caveat about how difficult and uncertain is deriving the spin parameters from their data).

Very recently, with spectroscopic observations of UDGs in Coma, Ferré-Mateu et al. (2018) showed that while most of their UDGs lie in positions expected of dwarf-like galaxies in different scaling relations, there is at least one UDG of their sample that does not follow the same trends, suggesting a different formation scenario: "DF26" (R_e=3.49 kpc, $\mu_{0,R}$=23.6 mag arcsec^{-2}) does not follow the same trend as other Coma UDGs of older galaxies being smaller (as a result of spending less time before quenching, with galaxies than quenched later became more extended); it also shows signs of interactions

and together with a few UDGs has been in Coma since earlier times than the rest of the UDGs, with accretion times similar to the massive galaxies of the cluster (Alabi et al. 2018).

Given all this, it is very likely that there are more than one efficient formation mechanisms of UDGs to explain the diversity in the observed properties (e.g. colors, shapes, total mass and dark matter fractions). A caveat that should be noticed is that usually all the above mentioned works use a slightly different definition of UDG and the nature of the studied galaxies could be slightly different (e.g. Di Cintio et al. 2017 used UDG-like galaxies that are slightly smaller what observationally is considered a UDG; in Leisman et al. (2017) their HI-bearing UDG galaxies have different morphologies and most likely different stellar populations that classical UDGs, and basically each work in the literature sets its own criteria in the surface brightness limit for defining a UDG), so this should be considered when comparing different works for understanding the formation and evolution of UDGs.

1.1.2 Is the evolution of cluster-UDGs driven mainly by internal processes or by the environment?

A natural question is: once UDGs are formed, what are the main drivers of their evolution? Simulations and observations have suggested some ideas about it.

Román & Trujillo (2017b) studied a set of six UDGs outside clusters, and compared them with cluster-UDGs, finding two very interesting features: i) UDGs can be separated in blue and red UDGs, with an evolutionary scenario of bluer UDGs being formed in isolation outside clusters, and becoming redder and fainter while their accretion into the clusters; and ii) that some parameters correlate with the projected clustercentric distance: the stellar mass, the Sérsic index and the effective radius decrease towards the center, in agreement with a picture of UDGs being disrupted due to environment interactions. In this scenario the importance of the environment is essential. Nevertheless we should say that their sample is very small to be accepted as totally representative and while the trends are somehow visible, when considering the scatter of their derived parameters they become hard to see.

On the other hand, from the NIHAO UDGs (Di Cintio et al. 2017), one may think that internal processes are more important than the effects of the environment for the evolutionary pathways of UDGs, in the sense that UDGs in isolation already show the

large size and faint surface brightness of cluster UDGs; features than, as we mentioned, can be reproduced by feedback driven gas outflows due to extended SFHs.

van der Burg et al. (2016) suggested two possible scenarios to explain the cluster UDGs: one where more compact galaxies, accreted on different orbits, became larger due to tidal heating by their interaction with the host cluster and somehow they managed to retain high dark matter fractions (to allow them survive in the inner parts of clusters), and other where UDGs were already large at their accretion times, explaining their large fraction of dark matter and their distribution at large projected distances; but as they mention, their analysis was not enough to distinguish between both scenarios. Also, Venhola et al. (2017) concluded that while the bluer color of UDGs in the outskirts might be a signal of the influence of the environment, and while low-mass clusters seem to have more elongated UDGs than more massive clusters, they did not find evidence of systematic differences in the whole population of UDGs in Fornax and Coma, even when they are very different environments, pointing towards an scenario where UDGs are not influenced by its environment.

So, as can be appreciated, it is not clear whether once UDGs have been accreted onto galaxy clusters, their morphologies and structural parameters are mainly driven by their environment (e.g. if a strong dependence on the projected clustercentric distance would be observed), or if internal processes are still dominating their shape and mass. Would the answer change depending on the evolutionary status of the cluster or its degree of virialization (for instance, maybe after a long time within the cluster potential the features due to internal processes are washed out by the effects of the environment)? Or perhaps there also are cluster UDGs formed in-situ (e.g. via central collisions of galaxies Baushev 2018)? Since galaxies in clusters with lower velocity dispersions are expected to have stronger interactions in the central regions (Le Févre et al. 2000; Venhola et al. 2017), would there be a trend in UDG properties as a function of the velocity dispersion/mass? These are some of the questions that we would try to give some light to along this thesis.

Notwithstanding, we should mention that to fully understand the population of UDGs (e.g. membership, stellar populations, rotational velocities, total masses, accretion histories, dark matter fractions), spectroscopic data is needed. There are no resolved spectroscopic measurements available, so we have no observational information about the angular momentum of UDGs or direct determinations of M/L. About detailed stellar populations,

we do not know very much yet because there are only a handful of studies (e.g. Gu et al. 2017; Ferré-Mateu et al. 2018; Ruiz-Lara et al. 2018) that derived rough SFHs and ages. So far the general picture is that cluster UDGs have relatively old stellar populations (~ 7 Gyr) and low metallicity, and be slightly alpha-enhanced. However, the S/N and resolution are usually too low for an accurate determination of SFHs.

With all this, it is clear that the nature of UDGs is still a matter of hot debate, and while waiting for spectroscopic data to get more information about their internal properties, it is important to collect more photometric data to keep constraining the nature of these faint galaxies and test all the suggested theories about their origin.

1.2 Galaxy clusters

Galaxies in the Universe tend to be grouped in groups or clusters. The difference between a group and a cluster is the number of galaxies they contain (from a few tens for a group to hundreds or thousands for a cluster). They are the largest gravitationally bound structures in the Universe with masses in a range of 10^{12-13}M$\odot$ for groups or 10^{14-15}M$\odot$ for clusters. Because of their high number density and diversity of inhabiting galaxies, these systems are perfect laboratories to study the processes that trigger and shape the evolution of their galaxies. Clusters can have very different degrees of virialization, richness, morphologies and levels of substructure, so there are different types of classifications that privilege one or another parameter above the rest.
A commonly-used parameter to quantify how large is a cluster is its virial radius, R_{vir}. Often, as an approximation of R_{vir}, the parameter R_{200} is used, defined as the radius at which the mean density $\langle\rho\rangle$ is 200 times the critical density of the universe $\rho(z)_{crit}$ at the cluster's redshift (it is found from simulations that an overdensity will collapse into a halo once it reaches roughly 200 times the critical density at the epoch of the collapse). From this, M_{200} is the mass enclosed within R_{200} assuming spherical symmetry and density $200\langle\rho\rangle$ (or viceversa if one determine the mass first).

Galaxy clusters strongly radiate in X-ray wavelengths, with typical luminosities of the order of $L_X \sim 10^{43-45}$ erg s^{-1}. This emission does not come from individual galaxies by themselves since it is found to be very expanded, but for a hot plasma with thermal bremsstrahlung radiation, the intracluster medium. Because of this, galaxy clusters are usually detected or characterized using X-ray studies. Perhaps the most interesting feature about its X-ray emission is that it has been found that the X-ray flux correlates

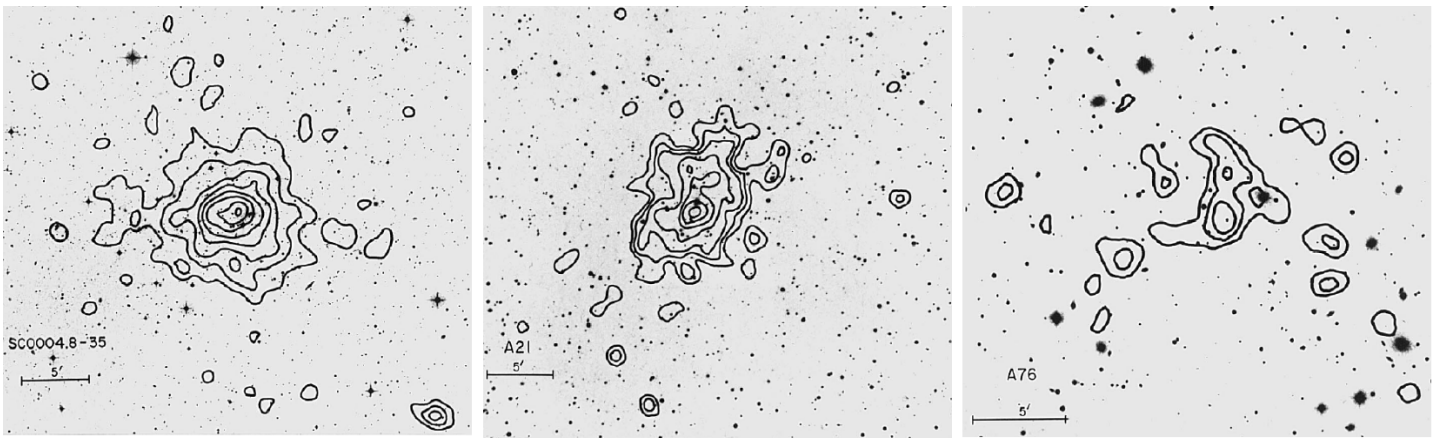

Figure 1.2: Example of three X-ray isocontours of galaxy clusters with different morphologies. The image was adapted from the original by Jones & Forman (1999).

with the velocity dispersion and the mass (e.g. Hoekstra et al. 2011; Reiprich & Böhringet 2002); with X-ray luminous clusters being more massive in a basically linear (in the log-log space, power law in normal space) relation.

X-ray observations are also a nice tool to know more about the relaxedness of a cluster via the shape of its X-ray isocontours. Since they trace the hot gas, symmetrical (round) isocontours imply relaxed or virialized systems, whereas distorted and asymmetrical contours would mean non-relaxed clusters. As a matter of illustration Figure 1.2 (adopted from Jones & Forman 1999) shows the X-ray contours of three galaxy clusters with different morphologies.

1.3 The WEAVE-Clusters Project

The new WEAVE spectrograph, to be installed in the near future at the William Herschel Telescope, will be a versatile spectrograph with 3 modes: a Multi-Object fiber-Spectrograph (MOS), allowing 1000 fibers to be observed simultaneously, a Mini-IFU (mIFU) mode, with 20 mini-IFUs, each with a field of view (FOV) of 10 arcsec × 12 arcsec, and a large IFU-mode, employing a large IFU of 1.3 arcmin × 1.5 arcmin. WEAVE's large FOV and high-multiplex MOS mode, combined with spatially-resolved spectroscopy from its mIFU mode, will allow us to make a huge and unique leap forward in understanding the processes that drive dwarf galaxy evolution in clusters. WEAVE will allow us to study: i) the faint end of the galaxy luminosity function; ii) the scaling relations of the

dwarf galaxies; iii) the orbits of dwarfs inside the clusters; iv) the distribution of matter in dwarf galaxies; v) its internal kinematics; vi) its stellar populations, metallicities and SFHs; and the vii) ionized gas inside them. No other survey that we are aware of can accomplish all of these goals for such a large number of dwarf galaxies.

Regarding galaxy clusters, WEAVE will do three different surveys, in three different "layers". The first layer, "Nearby cluster survey", observing 69 X-ray selected galaxy clusters at $z \leq 0.04$, on which we delve below; the second layer, "Cluster-infall regions survey", observing 20 clusters at $\langle z \rangle = 0.055$ with the aim of studying the galaxy transformation processes during their infall; and the third layer, "Cosmological clusters survey", for studying the evolution of galaxies in the central parts of clusters out to $z = 0.5$, as well as for constraining cosmological parameters and scaling relations. All the specifications about each survey can be found in the document "The WEAVE Surveys: Strategy and Planning", by Scott Trager and the WEAVE Science Teams.

As a preparation for WEAVE, particularly the Layer I, a team leaded by J. Alfonso L. Aguerri and Reynier Peletier, is carrying out a deep photometric survey on several of the clusters that will be spectroscopically observed with WEAVE (Layer I). This survey aims to detect the faintest galaxies in these clusters to study the influence of the environment on the evolution of dwarfs, LSB and UDGs. The sample, a subsample of the catalogue provided by Piffaretti et al. (2011), consists of 46 galaxy clusters that accomplish three main selection criteria:

- ⋆ Redshifts between $0.01 \leq z \leq 0.04$. The lower limit was determined to have clusters that can be observed with the FOV of WEAVE up to its virial radius, using one tile (nearer clusters would need more than one); while the upper limit comes from the expected observational limit in magnitude given the integration times planned (see next Chapter). The Coma cluster is excluded since it has been studied in detail in other photometric studies.

- ⋆ Clusters in the northern sky (so they can be observed in La Palma site). This also complements very nicely the WINGS clusters (WIde-field Nearby Galaxy-cluster Survey; e.g. Fasano et al. 2006) that cover galaxy clusters with $0.04 < z < 0.07$.

- ⋆ Clusters than are photometrically covered by SDSS, to have complementary photometry available.

This sample, reaching very low surface brightness, will be unique to study the properties of UDGs in clusters with a wide range in mass and dynamical states. We have developed dithering and data reduction procedures, allowing us to find and study quantitatively many low surface brightness features in the clusters. For this survey the observations are being performed at the 2.5-m Isaac Newton Telescope at the observatory del Roque de los Muchachos, in La Palma, Spain, where we are doing deep imaging in the $g-$ and $r-$band, as we will describe in more detail in the next Chapter.

1.4 This thesis

In this thesis we address the study of UDGs in low-z galaxy clusters, with the aim of understanding more about their nature and evolution, taking into account all the above mentioned. To do this, we use data from a deep photometric survey of the WEAVE-Clusters Project, and we find the UDGs in our sample. Using image-decomposition techniques we infer the stellar light properties of the UDGs in each cluster, as well as their spatial distribution, and we compare the results between clusters and between different types of galaxies via their scaling relations. Given the fact that the clusters have a variety of masses, and that our observations cover more than 1 R_{200} for all our sample, we are in position of studying the dependences of the observed properties as a function of the local (projected clustercentric distance) and global (dynamical mass of the host cluster) environment in which UDGs inhabit.
Along this work we adopt a ΛCDM cosmology with $\Omega_m = 0.3$, $\Omega_\Lambda = 0.7$ and $H_0 = 70$ km s^{-1} Mpc^{-1}, and magnitudes are in the AB system.
We have made an extensive use of the SIMBAD Astronomical Database, ADS (NASA's Astrophysics Data System), NED (NASA/IPAC Extragalactic Database), and Astropy services (a community-developed core Python package for Astronomy), as well as the cosmological calculators from Wright (2006) and from the International Centre for Radio Astronomy Research[1], for which we are thankful. We also want to thank Javier Román and Remco van der Burg for providing us with the data of their works as well as interesting comments and clarifications.

[1] http://cosmocalc.icrar.org/

CHAPTER 2

Sample, Observations and Data Reduction

In this Chapter we describe our observations, the main steps during the data reduction, and the criteria for selecting our final clusters sample.

2.1 Observations

As mentioned, the observations for the survey are done using the Wide Field Camera (WFC) at the 2.5-m Isaac Newton Telescope (INT), at the Observatory of Roque de los Muchachos, Spain. The WFC has 4 CCDs with a scale of 0.33 arcsec/pixel, and the edge to edge mosaic covers ~34 arcmin. For more specifications about the WFC the reader can look at the Isaac Newton Group website http://www.ing.iac.es/astronomy/instruments/wfc/ .

We use the SDSS-like filters g and r, and the total integration times per field are ~1800s and ~5400s, respectively (with single exposures of 210s), imaging several fields for each cluster to cover up to ~ 1 R_{200}. The observational strategy combines the short exposure times with large dithers between consecutive frames, which allow i) reducing the overheads by deriving background models directly from median combining and stacking the science images (see for instance Venhola et al. 2017); ii) reaching deep surface brightness limits keeping a high saturation limit; and iii) making sure that the region has a uniform depth thanks to the overlapping fields between dithers. The integration times were chosen during the planning and design of the survey, with the

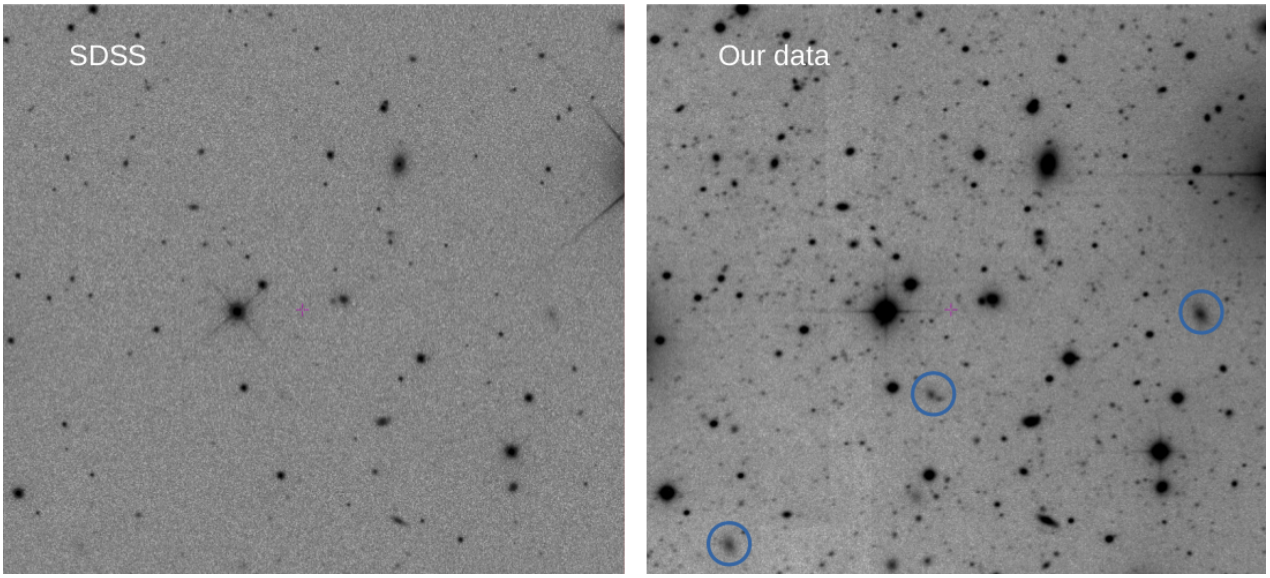

Figure 2.1: Example of our deepness vs. SDSS' depth. Our data allow us to reach fainter structures, as the highlighted galaxies that turned out to be UDGs in our final catalogue.

goal of reaching a typical surface brightness around 27.5 mag arcsec^{-2} at S/N=1 per arcsec^2.

In Figure 2.1, just as a matter of illustration, we show an example of a region in the cluster Abell 2152 from SDSS, and the same region in our image, to show that our data allow us to detect fainter galaxies.

The images were observed in different observational runs between 2015–2018[1], always in a homogeneous way. Bias, flat-field frames, and standard fields were also taken each night for being used during the data reduction process.

2.2 Data reduction

A good data reduction process is needed when dealing with extreme low surface brightness galaxies like UDGs, since the images can be quite contaminated by atmospheric background light at those faint levels; for instance, a typical sky night in La Palma has $\mu_V \sim 21.9$ mag arcsec^{-2} (Benn & Ellison 1998; Ruiz-Lara et al. 2018).

The data reduction of our data is done by modifying and adapting a pipeline, originally written by Aku Venhola, that works in the environment of Astro-WISE (McFaraland et al.

[1]Several observers have been involved, whom we thank a lot, including R. Peletier, J.A.L. Aguerri, P. Mancera, S. Sen, A. Ponomareva, K, Verro, N. Choque, and several master students

2013) using different data reduction recipes. The pipeline covers all the usual corrections and in general it goes trough the following steps for each cluster and for each filter:

1. In the environment and database of `Astro-WISE`, where all our images are ingested, it is possible to make queries to retrieve specific images, based for instance in the type of image (e.g. calibration or science image), the observation dates, the filter, the coordinates, or the class of the image (e.g. raw image, reduced image, regirdded image, etc). So, in the first step of the data reduction one specifies the coordinates of the center of the cluster to be reduced, and queries for all the raw science frames nearby those coordinates (i.e. $\pm$ 1 degree). Then, one can see the range in time in which the observations were held, the number of cluster frames, the standard fields, and the calibration images (bias and flat-field frames) that were observed for those dates.

2. With the details about the calibration frames and their dates, master flat and master bias frames are created for the dates that the cluster observations span. Bias and Flat-Field corrections are needed to take into account the electronic noise and the spatial differences in the sensitivity of the CCDs, respectively. From the individual bias frames, `Astro-WISE` creates a "master bias" frame using pre- and ovserscan regions in the image; the "master flat" frame is done by median-combining and normalizing the available twilight- and (if available) dome-flat-fields frames, and finally multiplying the averaged flat-fields by each other. These master frames will be later used for reducing the cluster images.

3. Hot- and Cold-Pixel Maps are built using the bias and flat-field images, respectively, to extract information about pixels with with very high (hot) or with not enough (cold) sensitivity. Cosmic rays and tracks from satellites are also detected and the information is stored, since will be essential for creating the weighted maps (see below).

4. Once this set of images has been created, the observed standard fields are selected, and they go through the routine "Reduce". This routine subtracts the bias images from the raw science frames and then it divides the raw science frames by a master flat frame. Once reduced, astrometric solutions are computed and applied to the standard fields using a set of astrometric catalogues, to transform from pixel to world coordinates; and then, by matching them with photometric catalogues,

photometric corrections are also computed, to be latter applied to the cluster images.

5. After these steps the cluster images are queried, and background subtraction is applied. This is essential since we need to separate the light from real sources from that of the background. Most of the atmospheric contamination vanishes in this process, because of the dithering done when observing: consecutive integrations will not have the same contamination in the same pixels, so by stacking all the images and taking the average, hot and cold pixels, cosmic rays, and fixed pattern noise are removed. The pipeline also allows to make de-fringing corrections, which is done with an automatic algorithm that uses the standard deviation of the pixel values in the de-bias and flat-fielded image to build a fringe map scale factor. Finally, illumination corrections, to remove systematic flux variations from the instrument that could not be removed by the flat-field correction, could also be applied, but we find no need for this in our images.

6. Subsequently, these cluster images go also to the "Reduce" task, where the corrections are applied in the same way as for the standard fields, and the bad artifacts are removed. Atmospheric extinction and air mass corrections are also applied automatically using the information of the standard fields reduction.

7. Astrometric solutions are also found for the cluster images, to derive transformations between pixel and world coordinates. Such transformation is done using the software `SCAMP` (Bertin 2006), with which the coordinates are transformed considering the shift and rotation stored in the image headers. Then, as explained in Venhola et al. (2018a, in prep.), the corrections are refined by matching sources in the science image with the 2 Micron All-Sky Survey Point Source Catalog (2MASS-PSC) (Cutri et al. 2003) and fitting the residuals by a second order polynomial plane. This polynomial correction is then applied to the data coordinates and the astrometry is ready. In this step the reduced science frames are re-sampled with a scale of 0.2 arcsec pixel^{-1} and all the cluster images are regridded, applying also here the photometric corrections previously derived.

8. For generating the final mosaic, i.e. the final coadded calibrated science image, all the fully calibrated individual exposures are median stacked using the program `SWarp` (Bertin 2010). A weighted map of the coadded image is created, containing the information about saturated or bad pixels (from the hot- and cold-pixel maps),

noise level and cosmic rays. In the weight image the bad pixels are set to 0. The weight map is essential during the later source detection, because it indicates the pixels' sensitivity, e.g. where the image is not sensitive enough or where there are artifacts than should not be taken into account.

To check the accuracy of the photometry, we compare the magnitudes given by SExtractor (see next Chapter) with the magnitudes from SDSS, for a set of bright non-saturated stars, after our zero-point corrections have been taken into account. The rms of the difference between our photometry and SDSS is very good, with a mean value of 0.040 mag and 0.046[2] mag, in the r- and g-band, respectively. Regarding the accuracy of the astrometry, also comparing with SDSS, we find mean values of the rms between both, right ascension and declination of the order 5×10^{-5} degrees. So, as we can see, the astrometry and photometry of the data reduction are quite good.

More information about the data reduction pipeline can be reviewed in Venhola et al. (2018a, in prep.); even when it describes the data reduction processes for OmegaCAM, most of the steps are consistent and analogous to those in the data reduction pipeline for the WFC. Also, the "howto's" of each process of Astro-WISE can be check in detail in http://www.astro-wise.org/portal/howtos/.

If the final images have good quality, with constant seeing over the full image and with a seeing smaller than 1.5 projected kpc, are not very patchy (without strong patterns of the different dithers used for the coadded image), and have homogeneous illumination in different regions they are considered for their analysis (see next section). If not, the images are re-reduced with a slightly different configuration, for instance rejecting exposures with seeing above some threshold or changing how the background subtraction is done. While not all the images are perfect they are very good, and good enough for our purposes. If the images are still bad after re-reducing (usually just because the seeing is to high), the corresponding clusters are scheduled for being re-observed in our observational campaign.

For illustration purposes, in Figure 2.2 we show an example of a small region of one cluster in the "Raw Science Frame" (just a single exposure of 210s), compared with the final image of the same frame used in our analysis once it went trough all the steps in Astro-WISE.

[2]Excluding the g-band calibration of A779 and RXCJ1223, which have an rms of 0.2 mag.

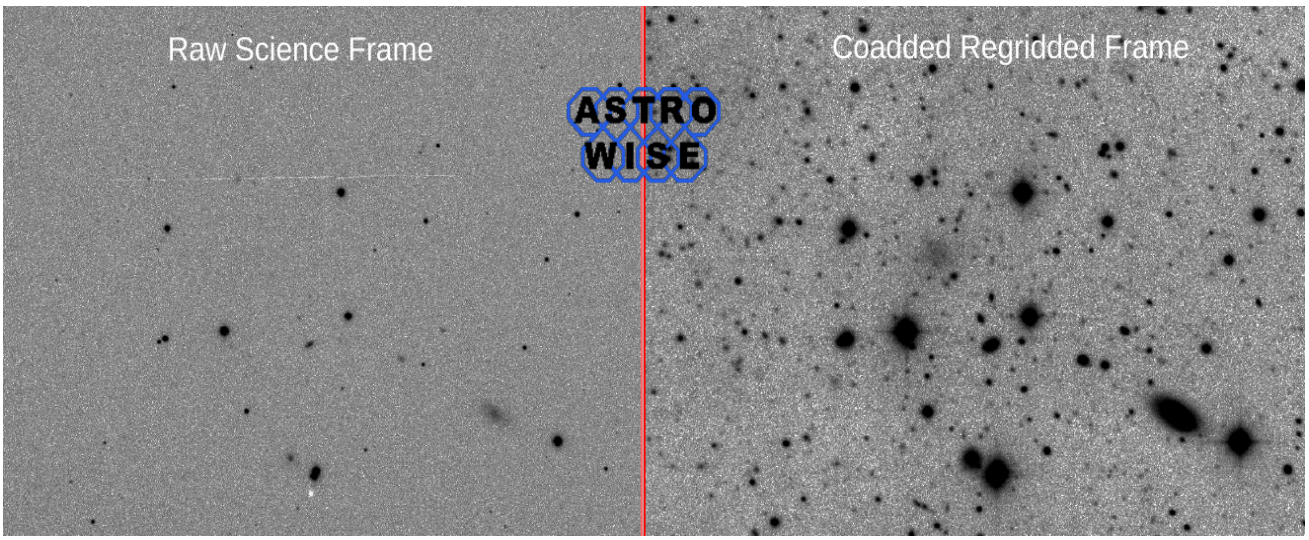

Figure 2.2: Comparison between a small region of a raw science frame and the final coadded image after it goes trough the data reduction pipeline.

2.3 Sample selection

As already mentioned, the WEAVE-Clusters sample includes galaxy clusters with a large diversity in properties like mass, virial radius and richness. Although this photometric survey is still an ongoing project, several galaxy clusters have been fully observed and reduced, and are selectable for being included in our study. The first step for the sample selection is doing management tasks to know exactly which clusters have been fully observed and reduced (and in which conditions), which have not, and whether or not the data has been ingested in the system.

To select the final sample between all the clusters, we give priority to clusters with the lowest possible redshift (to have better resolution) and the best possible image-quality. Also, we prefer clusters without a lot substructure behind and/or in front of them, according to spectroscopic data in the literature of galaxies in each FOV (to avoid strong foreground and/or background contamination), and that are as isolated (no other nearby clusters at the same redshift) and virialized as possible, and trying to cover a large range in mass. In order to have a representative sample, we select 8 clusters to be analyzed.

Fig 2.3 shows the location of the WEAVE Clusters (Layer I) in the sky, and in Table 2.1 we show the studied clusters in this work, as well their coordinates (J2000), redshift, average seeing in each observed band and physical scale (kpc/arcsec). The redshift for each cluster is determined by fitting a gaussian function to the redshift distribution of

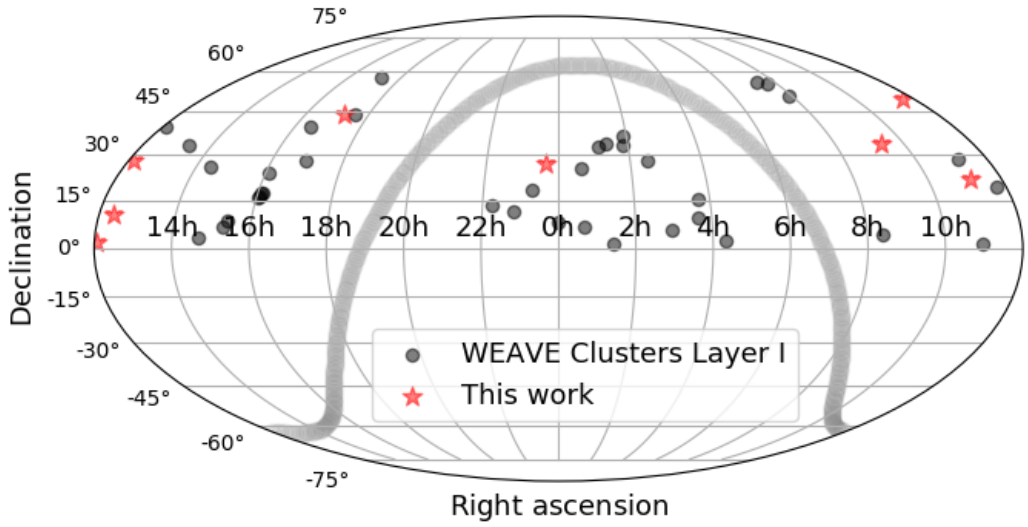

Figure 2.3: Location of the clusters being observed in our survey (black points) and those studied in this work (red stars). The gray band shows the location of the Galactic plane.

the galaxies in each FOV consistent with being at a redshift similar to the purposed redshift on the literature for each cluster, according with the spectroscopic sample of the SDSS Catalogue DR14 (Abolfathi et al. 2018) and complementing by cross-matching the coordinates with the NED database[3]. Figure 2.4 shows the histograms of the redshift distribution and the gaussian function fitted for each cluster. Not all the galaxies with spectra, in all the clusters, have color information in the different literature, so for sake of homogeneity we fit the gaussian to the redshift distribution, considering galaxies within 2 standard deviations of the peak of the distribution, without considering any constraint in the color of the galaxies (this is not only considering red sequence galaxies). This does not really affect the redshift determination for each cluster (since the peak of the gaussian is usually very prominent), but affects the width of the gaussian, which is later important for deriving the velocity dispersion σ, and thus the mass, of the clusters. We will address this issue later when determining the M_{200} and R_{200} for each cluster[4]. The inferred velocity dispersion of each cluster is also shown in Figure 2.4, and has been corrected by the expansion of the universe using $\sigma = \sigma_{obs}/(1+z)$.

[3] https://ned.ipac.caltech.edu/

[4] There are X-ray measurements of R,M_{500} in the literature, but, as mentioned in Giles et al. (2015), it is know from simulations that because hydrostatic estimations (X-ray) only consider thermal pressure and not random motions -supported pressure, the X-ray masses are bias towards lower values, so we decide not to use them. Some clusters have dynamical R,M_{200} estimations in the literature, but not in a homogeneous way, and not all of them, so we decide to derive these parameters by ourselves.

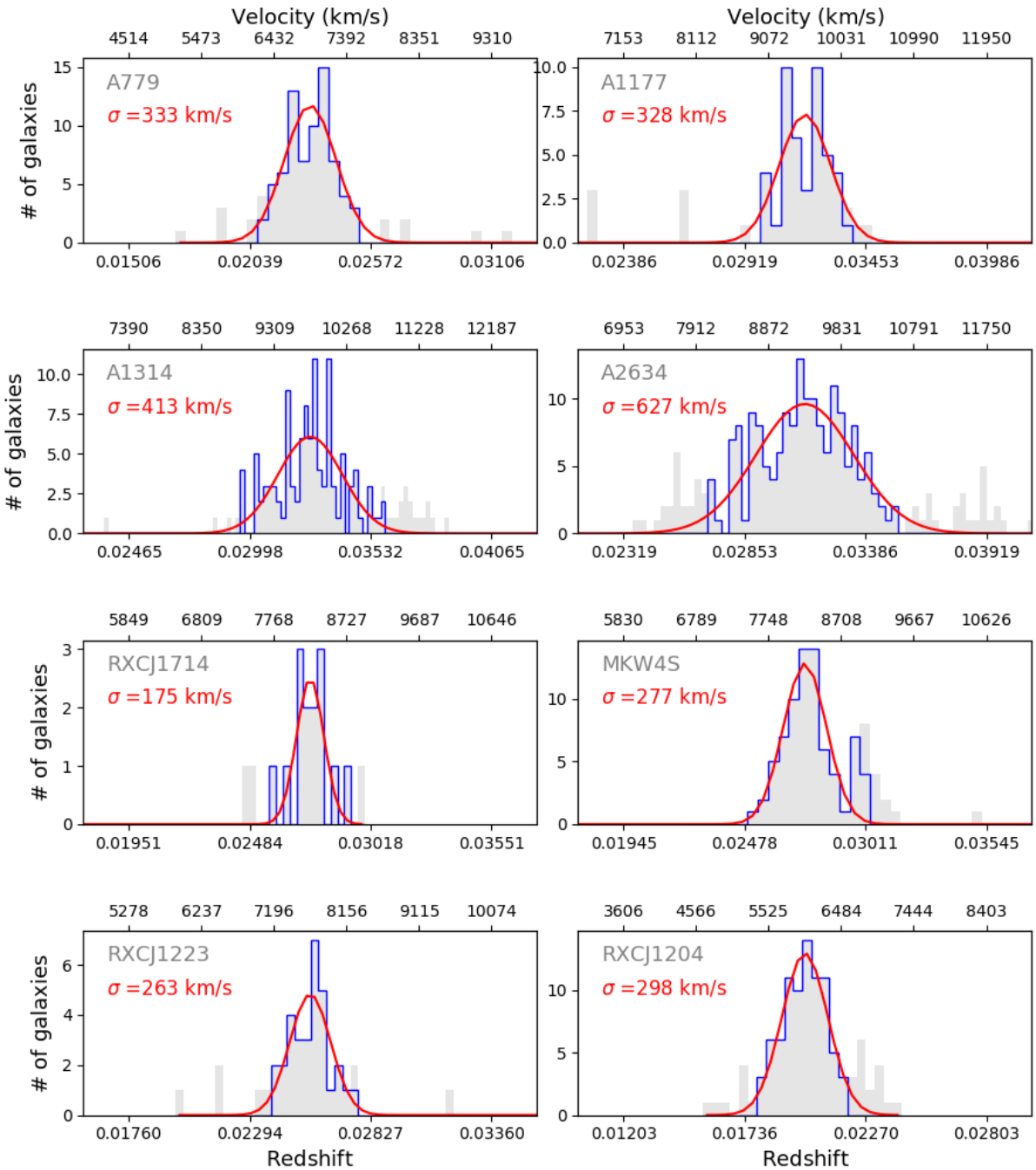

Figure 2.4: Redshift distribution of galaxies nearby each cluster, with spectra from SDSS and NED. For each panel the gray area shows the whole redshift distribution near the cluster's redshift, while the blue line encloses the galaxies considered for fitting the gaussian, the later showed with the red fit, and characterized for the sigma listed in each panel. Bottom x-axes indicate the redshift and the upper x-axes the recessional velocity of the galaxies in km/s.

Table 2.1: Coordinates, redshift, seeing and physical scale for the clusters in our sample. The ID is a short code for the full name of each cluster, while the coordinates end with any possible ambiguity.

Cluster	RA (J2000) (degrees)	DEC (J2000) (degrees)	Redshift	Seeing (arcsec) r	g	Scale (kpc/arcsec)
A779	139.9550	+33.7603	0.0231	1.41	1.35	0.466
A1177	167.4296	+21.7619	0.0319	1.51	1.52	0.637
A1314	173.7104	+49.0578	0.0327	1.54	1.58	0.653
A2634	354.6071	+27.0125	0.0312	1.55	1.59	0.624
RXCJ1714	258.5775	+43.6897	0.0275	1.32	1.49	0.552
MKW4S	181.6558	+28.1836	0.0274	1.43	1.46	0.550
RXCJ1223	185.7771	+10.6239	0.0256	1.64	1.41	0.515
RXCJ1204	181.1050	+01.9006	0.0200	1.51	1.65	0.405

CHAPTER 3

Ultra Diffuse Galaxies in the Sample

This chapter focuses on explaining i) the adopted definition of UDG in this thesis, ii) the estimation of the detection efficiency and the depth of our images, iii) the source extraction and preliminary photometry, iv) the identification of the potential UDGs based on their size and surface brightness, v) the final photometry of those potential candidates via galaxy modeling, and vi) the UDGs found in this work according with their final photometric parameters.

3.1 UDG definition in this work

As mentioned in the Introduction, since there was not a physical motivation in van Dokkum et al. (2015a) for defining a UDG with a surface brightness exactly μ(g,0)≥24.0 mag arcsec^{-2} and effective radius $R_e \geq 1.5$ kpc, the different works in the literature adopt different criteria in the surface brightness' and effective radius' lower limits.
For instance, Román & Trujillo (2017a) considered galaxies with μ(g,0) > 24.0 mag arcsec^{-2}, Román & Trujillo (2017b) used μ(g,0) > 23.5 mag arcsec^{-2}, Venhola et al. (2017) $\mu(r',0) > 23.0$ mag arcsec^{-2}, while Koda et al. (2015) and van der Burg et al. (2016) opted for using $\langle\mu(r,R_e)\rangle \geq 24.0$ mag arcsec^{-2}. As the last authors explain, the mean effective surface brightness within the effective radius ($\langle\mu(r,R_e)\rangle$) is more related to the detectability of galaxies than the central surface brightness, and has also the advantage that it depends on the magnitude, effective radius and axis ratio, but not in the Sérsic index.

These characteristics of the mean effective surface brightness, coupled with the fact that comparing with van der Burg et al. (2016) will be very interesting since they also studied the population of UDGs in different galaxy clusters, motivate us to also work with the quantity $\langle\mu(r,R_e)\rangle$. For the the forthcoming analysis we adopt the definition of a UDG being a galaxy with effective radius[1] $R_e \geq 1.5$ kpc and $\langle\mu(r,R_e)\rangle \geq 24$ mag arcsec^{-2}. Comparing with van Dokkum et al. (2015a), for instance, $\langle\mu(r,R_e)\rangle \geq 24.0$ mag arcsec^{-2} corresponds to $\mu(g,0) = 23.68$ mag arcsec^{-2} for an exponential profile and a color $g-r = 0.8$, and to $\mu(g,0) = 24.16$ mag arcsec^{-2} for a Séric index of 0.7, under the same color assumption. Additionally, we also demand a Sérsic index lower than 4, and a color $g-r$ (measured at the effective aperture) lower than 1.2 mag, to prevent from concentrated and background objects.

3.2 Detection efficiency and depths

The plan for making the catalogues of UDGs is to use `SExtractor` (Bertini & Arnouts 1996) for detecting all the sources in our images[2] as well as getting their preliminary photometry, and then `GALFIT` (version 3.0, Peng 2010) to extract accurate parameters for the most-likely UDGs candidates.

Nevertheless, before that, we perform a series of simulations to determine the typical detection limits for *each* image and to find what are the best parameters to run `SExtractor` with. This is important to make our `SExtractor` runs more efficient, which is essential considering the large sample we are dealing with. This will also give us the calibration between the "real" (modeled) parameters and the output from `SExtractor`.

Considering this, for generating the models we use the task *mkobjects* in `IRAF`[3], that allows us to model light profiles of galaxies in an easy and fast way. We model 9000

[1]We use the effective radius measured along the semi-major axis; different to the "circularized" effective radius $R_e \cdot \sqrt{b/a}$, because in this way we select objects with the same size without biasing the axis ratio distribution. Also should be notice that, in principle, R_e is bandpass-dependent; but as discussed later the dependences are not strong. As we will explain in more detail, here we work with R_e measured with the r-band because that is our deepest band.

[2]An important caveat that is worth to mention is that automatic detection techniques will always loose some galaxies and will not have a 100% level of completeness; however: i) most of the bright UDGs should be detected by this automatic technique, and ii) the strategy used in this work is very similar as those used in previous works, so our final sample should be comparable with other samples in the literature.

[3]`http://iraf.noao.edu/scripts/irafhelp?mkobjects`

UDG-like galaxies as follows:

- ⋆ We model 900 galaxies in ten different frames, each one of 10000×10000 pixels, for a total of 9000 galaxies. The minimal distance between them is slightly larger than twice the effective radius of the biggest galaxy, to avoid blending between nearby sources and get the intrinsic efficiency of our methods because of the faintness of the sources rather than get lower detection limits due to overlapping objects. The *mkobjects*' models take into account the gain for each cluster (that we know from the reduced image) and Poisson noise is added to each galaxy. The galaxies have the following parameters: effective radius between 1.5 and 7 kpc, mean effective surface brightness between 24 and 27 mag arcsec^{-2}, axis ratios in a range of 0.5-1.0, and an exponential profile. Except for the Sérsic index (n = 1) the other parameters are chosen randomly from each interval, but, as mentioned, the mean effective surface brightness do not depend on the Sérsic index, so the exponential profiles do not bias our results.

- ⋆ Then, the frames are convolved with a gaussian filter using a sigma equivalent to the mean seeing in r of each observed image; this with the aim of getting the same resolution as the real data. We use the seeing of the r–band because the detection of UDGs in the science images will be done in this filter, since the observations in this band are the deepest.

- ⋆ From a provisional run of `SExtractor` in the r–band images, we get for each cluster a so-called –OBJECT check-image (an image generated with the same background of the science image but with the sources extracted) and we cut different regions of the FOV, each region of 10000×10000 pixels. These images have spots with pixel values of zero where sources where extracted and look quite patchy. Because of this, we replace those null pixel values by random noise around the mean pixel value of each region and with its standard deviation. With this we are able to get a representative background of different regions of each image. While this procedure is not perfect, the generated background frames look homogeneous and are more realistic than generating a random background noise, where the imperfections of the real science image would not be present.

- ⋆ Finally, we inject the modeled convolved galaxies into the different background frames, and we end up with the 9000 simulated UDG-like galaxies. In Figure 3.1

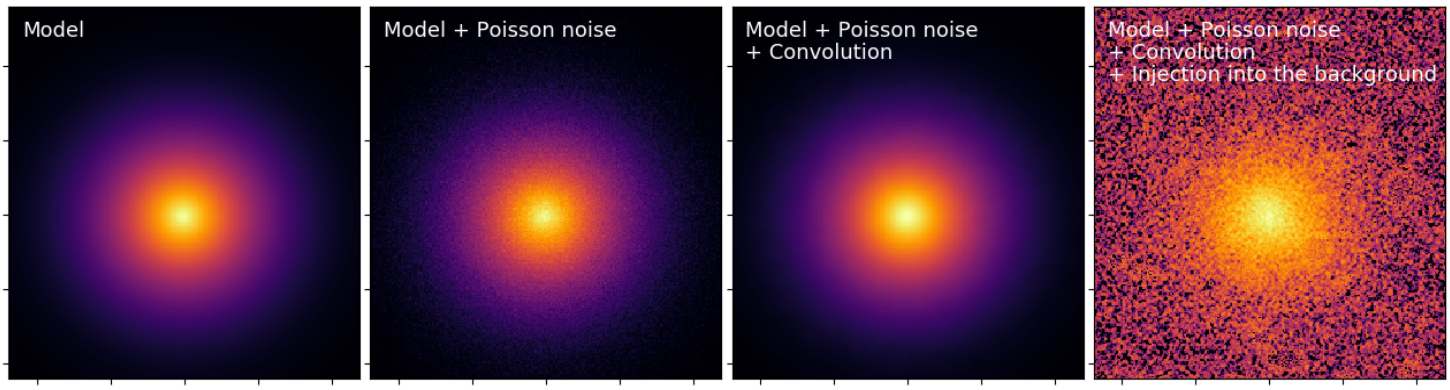

Figure 3.1: Appearance of a simulated UDG in the different steps of the model. From left to right: i) initial model, ii) i) + Poisson noise, iii) ii) + convolution, iv) iii injected into the background.

we show an example of one arbitrary mock galaxy and its appearance in each different step of the process.

With these detection images, we run `SExtractor` in all our images, with different parameters in its configuration file, specially varying the detection parameters of the detection threshold (`DETECT_THRESH`) and the minimal detected area (`DETECT_MINAREA`). We test different combinations by cross-matching (Taylor 2005, 2006) the catalogues from `SExtractor` with the modeled galaxies (allowing a maximum distance in pixels equivalent to 1 kpc at the cluster's distance) and looking at the recovering fraction (ratio between simulated and detected galaxies), the number of "ghost" detections (detections found where no galaxies were simulated) and at which threshold-value using a lower value of `DETECT_THRESH` does not increase significantly the recovering fraction but increase severely the number of "ghost" detections (according to the simulations we would expect a contamination below ~10% of the number of real detections for all the clusters). This is important given the extension of our dataset since we should try to be as efficient as possible. After reviewing the different possibilities we choose the best combination of the two parameters taking into account all the above mentioned tests.

We present the results for the detection efficiency of all the images in Figure 3.2. There we show the effective radius–surface brightness plane for the simulations on each cluster r–band image, with the color representing the recovery fraction between detected and simulated galaxies per bin.

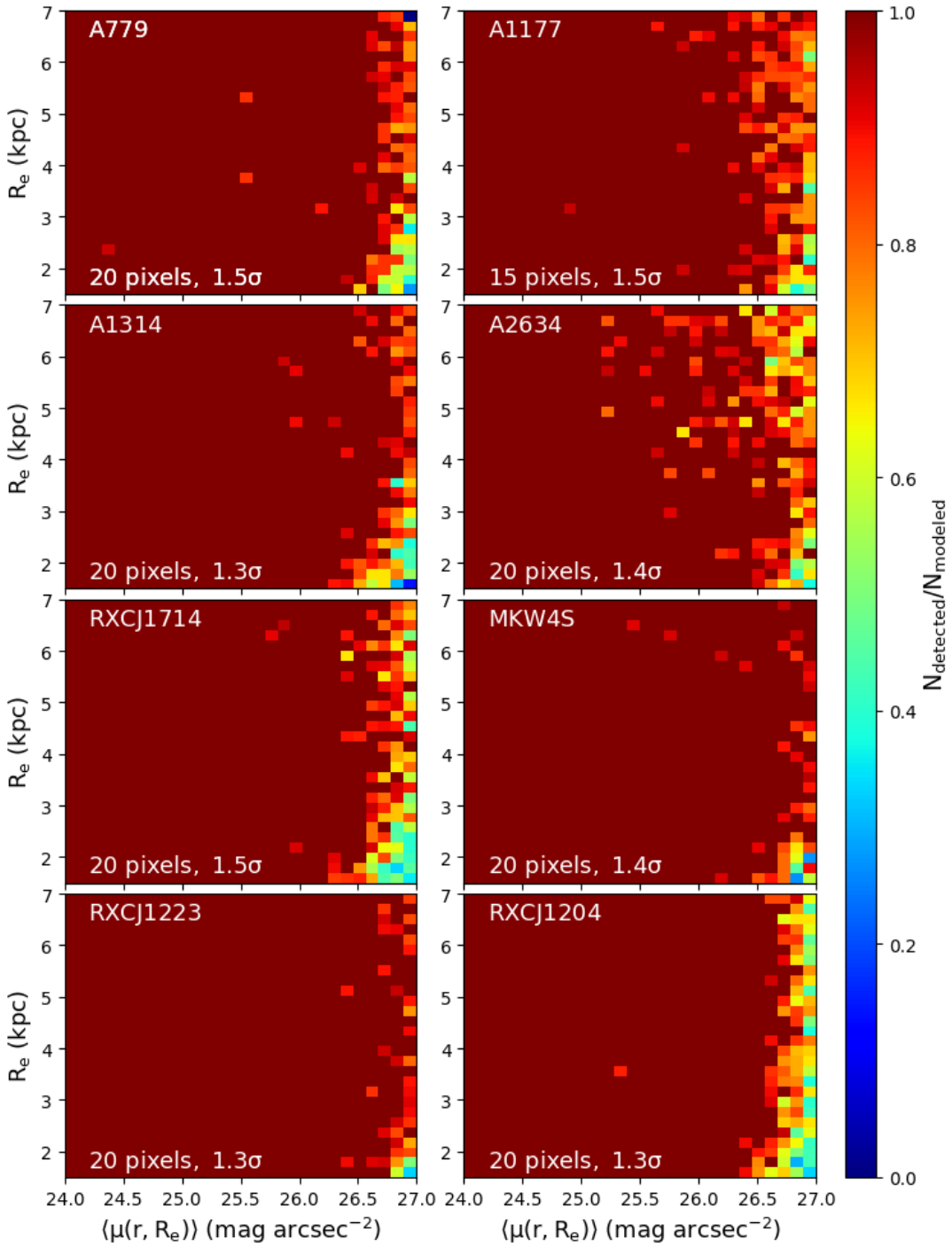

Figure 3.2: Detection efficiency of the simulated galaxies from the `SExtractor`'s output. The name of the cluster, as well as the `DETECT_TRESH` and `DETECT_MINAREA` parameters used in `SExtractor` are labeled in each box.

A natural idea would be using those simulations to get the intrinsic detection limits and completeness level of our images, something essential to make fair comparison between our sample and the data in the literature. This is by itself a bit tricky because the completeness depends of course in the surface brightness and in the size, but also on the characteristic of the observations; however, our simulations include all those ingredients, so in principle should be feasible to give us rough detection limits. Nevertheless, we have to keep in mind a couple of different factors. First, even when we incorporate realistic effects, the simulations could still be a bit idealized (see also next Chapter regarding *mkobjects* models), so it may be the case where the simulations are systematically brighter than the real galaxies. Second, our simulations are by construction blending-corrected, since each galaxy is at least at some minimum distance from its closest neighbor; something that does not happen in the real data. Also, it could be that the real psf function of the data makes the galaxies harder to detect than the gaussian filter we applied to the simulations. And moreover, it could also be that we actually detect the faintest galaxies, but they are that low surface brightness that the measurements from `SExtractor` are too off from the real values, that they do not enter in our UDG searching region; this makes sense because the faintest UDGs should have very week wings, and most likely `SExtractor` would only detect the center of the profile, measuring a non-representative effective radius and surface brightness. Therefore, we conclude that our simulations are very useful for determining the best configuration for `SExtractor`, but the detection limits are not 100% realistic.

Because of this, we decide to measure the depth of each image, by measuring the background on them. In practice, for each image we measured several regions where only background signal is detected, and we get the dispersion of the pixel values. We then transform the pixel values to surface brightness, as is usually done in the literature.

In Table 3.1 we give the mean depth of our images (measured at a 3σ level in boxes of 10×10 arcsec. The mean of our r-band images is ~ 29.3 mag arcsec^{-2}, in good agreement with the typical depth of studies on UDGs (see for instance Section 7 in Román & Trujillo 2017b).

3.3 All-sources Catalogue

To get our "All-sources Catalogue" for each cluster, we run `SExtractor` in the dual mode, with the best combination of the `DETECT_TRESH` and `DETECT_MINAREA` parameters. The dual mode allows us to do the source detection in the $r-$ band image, and then, using the

Table 3.1: Mean depth in surface brightness of our images, measured at a 3σ level and in boxes of 10 arcsec × 10 arcsec.

Cluster ID	Mean depth mag arcsec^{-2}
A779	29.1
A1177	29.3
A1314	29.3
A2634	29.3
RXCJ1714	29.3
MKW4S	29.5
RXCJ1223	29.5
RXCJ1204	29.1

same positions and apertures, do the photometry in both bands. The main parameters obtained from SExtractor are ALPHA_J2000, DELTA_J2000, MAG_AUTO (Kron–like magnitude), FLUX_RADIUS, MU_MEAN_MODEL, FWHM_IMAGE, FLAGS, and the CLASS_STAR index. If a source has FLAGS[4]$_{g,r}$ < 4, it is included in the final cluster catalogue.

During the calibration process with ASTRO-Wise preliminary zeropoint corrections are taking into account, but sometimes they are not perfect, so we perform one more zeropoint-like correction, where we compare our magnitudes with those from the SDSS catalogue DR14 (Abolfathi et al. 2018). For getting an accurate estimation, we select objects from our catalogues with FLAGS$_{g,r}$ = 0, MAG_AUTO < 16.0 mag (to avoid saturated stars) and CLASS_STAR[5]$_{g,r}$ ≥ 0.9, to make sure we are taking only point-like sources (stars) with a photometry as good as possible, and we compare them with the SDSS catalogue. We add the $2-\sigma$ clipped median value of difference in magnitude between both catalogues, and this value is almost always below 0.15 mag, and the accuracy of the photometry is the same as reported in the previous chapter.

Figure 3.3 presents all the CMDs for the selected galaxies-like objects in each cluster of our sample.

[4]FLAGS$_{g,r}$ is a "label" or warning that lets you know how well the photometry was done by SExtractor. FLAGS$_{g,r}$ < 4 allows for blended objects and objects with close neighbors.

[5]The CLASS_STAR parameter, also call stellarity index, is a probability that SExtractor gives to a source for being a star: 1 means the source is likely a star and 0 a galaxy.

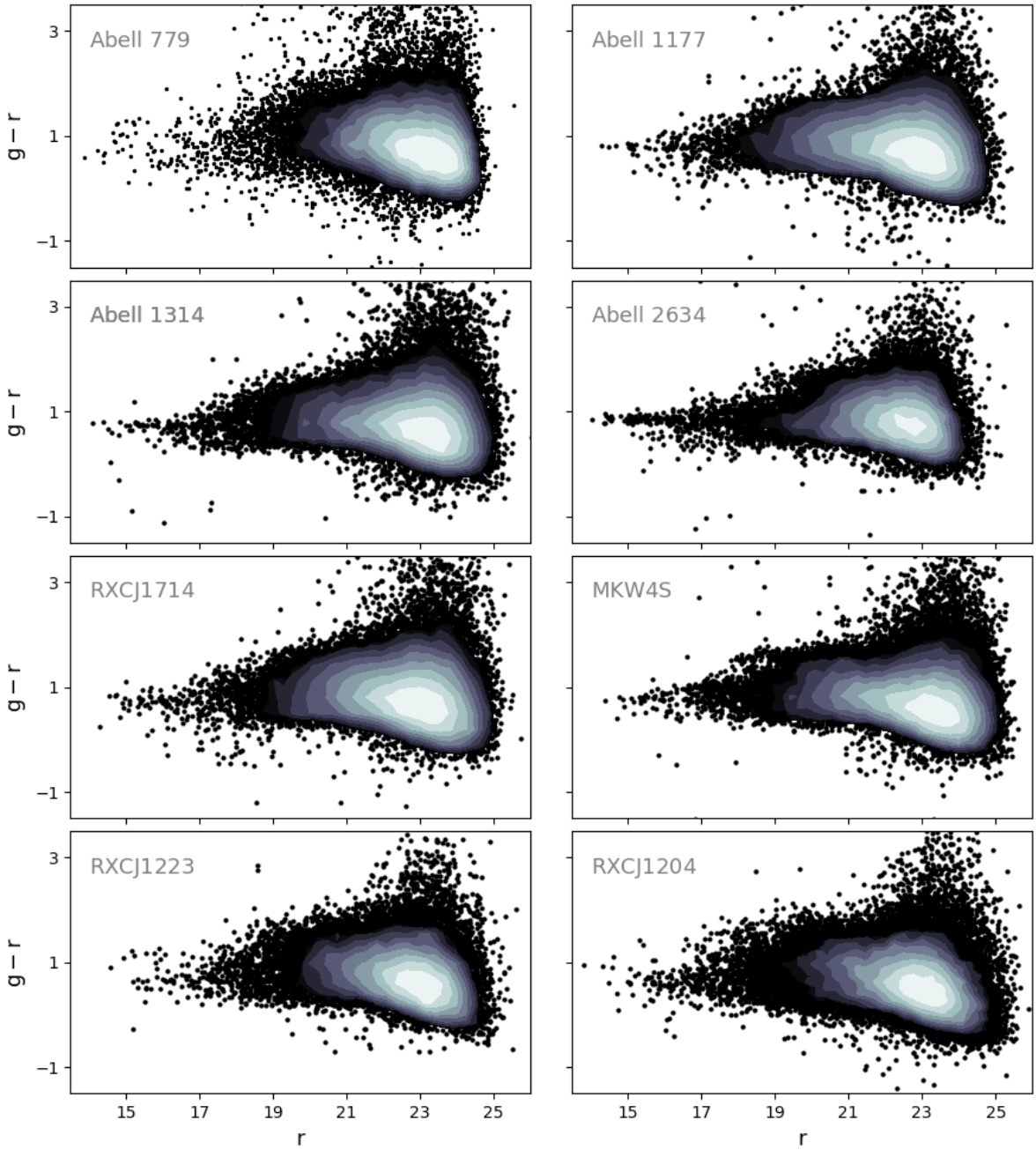

Figure 3.3: Color-magnitude diagrams for the classified galaxies in each cluster. Contours illustrate the density of points in the diagrams.

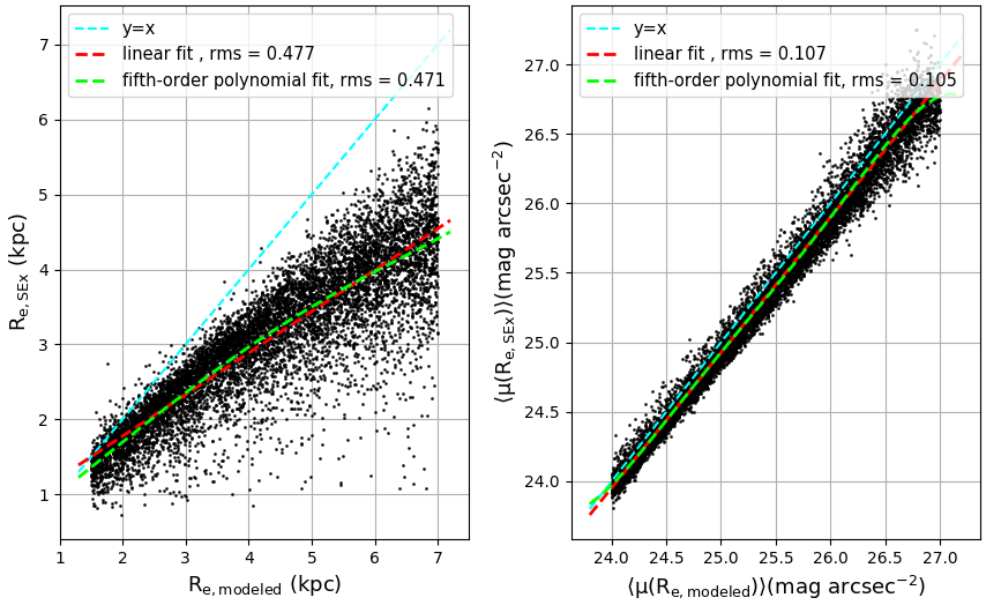

Figure 3.4: Example of the difference between the modeled and the SExtractor recovered effective radius and surface brightness for one galaxy cluster. See text for details

3.4 Selection of potential UDG candidates

For finding the potential UDG candidates we use our defined selection criteria based on size and surface brightness. We do this using the modeled galaxies described before, this time looking at the difference between the modeled parameters and those determined by SExtractor. We are particularly interested in how big are the difference between effective radius and surface brightness at the edges of our lower selection limits, since this will determine the selection criteria we should use considering the photometry of SExtractor. To illustrate this point, an example of the comparison between the effective radius and the surface brightness from SExtractor and from the original model is shown in Figure 3.4, where only objects with $\mathtt{FLAGS}_r < 4$ are used.

As we can see, the surface brightness comparison shows a good agreement, but the comparison of the effective radius is not quite good. As noticed by authors like Hammer et al. (2010) or Román & Trujillo (2017b), the effective radius from SExtractor is usually a trusty measure of the actual effective radius, but becomes less and less accurate as we go to fainter and fainter magnitudes, where it underestimates the size of the objects; this defect is also very clear in our sample of simulated UDGs. We fit a linear regression and a fifth-order polynomial to the relation and we look at the difference between them and

a line y = x, at R_e ~1.5 kpc; the fitted line and the fifth-order polynomial have always the same behavior, but the polynomial produces a slightly smaller rms, so we compare that fit with the line y = x. We measure the difference between both, and, in order to loose some fewer candidates we adopt an offset of two times the measured differences. The considered offset for each cluster is listed in the second column of Table 3.2 and the offset is corrected for our further selection. The fact that the recovered effective radius is not that accurate is not as bad as it seems to be because we select *all* the objects *above* 1.5 kpc - the offset. Moreover, these radius are not used anymore afterwards for characterizing our galaxies.

For the surface brightness the fifth-order polynomial generates also a slightly lower rms than the straight line, and it seems to mimic the flatness seen in some clusters at the faint surface brightness regime, but both are basically the same at all our range in surface brightness; and at $\langle\mu(r,R_e)\rangle$ = 24 mag arcsec^{-2} the rms of the difference between the output from `SExtractor` and the modeled galaxies is always ~ 0.1 mag arcsec^{-2}. Again, to "be on the safe side", trying to loose as few UDG candidates as possible, we decide to take a "cushion" difference of three times the rms of the relation for each cluster, and that value is listed in the third column of Table 3.2. We have to take these corrections into account when fine-tuning the settings of our selection criteria for the search of UDGs.

As mentioned, it is clear that we will loose some truly UDGs because bad measurements with `SExtractor` (for instance due to discrepancies in the effective radius), plus those that are not detected, but this is a problem in all the automatic detection techniques so far and at least we should be selecting the vast majority of the UDG-like sources, with a completeness comparable to previous works[6].

To select then the most-likely UDGs from the catalogues, we build the size-surface brightness plane and we select the objects that meet our selection criteria. The limits that we consider in effective radius and surface brightness come from subtracting the `SExtractor`'s corrections (Table 3.2) to the limits we choose for defining a UDG. If a object lies within the searching region, and it is classified as galaxy (`CLASS_STAR`≤0.2), it goes to the next step where we do a visual cleaning of the candidates to remove false

[6]Tests on mock galaxies by Aku Venhola, using the software `MTObjects`, developed by the astronomy-computer science group of the University of Groningen, show very encouraging results, in the sense that `MTObjects` seems to find LSB galaxies that `SExtractor` does not, and also the preliminary photometry is more accurate. A possible improvement for the future would be to use this software in our images to find missed UDGs.

Table 3.2: Differences at the edges of our selection criteria between the modeled values and those measured by SExtractor.

Cluster	ΔR_e (2 × offset) (kpc)	$\Delta\langle\mu(r,R_e)\rangle$(3 × rms) (mag arcsec^{-2})
A779	0.33	0.37
A1177	0.29	0.37
A1314	0.31	0.37
A2634	0.29	0.38
RXCJ1714	0.27	0.37
MKW4S	0.35	0.33
RXCJ1223	0.30	0.32
RXCJ1204	0.35	0.36

positives.

For the visual inspection, we generate individual stamps of all the objects that fulfilled the last step, and we briefly look at them to reject objects that are not really UDG-like. Typically the rejected objects are multiple detections in: halos of very bright elliptical galaxies, pikes of saturated stars, arms of spiral galaxies, noise at the border of the image; or just cases where objects are very close to each other or to very massive galaxies at such extent that we are not sure about the reliability of separate the light contribution of each of them. The remaining galaxies are those that will be studied with GALFIT, as we will discuss in the following section.

3.5 Galaxy modeling to get the final photometry

To get the final photometric parameters, we run GALFIT over stamps of all the potential UDG candidates for each cluster. The main pipeline for this was written by Aku Venhola and is described detail in Venhola et al. (2017) and Venhola et al. (2018a, in prep.). It was written originally for data from OmegaCam at the VLT, so we modify slightly the pipeline to make it adequate for the WFC. In general process is as follows:

1. To take into account the PSF effects, we stack several stars from our images in each filter, using only sources with FLAGS = 0, CLASS_STAR ≥ 0.8, and MAG_AUTO

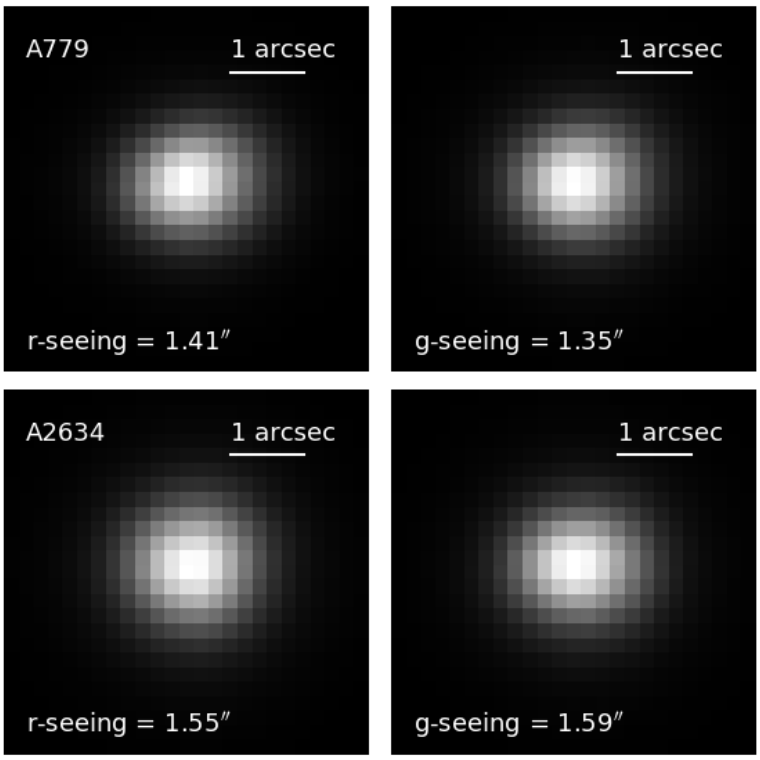

Figure 3.5: Examples of PSF profiles for the GALFIT fitting for different clusters, constructed by stacking and combining the best stars in each field.

between 16-19 mag, to avoid saturated and very faint stars. Examples of two PSF images are shown in Figure 3.5.

2. We mask, for the stamp of each candidate, the nearby sources; using an automatic masking routine plus manual masking when needed. When two galaxies are that close one another that masking is not feasible, both are modeled with GALFIT.

3. The parameters from the SExtractor's output are used as initial seeds for GALFIT, and we fit Sérsic profiles to all the galaxies. Some studies have studied the fraction of nucleated UDGs (e.g. Koda et al. 2015; Venhola et al. 2017), but the resolution of our data does not allow us to observe nucleation.

4. A fitted model is considered good if i) it visually resembles the real galaxy, ii) the model produces a radial profile that mimics the observed radial profile and iii) the residuals are low and the fit produces a reasonable χ^2_ν parameter (for all the clusters the mean χ^2_ν is around 0.8). Bad fits use to appear if the masking is not good enough or if the fitting areas are to small (because GALFIT needs a

good measurement of the background level for such faint galaxies); in those cases we run GALFIT again with a slightly different configuration, for instance varying the center of the galaxy or the fitting area, or slightly modifying the masks. All our models converge with reasonable values and are double checked. If the final residuals show strong substructure we rejected the candidates, since substructure is not expected in UDGs and could be just background galaxies.

From GALFIT's output we are able to derive the position of the center of the object, its effective radius, total magnitude in each band, axis ratio b/a, Sérsic index, n, and its position angle. It is important to explain that while we fit models to both bands, we consider the parameters than come out from the r-band fitted models, since the S/N is higher and since the r-band is less affected by young stars.

3.5.1 Color determination

Following Venhola et al. (2017) and Venhola et al. (2018a, in prep.), we decide to work with colors derived from measuring the g and r magnitudes using the effective aperture derived from GALFIT (using its center, effective radius, axis ratio and position angle). This is more stable than using the total color because for most of the galaxies they are the same (the mean difference is 0.04 mag), but using measurements at the effective aperture significantly reduces the error in the magnitudes, basically because it is less dependent to systematic errors in the sky background determination. So, for getting these magnitudes and color we just measure the flux in the elliptical effective aperture, and are these magnitudes and colors the ones that we use for the forthcoming work. The measurements in the g-band are done using the r-band derived aperture.

3.5.2 Errors on GALFIT parameters

Inferring realistic errors for the GALFIT parameters is very important, but the errors automatically generated by GALFIT are sometimes too small and not that realistic. For estimating the errors in a more proper way, and following Venhola et al. (2017) we use a different approach based on mock galaxies.

We simulate mock galaxies with known parameters, and we compare their original parameters with the output of GALFIT, as a function of the surface brightness (since the S/N dominates the uncertainties in this type of LSBs). However, for doing this we use a slightly different approach than in the simulations for getting the detection rates: as noticed by Dr. C. Y. Peng on the GALFIT's Manual (see https://users.

obs.carnegiescience.edu/peng/work/galfit/TFAQ.html), *mkobjects* from IRAF and GALFIT differ in how the photometry is done (IRAF photometry is somehow idealized) and their parameters are not one-to-one comparable (for more details the reader can go to https://users.obs.carnegiescience.edu/peng/work/galfit/TFAQ.html#misconception1). Dr. Peng also explains that even when the comparison is more fair for low-Sérsic index galaxies (like UDGs) than for high-Sérsic index galaxies, and considering a proper set-up of the configuration files for *mkobjects*, it is still very hard to produce consistent and reliable agreements to better than 5-20%. Because of this we decide to generate a few mock galaxies via another method, for their further GALFIT analysis to get expected typical errors from the fits.

We generate 500 new mock galaxies in totally random positions, using a 2D-Sérsic profile determined by their mean effective surface brightness, effective radius, axis ratio and Sérsic index. We make sure of covering all the parameter space with good statistics to have a representative sample, sampling a distribution with a range in mean effective surface brightness of 23.7–27 mag arcsec^{-2} , 0.2–1.0 in axis ratio, 1.5–7 kpc in effective radius, 0.1–2 in Sérsic index and random position angles. Once the distributions are drawn, we model the flux of the galaxies using the equation (Peng 2010):

$$F_{tot} = 2\pi r_e^2 \Sigma_e e^{b_n} n b_n^{-2n} q,$$

where F_{tot} is the total flux, r_e the effective radius in pixels, Σ_e the pixel surface brightness, n the Sérsic index, q the axis ratio, and the b_n parameter is computed following the power series expansion on n by Ciotti & Bertin (1999) if $n \geq 0.36$ or MacArthur et al. (2003) if $n < 0.36$.

We also add Poisson noise to the galaxies, and they are convolved with the kernel of the PSF profile of one cluster. We choose the PSF of MKW4S since its seeing (1.43”) is close to the mean of the mean seeing of our sample (1.48”). Finally the galaxies are injected into a region of the science image of MKW 4s. In practice we realize several runs, injecting 20 galaxies per time. Figure 3.6 shows examples of the generated mock galaxies.

Once the images are ready, they go trough the same process as the real galaxies, meaning that they are detected and measured by SExtractor and using the output from this one as seed values for GALFIT.

The comparison between modeled and derived parameters is analyzed as a function of the surface brightness and the result of this is shown in Figure 3.7. As can be seen, the

Figure 3.6: Some examples of the simulated UDGs for testing the accuracy of fitting our data using GALFIT.

differences between the modeled and recovered parameters increases towards fainter surface brightness, but the agreement is very good (see for instance Fig. 11 in Venhola et al. (2017) for a comparison with a better data under the same analysis). We find 2σ mean offsets (model – GALFIT, blue lines) for each parameter of $\bar{\Delta}$mag = -0.074 mag, $\bar{\Delta}R_e$ = -0.082 kpc, $\bar{\Delta}$n = -0.017, and $\bar{\Delta}$b/a = -0.003. The fact that the negative half of the Δmag plane is more populated makes sense if one thinks that at these faint magnitudes, the wings of the Sérsic profile are very weak and probably GALFIT cannot detect them, making it missing some outer light of the galaxies, and measuring higher (fainter) magnitudes.

For characterizing our uncertainties we measure the standard deviation, at a 2σ level, of each parameter for different bins of surface brightness (vertical red solid lines), and we fit to them a second degree polynomial of the form $\Delta = ax^2 + bx + c$ (red dotted lines), and we assume this one to be the uncertainty for each of our measurements. Table 3.3 gives the values for the a, b and c constants for each analyzed quantity. The errors in our reported surface brightness come from propagating the errors of the magnitude and

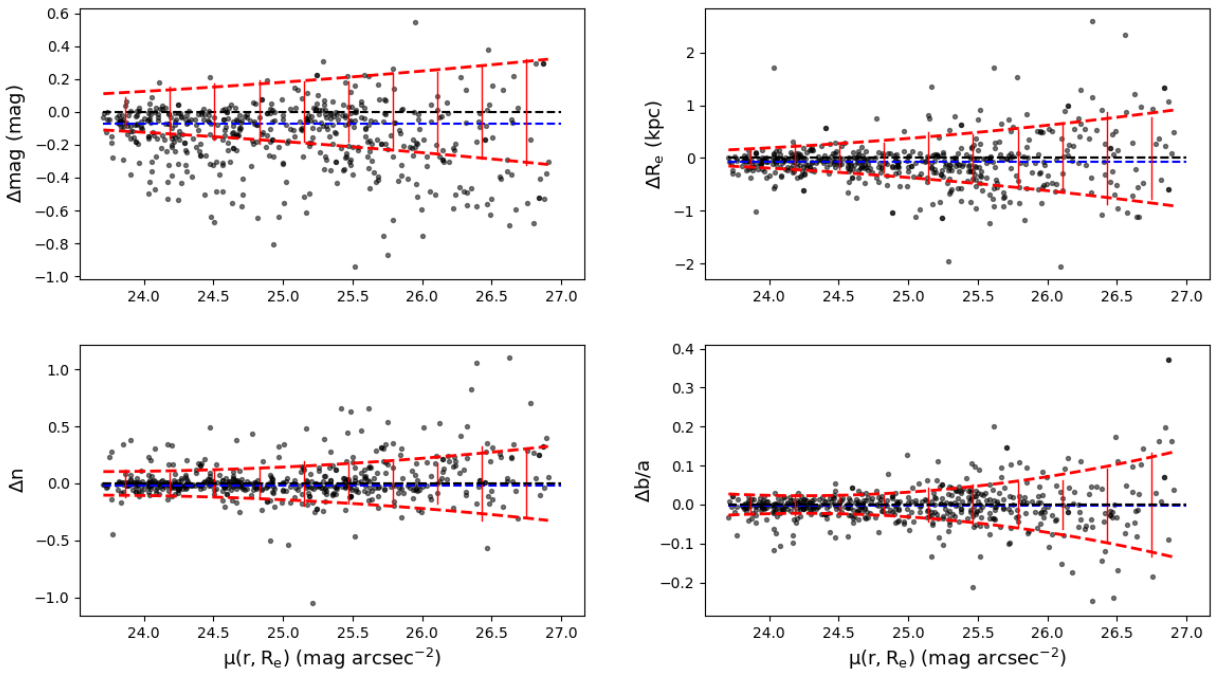

Figure 3.7: Comparison between the modeled parameters of the mock galaxies with those recovered with GALFIT, used to estimate the uncertainties in our real data. The Δ refers to model-GALFIT values, the black and blue lines show the zero and the offset position of the differences, and the red solid vertical and red dashed lines are the 2σ errors in bins of surface brightness, and the second degree polynomial fitting to them, respectively.

Table 3.3: Parameters of the second degree polynomials used for deriving the uncertainties associated with each quantity fitted with GALFIT.

Parameter	a	b	c
Δ_{mag}	0.00604	-0.24012	2.40846
Δ_{Re}	0.03562	-1.56724	17.28818
Δ_{n}	0.02003	-0.94497	11.24596
$\Delta_{b/a}$	0.01577	-0.76446	9.28807

effective radius.

It is very important to clarify that our errors in the aperture magnitudes and aperture colors are not the same as the just previously shown uncertainties in the total magnitude, because, as already mentioned, the measurement of these quantities was done by determining the flux within the effective aperture. The errors associated with

the color are determined following eq. (7) in Venhola et al. (2017):

$$\sigma^2_{g-r} = \sigma^2_{ZP,g} + \sigma^2_{ZP,g} + \left(\frac{2.5}{I_r ln10}\right)^2 (\sigma_{I,g} + \sigma_{sky,g})^2 + \left(\frac{2.5}{I_g ln10}\right)^2 (\sigma_{I,r} + \sigma_{sky,r})^2,$$

with $I_{g,r}$ the mean intensity within the effective aperture in each band, $\sigma_{I,g,r}$ its error, and $\sigma_{ZP,g,r}$ and $\sigma_{sky,g,r}$ the error in the zero-point and sky determination, respectively. Along the rest of this work we will work with these colors, and the uncertainties associated with them. These measurements are much more robust, and the typical uncertainties associated with the color are of the order 0.2 mag.

3.6 UDGs in our sample

Once we retrieve all the parameters of the cluster UDGs from `GALFIT`, we use them to infer the mean effective surface brightness of each galaxy, to see whose of them can be classified as UDGs according to our definition.

The equation that we use to derive the mean effective surface brightness, using the integrated magnitude within the effective aperture, $m(< Re)$, and taking into account an elliptical aperture, is:

$$\langle \mu(r, R_e) \rangle = m(< R_e) + 2.5 \log(\pi (b/a) R_e^2) \ ,$$

Finally, Galactic extinction– and K–corrections are taken from Schlafly & Finkbeiner (2011) and Chilingarian & Zolotukhin (2012), respectively (for the K–correction the redshift of the cluster and the color of each individual galaxy is considered), and, while basically negligible, cosmological dimming (Tolman 1930, 1934) is also considered.

3.6.1 Final UDG classification

The original idea for the final step on the UDGs classification is using the CMD diagram for each cluster, and keeping only objects with a distribution similar to the RS of each cluster, since most of the cluster UDGs are known to have old, passively evolving, stellar populations. However, this is not straightforward: if one wants to make a fair color comparison between UDGs and elliptical galaxies that populate the RS, their magnitudes should me measured in the same way. This means that we should fit the elliptical galaxies with `GALFIT` as we did with the UDGs, but this is more complex because while UDGs have a simple one-component Sérsic profiles, ellipticals can have different components and not only a de Vaucouleurs profile, for instance. We try fitting

one-component Sérsic profiles to the giant ellipticals but the residuals are high for most of them (see for instance Venhola et al. 2018a, in prep., where the same problem is studied in some more detail), and a careful fitting analysis for each elliptical galaxy is out of the scope of this work, so we do not try more in this direction.

Another natural option would be using the preliminary photometry from `SExtractor` (that was done homogeneously for all the sources) with the same idea of keeping only UDGs that lie within the RS; however as we saw in the comparison between the model and the `SExtractor` photometry, at the faint magnitude levels typical of UDGs, the scatter is way higher than at bright magnitudes, typical of RS galaxies, so this idea is also rejected.

Finally, something else that should be considered is the fact that the behavior of the RS could not be homogeneous at faint UDG-typical magnitudes. For instance Roediger et al. (2017) showed that the RS in the Virgo Cluster flattens around -14 ≤ M_g ≤ -13, what is also observed in the Fornax Cluster (Venhola et al. 2018a, in prep.); so a simple straight line fit to the RS in our sample may be not very precise at the magnitude of faint UDGs, and we could loose some truly UDGs.

Keeping all this in mind, for simplicity we decide to keep all the UDGs except for those with extreme colors which cannot be consistent with stellar population models, and thus should be background galaxies. This is usually done in the literature with colors ranging form $g-r \sim 0.9$–1 mag (e.g. Agulli et al. 2014; Venhola et al. 2018a, in prep.) so we follow the same approach considering a color slightly redder to account for the higher uncertainties at faint magnitudes. This is why we adopt the mentioned threshold of a color, measured within the effetive radius, $g-r \leq 1.2$ mag. Table 3.4 gives the total number of UDGs found in all our FOVs, showing also the number of galaxies rejected due to their Sérsic index and color selection criteria. The structural parameters of the final UDGs are studied in detail in next Chapter, and a few examples of the r-band image of UDGs are shown in Figure 3.8.

Table 3.4: Number of UDG-like galaxies in each cluster. We make the distinction between the number of galaxies that meet the size and surface brightness criteria, but do not meet the Sérsic index and color criteria, and those that do.

Cluster	N(UDG-like)	N(UDG)
A779	32	31
A1177	42	39
A1314	102	91
A2634	131	120
RXCJ1714	44	43
MKW4s	44	42
RXCJ1223	42	37
RXCJ1204	45	39

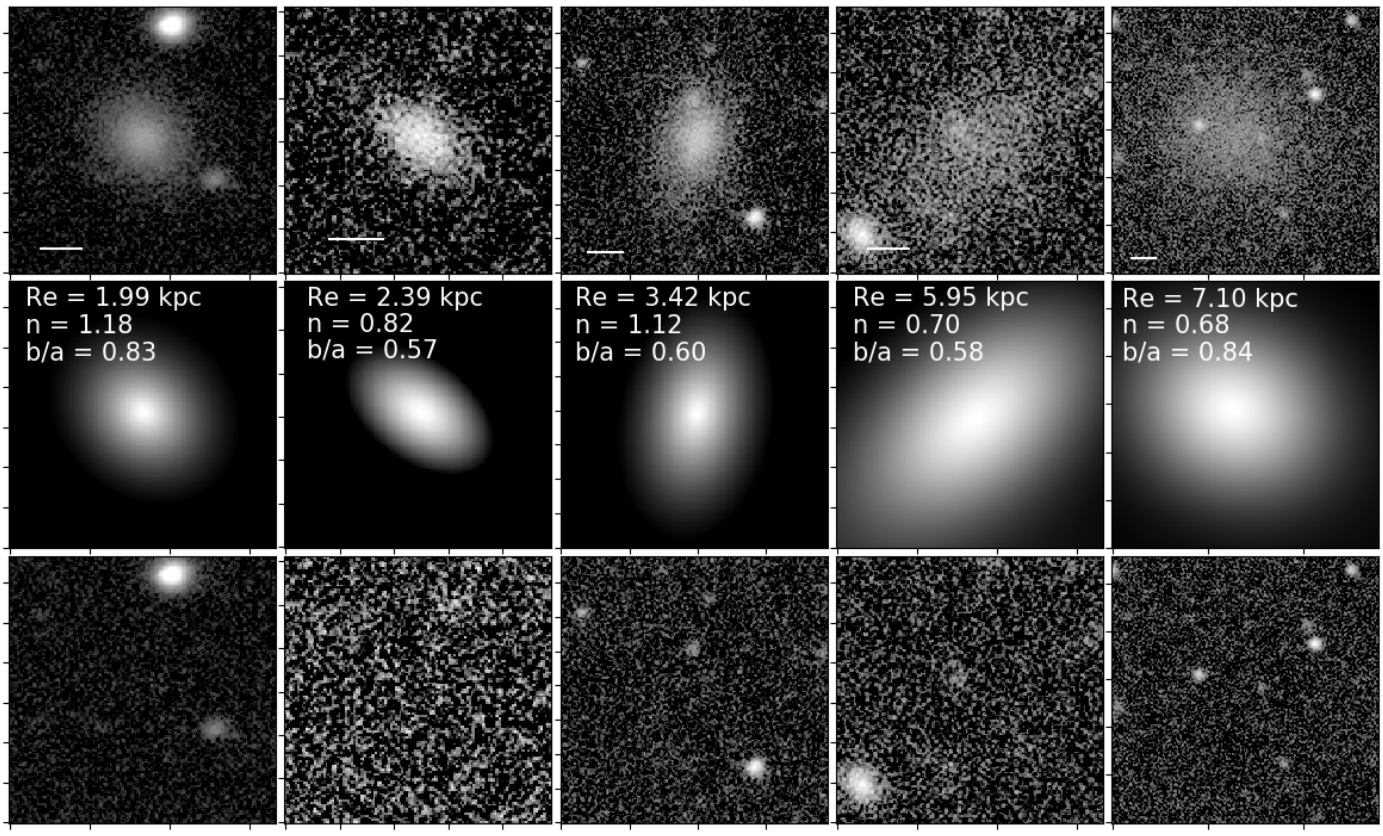

Figure 3.8: Examples of 5 UDGs found in different clusters. Top panels show the r-band image of the UDG, middle panels the GALFIT models with their structural parameters, and bottom panels the residuals of the fits. The color-scale is logarithmic to highlight the low surface brightness structures and the white bands in the top panels show the scale of 5 arcsec.

CHAPTER 4

PROPERTIES OF THE UDGS

This Chapter focuses on analyzing the photometric parameters obtained via the GALFIT modeling explained in last Chapter. We build different scaling relations for UDGs, putting them first in context with other types of galaxies, and then focusing on UDGs only. Finally, we asses the relation between the number of UDGs within R_{200} and M_{200}, using our sample and samples in the literature, derived for the first time in a homogeneous way.

4.1 Structural parameters

We find 442 UDGs in our eight FOVs, 247 of them lying at projected clustercentric distances smaller than 1 R_{200}. As a whole population, our UDGs have median (mean) values of $g-r$ = 0.59 (0.59); R_e = 1.91 (2.16) kpc; n = 0.96 (1.01); and b/a = 0.67 (0.67). Figure 4.1 shows the histograms of each parameter for our full sample. These parameters are in good agreement with the values reported in the literature (e.g. Yagi et al. 2016; Román & Trujillo 2017b; Venhola et al. 2017).

As expected, the bulk of our UDGs show a color characteristic of passively evolving old stellar populations, although a small fraction of the UDGs show also colors as blue as $g-r \sim 0$. This is observed in a few other cases in the literature, and are examples of UDGs than could still host ongoing star formation processes. Regarding the effective radius the histogram is dominated by the UDGs smaller than 2 kpc, a phenomena present in all the clusters studied in the literature, where the lack of large UDGs is very

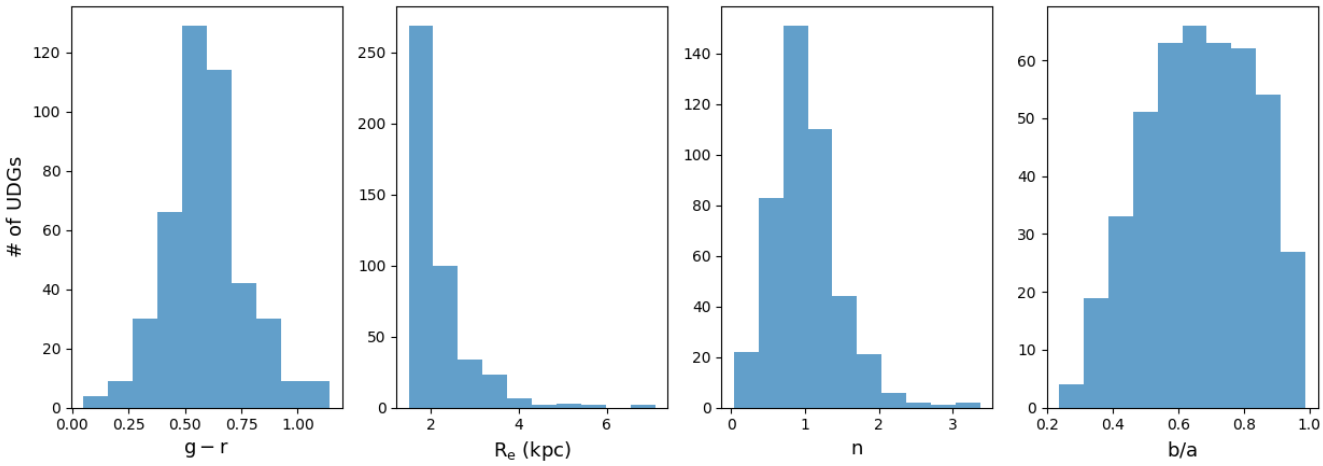

Figure 4.1: Histograms of color, effective radius, Sérsic index and axis ratio of the UDGs found in this work.

clear. Curiously, we find that our UDGs follow mostly exponential profiles as first defined by van Dokkum et al. (2015a), and slightly higher than the 0.7-0.9 range found in other works. Finally, regarding the (apparent) axis ratio distribution, presumably it resembles more the expected distribution of thick disks, but it is also very likely that there is a mix of shapes of UDGs and we are observing a combination of them.

Of course the mean and median values, as well as the histograms just described, are dominated by the more massive clusters that have more UDGs, so we also look at the value of the structural parameters in each cluster. Table 4.1 gives the mean, median, maximum value, minimum value and standard deviation of each structural parameter for the UDGs inside R_{200} (see below). Taking the mean of all the medians of each parameter (denoted by $\langle\ \rangle$), we find that in our sample, within R_{200}, our galaxies have $\langle g-r \rangle$ = 0.61; $\langle R_e \rangle$ = 1.95 kpc; $\langle n \rangle$ = 1.00 and $\langle b/a \rangle$ = 0.72. We see that overall, our parameters are in very good agreement with the literature for both the whole sample of UDGs and those within the R_{200} of each cluster.

Table 4.1: Mean, median, minimum and maximum value, as well as the dispersion on each structural parameter in the inner 1 R_{200} region. The order of the clusters here is different that in previous tables: here they are ordered from low to high masses. For reference, last column indicates the M_{200} of each cluster.

$g-r$							
	Cluster	mean	median	min	max	σ	M_{200} ($\times 10^{13}$ $M_\odot$)
	RXCJ1714	0.58	0.56	0.50	0.66	0.05	0.58
	RXCJ1223	0.55	0.55	0.45	0.65	0.05	1.98
	MKW4S	0.58	0.62	0.30	0.98	0.17	2.31
	RXCJ1204	0.59	0.55	0.36	0.92	0.16	2.88
	A1177	0.64	0.64	0.46	0.84	0.12	3.82
	A779	0.74	0.72	0.52	0.94	0.13	4.02
	A1314	0.63	0.65	0.37	0.91	0.12	7.62
	A2634	0.56	0.57	0.22	0.89	0.13	26.60
R_e (kpc)							
	RXCJ1714	2.09	1.77	1.64	3.32	0.55	0.58
	RXCJ1223	2.62	2.34	1.52	7.04	1.33	1.98
	MKW4S	1.85	1.82	1.53	2.47	0.32	2.31
	RXCJ1204	1.97	1.91	1.57	2.98	0.33	2.88
	A1177	2.08	1.93	1.53	3.63	0.52	3.82
	A779	2.26	2.03	1.51	3.95	0.64	4.02
	A1314	1.97	1.80	1.51	3.35	0.45	7.62
	A2634	2.13	1.96	1.50	5.70	0.68	26.60
n							
	RXCJ1714	0.93	0.79	0.62	1.60	0.31	0.58
	RXCJ1223	0.93	0.95	0.48	1.35	0.20	1.98
	MKW4S	0.98	0.95	0.04	1.65	0.40	2.31
	RXCJ1204	1.03	1.04	0.55	1.75	0.31	2.88
	A1177	1.14	1.14	0.58	1.89	0.31	3.82
	A779	1.14	1.06	0.24	2.98	0.56	4.02
	A1314	1.03	1.05	0.37	1.83	0.39	7.62
	A2634	1.03	0.98	0.17	2.33	0.46	26.60

Continued on the next page

	Cluster	mean	median	min	max	σ	M_{200} ($\times 10^{13}$ $M_\odot$)
b/a							
	RXCJ1714	0.79	0.82	0.62	0.89	0.10	0.58
	RXCJ1223	0.71	0.72	0.38	0.98	0.16	1.98
	MKW4S	0.68	0.65	0.38	0.92	0.16	2.31
	RXCJ1204	0.74	0.77	0.36	0.95	0.15	2.88
	A1177	0.73	0.70	0.60	0.93	0.11	3.82
	A779	0.71	0.69	0.38	0.96	0.17	4.02
	A1314	0.71	0.73	0.38	0.97	0.15	7.62
	A2634	0.67	0.68	0.33	0.97	0.16	26.60

Table 4.1: Continuation.

4.1.1 Stellar mass estimation

Deriving dynamical mass of UDGs is extremely difficult and, as discussed in the Introduction, the best we can do today is using other traces like globular clusters, or try to use integral field spectroscopy to derive the real stellar kinematics; something that will be done soon probably.

Nevertheless, estimating (rough) stellar masses based on the light we get is relatively simple, and has been done in the literature (e.g. van Dokkum et al. 2015a,van der Burg et al. 2016, Román & Trujillo 2017a,b). It is usually done using M/L ratios derived from the color information, or using stellar population models assuming some age and metallicity.

For simplicity, with the aim of derive rough stellar masses of our sample, we use here the approach via M/L ratios. In particular, we use the relation given by Roediger & Courteau (2015) that allows us to derive M/L based on our g- and r-filters. The M/L relation assumes a Chabrier Initial Mass function (Chabrier 2003), and according with Roediger & Courteau (2015) the results are comparable to use SED fitting techniques.

We derive M/L using the $g-r$ color and the r-band absolute magnitude, and we transform to mass assuming an absolute magnitude in the r-band for the Sun of 4.65 mag (from `http://mips.as.arizona.edu/$\sim$cnaw/sun.html`). Figure 4.2 shows the histogram of the distribution of stellar masses for the UDGs in our sample. From propagating the uncertainties we estimate that the accuracy is roughly of a factor 1-2 of the determined stellar mass. The median (mean) stellar mass of our UDGs is $M_\star$ =

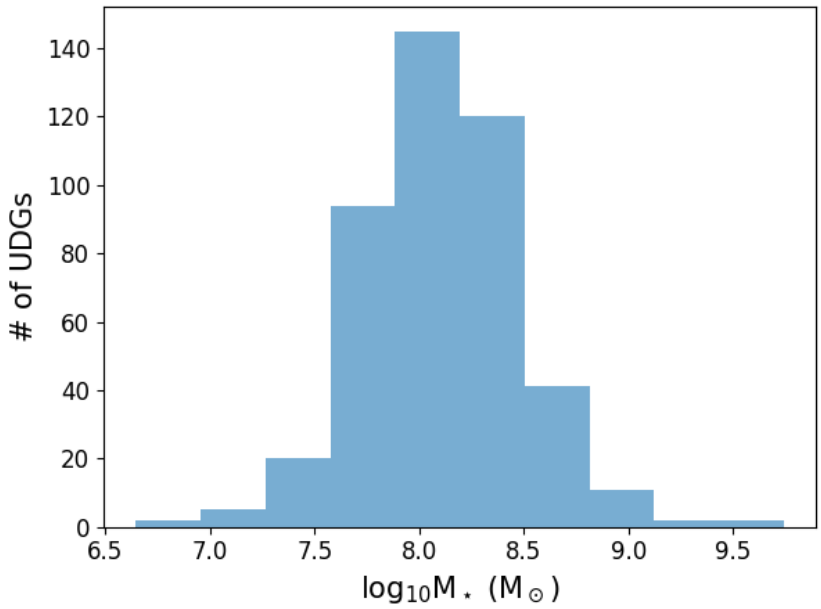

Figure 4.2: Histogram showing the distribution of stellar masses of the UDGs in our sample. See the text for details.

1.3×10^8 (2×10^8) $M_\odot$, in agreement with the values reported in the literature.

4.2 Scaling relations

In this Section we will show how all the structural parameters of UDGs as a population correlate with each other, putting them in context when compared to other types of galaxies, and we will later focus on specific scaling relations of particular interest like the planes color vs. R_e, or axis ratio vs R_e, only for the UDGs.

For comparing with other types of galaxies, we use a set of bright galaxies from the low-redshift clusters sample of WINGS (Fasano et al. 2006; Sánchez-Janssen et al. 2008), the catalogue of the Fornax Cluster (Venhola et al. 2017, 2018a, in prep.), the stellar hosts of blue compact galaxies (Amorín et al. 2009), and a set of dwarf elliptical galaxies (Aguerri et al. 2005). The structural parameters of these works were not derived exactly in the same way as ours, but all of them used the Sérsic profile fitting technique. For making a fair comparison we do as follows:

In the case of the WINGS bright galaxies, Sánchez-Janssen et al. (2008) characterized their sample by fitting a bulge+disk model, and also a Sérsic profile, which we use. From

there we get the Séric index, effective radius, axis ratio and magnitude. The authors derived the Sérsic fits using V-band data, but we do not expect considerable pass-band dependencies[1]. In any case, we do transform their V magnitude and $B-V$ colors to our g and r filters. For doing that we use the relation by Bilir, Karaali & Tunçel (2005), which includes the color terms $B-V$ and $g-r$. Then, we also correct for the differences in cosmologies to re-derive physical sizes and absolute magnitudes; this change is not very strong: the median of the difference in the original and new physical scale (kpc/arcsec^{-2}) is 0.067, and between the luminosity distances is 15 Mpc (i.e. less than 7% of the distance to the clusters). Finally, we apply K-corrections (the magnitudes were already corrected by Galactic extinction) and cosmological surface brightness dimming in the same way as for our data. While there may be some systematic differences in the data we do not expect them to be very strong.

Regarding the Fornax Catalogue the comparison is straightforward, since the authors used exactly the same analysis with GALFIT, and OmegaCAM uses SDSS filters, so we only apply K-corrections and surface brightness dimming.

For the blue compact galaxies (BCGs[2]), the procedure is the same as for the WINGS galaxies. We decide to work with the structural parameters derived from the R-band, since it is the most similar to our r filter.

Finally, the dEs from Aguerri et al. (2005), which are all Coma members, go under the same cosmological and photometric conversions, but this time the photometric conversion uses the equations derived by Robert Lupton[3]. Again, R-band derived structural parameters are used.

Figure 4.3 shows all the derived structural parameters for the UDGs and the comparison galaxies. Since our work deals with the lowest surface brightness galaxies of all (except for some dwarfs in Fornax, but those observations are deeper than ours), we assume that the uncertainty in our data (see last Chapter) is the uncertainty that dominates the scaling relations here presented. However, it should be mentioned that small systematics in the cosmological and photometric conversions might also be present. To not saturate even more the figure, error-bars are not plotted here, but can be appreciated in the following figures of this Chapter.

[1]See for illustration the Appendix B of Román & Trujillo (2017a) for a comparison between SDSS bands; or Amorín et al. (2009) for VBRI photometry.

[2]Do not confuse with the same acronym for brightness cluster galaxies. Blue compact galaxies, as mentioned in Amorín et al. (2009), are "gas-rich galaxies with bursty ongoing star formation".

[3]Available at http://www.sdss3.org/dr8/algorithms/sdssUBVRITransform.php

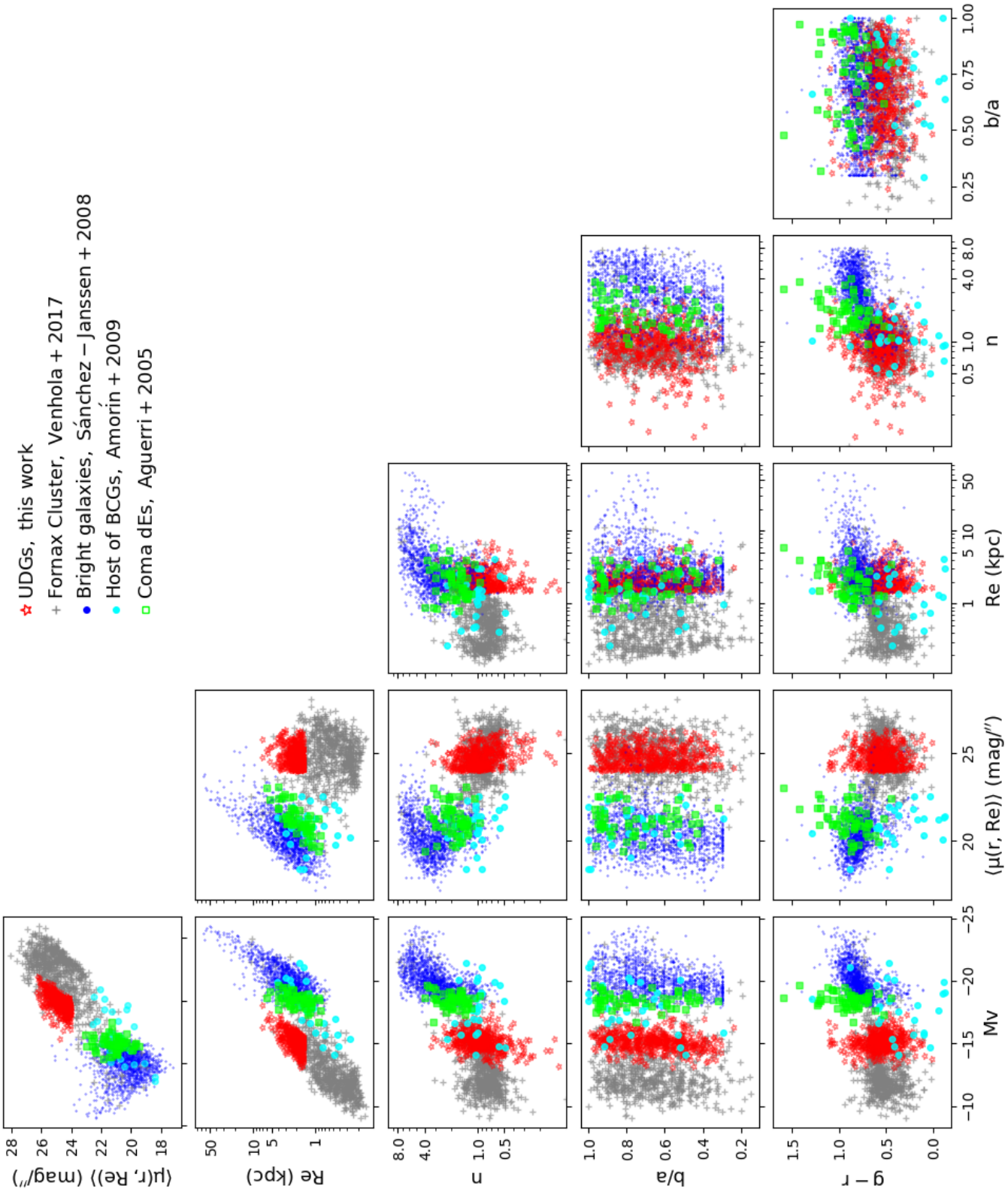

FIGURE 4.3. Structural parameters of UDGs compared with other types of galaxies. See the text for details.

We can see that UDGs fit very well with the general trend that goes from the small dwarfs to the very bright galaxies, just standing out against other galaxies of the same luminosity for being larger and lower surface brightness. They are also part of the continuous relation in the color-magnitude diagram between the brightest and faintest galaxies, although there are also two groups of UDGs, showing respectively slightly redder and bluer colors that other UDGs and galaxies of their same luminosities. Some of them have colors as red as the giant ellipticals, which may be an indication of some UDGs being as massive as them, but the size of our uncertainties in colors should also be considered and might be the reason of a larger spread in colors of the UDGs at any luminosity. When considering the dependencies on the luminosity, as mentioned, UDGs fit very well on a continuous relation between small and giant galaxies. Interestingly there seems to be a different slope for giant and dwarf galaxies in the surface brightness vs. absolute magnitude plane; and also here UDGs behave as a subset of the dwarf galaxies. Besides this, apparently UDGs do not follow a totally vertical distribution in the axis ratio vs. absolute magnitude plane, where a very shallow slope is visible. That would mean that brighter UDGs tend to be more slightly more roundish.

When looking at the surface brightness dependencies, again UDGs behave just as galaxies at the tip of the distribution of effective radius for dwarfs; with Sérsic index and axis ratio mixed between the other types of galaxies, and showing the mentioned larger spread in colors.

As a function of the effective radius, UDGs, as expected, build the bridge between the smaller dwarfs of the Fornax catalogue and the brighter cluster galaxies. Particularly the n vs. R_e plane reflects both the R_e vs. Mr and n vs. Mr planes, in the sense that brighter galaxies tend to be larger and to have higher Sérsic index.

UDGs also show a tail, as Fornax dwarfs do, of objects with small radii having very flat surface brightness profiles. However, the tail is magnified due to the logarithmic scale, and the difference of the Sérsic index of the tail and the bulk of UDGs is only around ~ 0.25; which is not an unexpected deviation of the real values at those faint surface brightness, as we saw with our simulations in last Chapter.

Additionally, we can see that UDGs follow, with a larger scatter, the same color–Sérsic index relation with relatively high-Sérsic index galaxies showing redder stellar populations, when one goes from disk-like to more elliptical-like structures. The panel with the color as a function of the axis ratio illustrates nicely how UDGs, as well as the Fornax dwarfs, agree very well with the massive cluster galaxies, but having in general slightly bluer colors. From here it is also easy to distinguish the a few UDGs as red as

the massive galaxies. As can be seen in all the panels with the color in the y-axis, these galaxies stand out from the rest only in its color, but the rest of their parameters are in agreement with the parameters of the bulk of the UDG population, which make us believe that the red colors are not a result of a bad fit. Interestingly, when looking in detail to the parameters of these red galaxies ($g - r > 1$, 12 galaxies), we realize that they are present in different clusters, but always at projected clustercentric distances larger than 1 R_{200} and between the outermost of all UDGs in each cluster. Considering, as pointed out above, that the fits seem to be fine, there are four possible explanations (or a combination of them) of the observed red colors: i) that this set of UDGs have truly redder stellar populations (which seems to be unlikely since they are far away from the center); ii) that they are very large galaxies at high redshift (which at least of the large ones seems unlikely given the size they should have at higher redshifts); iii) that these UDGs have more dust than the rest; or iv) that being these galaxies near the edges of our cluster images, their g-band photometry is not very deep and we are slightly biased to observe redder colors in them.

As mentioned in Chapter 1, most of the UDGs are believed to be dwarfs, and since they have old stellar populations it is interesting to compare their physical properties with dEs. From Figure 4.3 we see that as a function of the absolute magnitude and surface brightness, they complement extremely well each other, again UDGs just being slightly fainter and having bluer stellar populations that dEs (some dEs show a very red color). About the shapes and light profiles, UDGs extend towards lower axis ratios, and have lower Séric indices. We check and their positions are also well matched with the dEs and dIrr in Fornax.

As a conclusion of this comparison between the scaling relation of UDGs and other types of galaxies, we see that apart from being the faint and large tail of dwarfs, they occupy their same locus in the different planes we studied; following all the continuous relations from the small to the giant galaxies. In the photometric parameters space, it seems like there are no signals of UDGs sharing common regions with galaxies with massive halos, but of course this is not unexpected and the ultimate comparison should be done in the future with total mass determinations. We will now focus on two of these scaling relations of particular interest, but only for the UDGs, to see if the observations can support any of the proposed theories about their formation and evolution.

4.2.1 Scaling relations of UDGs

4.2.1.1 Axis ratio vs. effective radius

One of the predictions of the model by Amorisco & Loeb (2016) is that UDGs with higher angular momentum are larger than UDGs with lower angular momentum, since the spin parameter is proportional to the radius. As a consequence, large UDGs are prone to be more elongated; but in general the consequence would be that the axis ratio distribution is flat-like, as expected for disky galaxies. Nevertheless, according to Di Cintio et al. (2017), UDGs become larger due to strong feedback-driven outflows, without the requisite of inhabiting high-spin halos.

In a previous observational work, Venhola et al. (2017) compared the relation between R_e and the axis ratio for the Coma and Fornax clusters, finding that large UDGs in Fornax are more elongated than smaller UDGs, a phenomena not observed in Coma. Additionally, these authors mention that apparently low-mass clusters or galaxy groups contain more large and elongated UDGs than in more massive systems.

We plot in Figure 4.4 the effective radius–axis ratio plane for all the UDGs in this work. From the panel "a" in the figure we conclude that while there is not a very strong trend, in general one can see how the distribution changes from smaller to larger sizes, with larger UDGs preferring lower axis ratios. Then, since Di Cintio et al. (2017) and Amorisco & Loeb (2016) considered UDGs in isolation, we compare the distribution for the UDGs within 1 projected R_{200} (panel "b") and those outside R_{200} (panel "c")[4], that can be considered more isolated that the UDGs closer to the cluster center. The white stars in the last two panels show the medians of the bins in effective radius and their standard errors (sampling more where we have more data)

Interestingly, when the separation in "inner" and "outer" UDGs is done, one can see more easily (form the spread in the color of the hexagonal bins) that for the inner ones, the distribution tends to be more concentrated in higher axis ratios than the distribution of the outer ones (see also Figure 5.5 in next Chapter), where the distribution becomes more flat or disky. The effect is also appreciated with the median values of the inner UDGs being shifted towards higher axis ratios (and with lower errors) with respect to the outer ones (considering specially the effective radii up to 3.5 kpc, where we have more data points). This would mean that our observations of the relatively isolated UDGs are in agreement with them having been originated according to the model by Amorisco &

[4]Of course it should be reminded that we do not fully spatially cover the outer regions of the clusters.

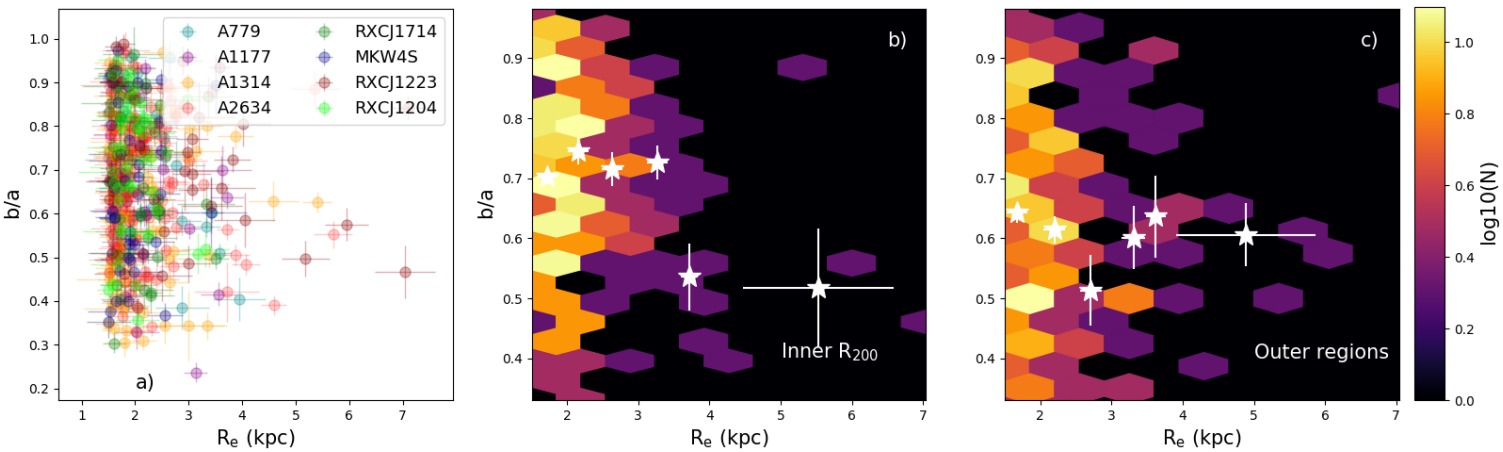

Figure 4.4: Axis ratio vs. effective radius plane for the UDGs found in this work. Panel a) shows the whole sample, panel b) the UDGs in the inner R_{200} and panel c) the UDGs outside R_{200}. The white stars show the median of the binned data and its standard error.

Loeb (2016). Moreover, it could also be a sign of the cluster environment shaping the UDGs, making them more round.

In Figure 4.5 the UDGs in each FOV are plotted separately, to see if the distribution is the same in them, also studying the correlation with the color. In general, they do not have a behavior different than the general trend. Nevertheless, it is interesting to see that some clusters have a tail of large UDGs showing relatively lower axis ratios; as mentioned in Venhola et al. (2017), this UDGs could have a different origin, or at least their large radius be consequence of tidal disruptions. There is not evident correlation with the color, but in next subsection we study this in more detail.

From this scaling relation, we conclude that, while more and better data is desirable to make stronger conclusions, it seems like the UDGs in our clusters agree with the proposition by Amorisco & Loeb (2016) in the sense that the axis ratio distribution of relatively isolated UDGs is flat, and there seems to be a general trend of larger UDGs (which should have larger spin) being less round . The fact that the trend is stronger in the galaxies that lie at a projected clustercentric distance smaller than 1 R_{200} could be an indication that the cluster environment may be playing a role here. Notwithstanding, large UDGs are not very abundant, so increasing the numbers here is necessary to have a statistically robust conclusion.

A natural question that also comes out from this is if those UDGs with low axis ratio but small effective radius had a different formation mechanism, or if they ended-up like

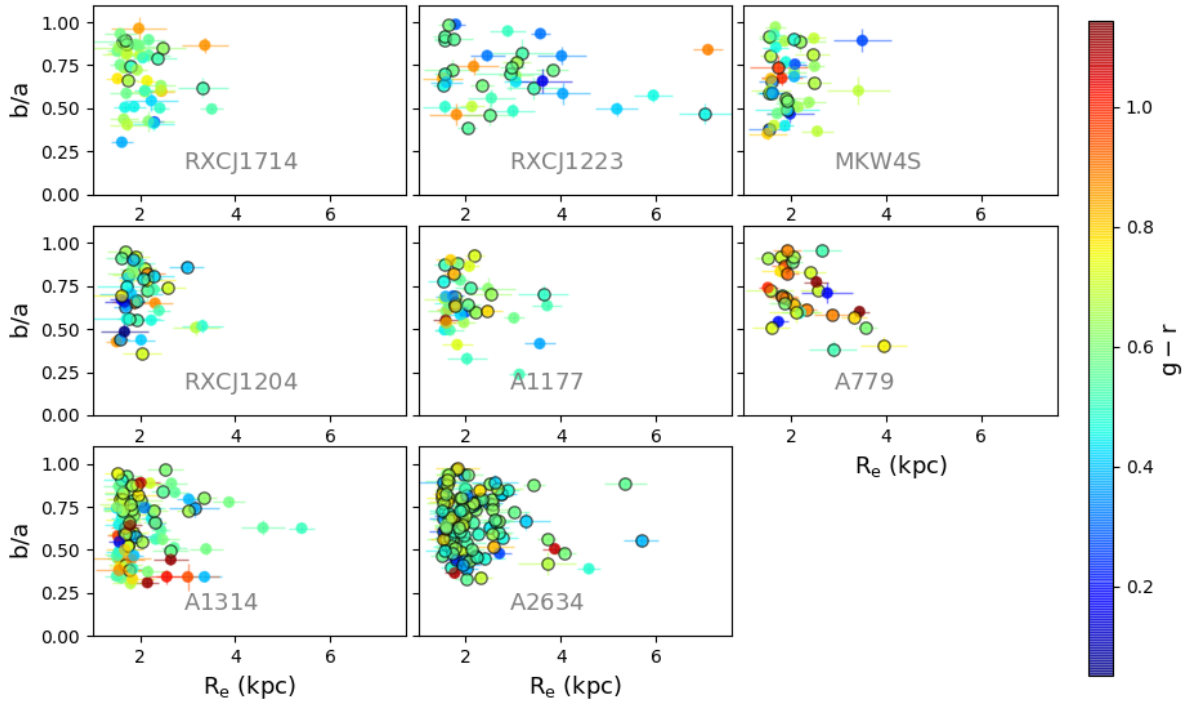

Figure 4.5: Axis ratio vs. effective radius plane for the UDGs in each FOV. The colors indicate the $g-r$ colors of the galaxies, and those UDGs in the inner projected R_{200} are highlighted with a black circle.

they are now due to more cluster interactions.

4.2.1.2 Color vs effective radius

As mentioned by Papastergis et al. (2017), according with the formation scenario proposed by Di Cintio et al. (2017) for isolated UDGs, more extended UDGs should have higher gas content and younger stellar populations. Under the assumption that galaxies with more gas are capable to form more stars, one could expect those more extended UDGs having bluer colors. Of course in a cluster environment galaxies are not expected to be gas rich, because the interactions with the cluster environment (e.g. galaxy harassment, tidal stripping, and ram-pressure striping) would have remove most of their gas quenching their star formation, but it is still interesting to look for signs of that phenomena in our clusters. This is studied in Figure 4.6.

In this case, while a tail is visible, the second and third panel, show that the general behavior of the color distribution is the same for the inner and outer UDGs; as also shown with the medians of the binned data. The mentioned tail of large UDGs ($R_e \geq 4$ kpc)

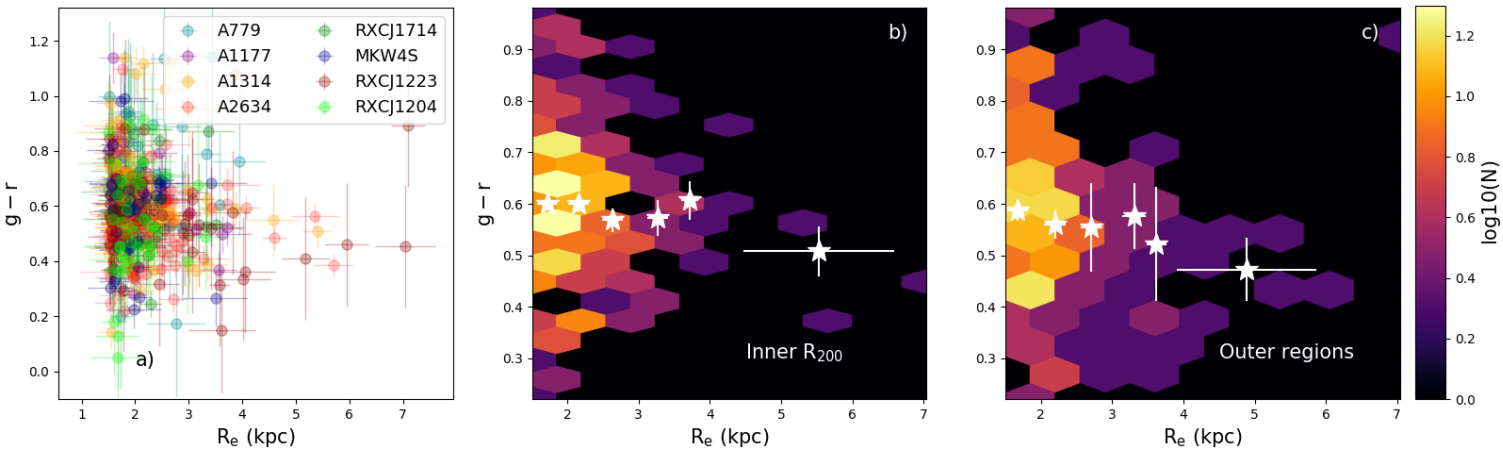

Figure 4.6: Color vs. effective radius plane for the UDGs found in this work. Panel a) shows the whole sample, panel b) the UDGs in the inner R_{200} and panel c) the UDGs outside R_{200}. The white stars show the median of the binned data and its standard error.

having slightly bluer colors ($g-r \sim$ 0.38-0.56, while the bulk of UDGs have $g-r \sim 0.6 \pm 0.12$) is interesting since probably they have considerable younger stellar populations. However on has to be cautious because with that few UDGs with $R_e >$ 3-4 kpc are probably not statistically different than the rest of the distribution.

The fact that the largest galaxies have bluer colors can be explained if one considers that the larger UDGs are probably the most massive ones, that should have a stronger potential and then would have been able to retain a higher gas fraction; they form more stars, and are therefore bluer.

The fact that large and small UDGs have similar colors is very interesting because it means that the large size of some UDGs should be explained by a mechanism other than large UDGs having a more bursty SFH than the smaller UDGs. Consequently, except for the mentioned weak tail, these observations do not favor an evolutionary scenario of UDGs driven by their SFHs (Di Cintio et al. 2017), but do not contradict the idea of the angular momentum of Amorisco & Loeb (2016) or the tidal disruption, as mentioned in Venhola et al. (2017). Figure 4.7 shows the relation for the different clusters, showing the same demeanor.

Overall we warn the reader that these results should be cautiously taken; the color of galaxies is affected by age, metallicity and dust reddening, so an interpretation of this scaling relation is hard to do from a mere photometrical point of view.

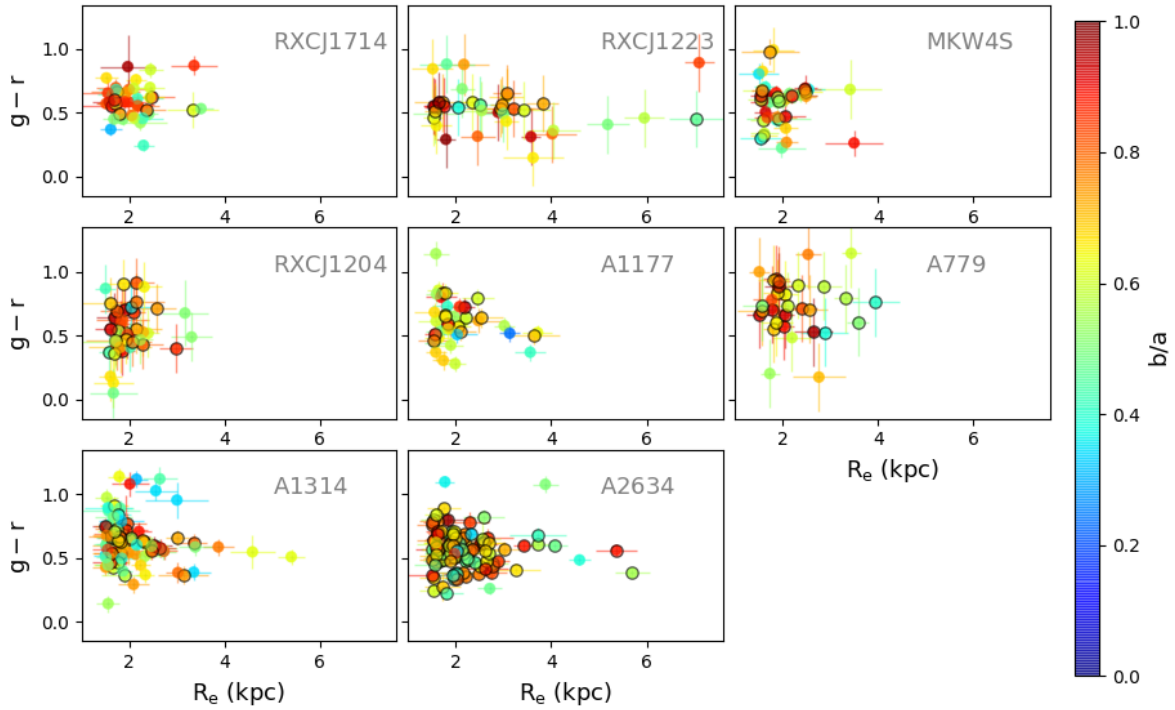

Figure 4.7: Color vs. effective radius plane for the UDGs in each FOV. The colors code the axis ratio of the galaxies, and those UDGs in the inner projected R_{200} are highlighted with a black edge.

4.3 The abundance of UDGs in nearby galaxy clusters

As first noticed by van der Burg et al. (2016), there is a strong correlation between the number of UDGs within R_{200} and the M_{200} of their host clusters. Regardless of the environment (UDGs in clusters or in groups), this relation holds remarkable well (in a logarithmic space), but different slopes have been proposed. Furthermore, observations show (e.g. van der Burg et al. 2016; Venhola et al. 2017) that large UDGs ($R_e \geq 2.5$ kpc) follow a less steeper relation than their smaller counterparts, meaning that they appear to be less abundant towards the most massive clusters.

In the literature, when the relation is shown, people usually just take the number of UDGs reported in each different paper and uses its blindly, regardless the fact that each work uses its own definition of UDG. Moreover, some authors consider the total number of UDGs they found, while others only consider those inside R_{200} as originally proposed. The fact that most of the studies in the literature have more or less the same

depth due to current-day instrumental limitations, that the definitions of UDGs are not the same but similar, and that most of the works use the same software for detecting and characterizing the UDGs, makes the comparison roughly fair; but still the situation is not the ideal because the intrinsic differences in the samples could be affecting the relation . This also makes it hard to study if the scatter in the relation is intrinsic, or it is mainly an artifact due to the different definitions. Because of that, we pay special attention to use a homogeneous sample for studying this relation.

This relation is very interesting because it gives hints about the environment in which UDGs preferably detected (and presumably formed, or at least where they survive the easier; see for instance Román & Trujillo 2017b; van der Burg et al. 2017).

In the first observation of this relation, van der Burg et al. (2016) found that $N \propto M_{200}^{0.96\pm0.16}$; then Román & Trujillo (2017b), extending the relation towards lower masses in the regime of galaxy groups, reported $N \propto M_{200}^{0.85\pm0.05}$. More literature populated the relation, but as mentioned, not in a homogeneous way, and leaving a gap, with few points, between very massive galaxy clusters with $M_{200} \sim 10^{14}$ $M_\odot$ and small groups with $M_{200} \sim 10^{12}$ $M_\odot$.

Recently, van der Burg et al. (2017), attempted to fill the gap in the relation using galaxy groups. They found this time $N(UDG) \propto M_{200}^{1.1\pm0.07}$, suggesting that UDGs are more abundant, per unit halo mass, in clusters than in groups, meaning that either groups destroy their UDGs easier, or that clusters are capable to create UDGs, as opposite as the conclusions from Román & Trujillo (2017b) (although their slopes are still in agreement considering both error-bars). This work also showed for the first time, that several galaxy groups are consistent with having zero UDGs; i.e. when the virial mass of the galaxy group is very low, it cannot host satellite UDGs.

Recently, Amorisco (2018) used the linearity of the relation found by van der Burg et al. (2017) to constrain the mass function of UDGs and estimate the fractions of MW-sized and dwarf-sized UDG' halos. So, the abundance of UDGs is very important in different aspects for studying their formation and evolution.

However, in our opinion there are some discrepancies between the analysis by van der Burg et al. (2017) and the rest of the literature, and one has to be careful before comparing straightforwardly.

The main discrepancies are: i) the sample is not as deep as the rest of the literature, being at least 0.5 mag arcsec^{-2} shallower; ii) colors are not studied, so the result is obtained using only $r-$ band photometry, which increases the chances of including

background galaxies; iii) it goes up to z ~ 0.1, so again this could affect the purity of the sample and the cosmological dimming at that redshift (not considered by the authors) is as high as ~ 0.5 mag arcsec^{-2}; iv) the size-criterion for the selection of potential UDG candidates was done in angular units and the selection is not complete for galaxies at z = 0.01 (although they rely on the assumption that the Universe at z = 0.01 is not very different than the Universe at z = 0.1, which is reasonable); v) they found a median Sérsic index for UDGs in groups of n = 2.2, which seems suspicious since there are very few low-z, highly resolved, UDGs with n > 2 (e.g. Román & Trujillo 2017a,b; van der Burg et al. 2016; Venhola et al. 2017, this work), and this could be a strong bias due to background contamination; and vi) given the fact that the authors found that at M_{200} ~ 10^{12} only 1 out of 10 groups host a UDG, and that they analyzed ~ 320 groups (from the GAMA Survey, with groups being defined by a friends-of-friends algorithm), they built the N-M_{200} relation by binning their groups in bins of mass; which is not something wrong and is statistically interesting, but it is not exactly as in the rest of the literature and might be more prone to errors. About this last point, it is also worth to mention that while not finding UDGs in structures with M_{200} ~ 10^{12} M⊙, is a bit surprising that the authors also found several structures up to M_{200} ~ 5×10^{13} M⊙ without UDGs, in mases where other works have found many UDGs (e.g. Muñoz et al. 2015; Román & Trujillo 2017a, this work).

van der Burg et al. (2017) made careful corrections, sanity and robustness tests to ensure the results are as reliable as possible, but it may be the case where the discrepancies between the above mentioned points and the literature could lead to a non-accurate conclusion. Having said all this, we think the work by van der Burg et al. (2017) represents a big effort of understanding UDGs in low-mass environments, but there are several things that could be improved, and the results should be taken with caution.

Therefore, this work is also relevant because our eight clusters have masses between 10^{13-14} $M_\odot$, and as reviewed in Chapter 3, the depths are as deep as previous works, so they can populate the gap in the literature (we do not have systems with M ~10^{12} $M_\odot$, though), but this time being studied with more consistency and homogeneity. For all the above reasons, the results from this section are some of the most important ones from the thesis.

4.3.1 Background decontamination

Even with the applied cuts in color, we will likely have interlopers, mostly background galaxies, contaminating our sample. This is because even when our color cut selects against red background galaxies, a blue disky galaxy, at a higher redshift than our sample of clusters, could look like a UDG, since it would have an exponential-like light profile, and its redshift reddening would put it at a typical red color of low-redshift red sequence galaxies.

Since taking spectra of all our sources is not feasible, we statistically decontaminate our sample. To do this we observe a control blank field, with the aim of detecting UDG-like objects there, estimate their number density, and infer how many of their counterparts could be classified as UDGs in each of our catalogues. The observed field is the so-called `CaBLANK1`[5] (RA:26.90°, DEC:+02.33°(J2000)), and is observed also at the INT using the same filters (with seeing of 1.76″ and 1.62″ in r and g, respectively) with the same integration times and procedures as the cluster observations, in order to have a fair comparison (and it has a depth, measured at a 3σ level in boxes of 10×10 arcsec, of 28.7 mag arcsec^{-2}). From `SDSS` spectra we check that while being a blank field, `CaBLANK1` has substructures at higher redshifts, in a similar manner as our FOVs, so the approach of the blank field is also realistic in that sense.

We run `SExtractor` to identify the UDG-like galaxies, and analyze them in the same way as the cluster UDGs. The CMD (only sources with `CLASS_STAR` ≤ 0.2) of the blank field is shown in the left panel of Figure 4.8, and the right panel shows the effective radius vs. surface brightness plane.

To estimate the expected number of interlopers, once `GALFIT` has been run over all of them, we take that size-surface brightness plane, corrected by Galactic extinction, and we assume it is at the distance of each of our clusters. Then, we apply the corresponding redshift corrections and we count how many of the objects lie within the selection criteria limits of each cluster, plus setting the same constraints on color and Sérsic index as we did for the clusters sources. Subsequently, we take into account the difference between the areas of the blank field and the areas subtended by each R_{200}, and we finally get the expected number of interlopers within each cluster.

It is also worth to mention that given our UDG selection criteria of rejecting very red or concentrated galaxies, as well as rejecting any fit with residuals showing bar-like structures, we do not expect a strong contamination. This is because a galaxy that has an angular size that corresponds to UDG-like physical sizes at our clusters' redshifts,

[5] see http://www.ing.iac.es/astronomy/instruments/wfc/blanks.html

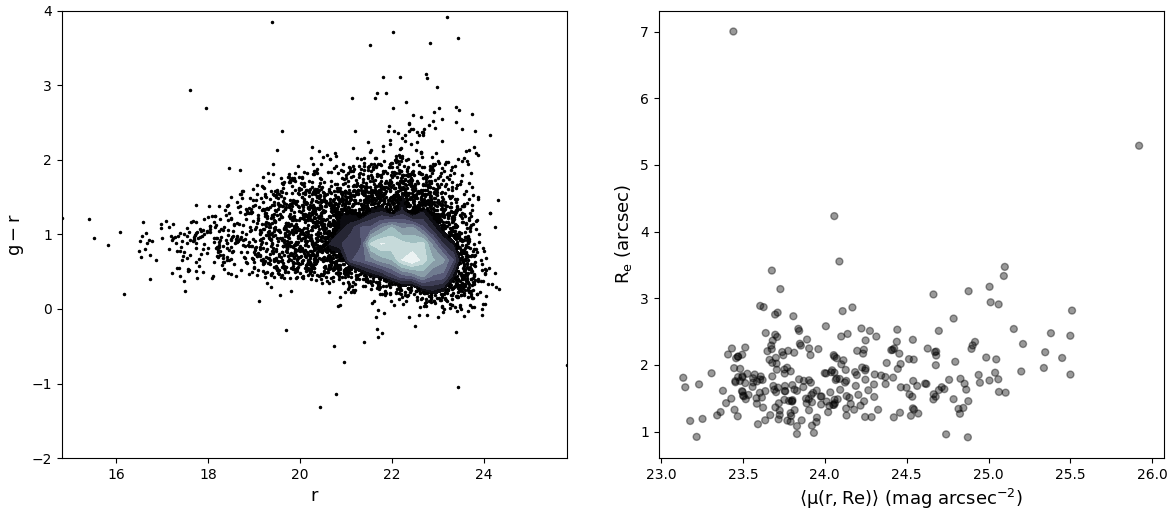

Figure 4.8: CMD and R_e vs. $\langle\mu(r,R_e)\rangle$ plane of our control blank field used to statistically decontaminate our sample.

would need to be very large. For instance, a galaxy with some angular size that at z = 0.02 implies R_e = 1.5 kpc, would need to have a truly size of R_e = 6.83 kpc if at z = 0.1.

4.3.2 The N(UDG)–M_{200} relation

Now we briefly summarize how do we get the "ingredients" to study this relation. First of all, for getting the M_{200} of each cluster, we obtain the value of the velocity dispersion, σ, of each of them, using their redshift distributions (see Chapter 2, Fig. 2.4). Then, for converting it to mass[6], we use the relation given by Munari et al. (2013):

$$\frac{M_{200}}{10^{15}M_{\odot}} = \frac{1}{h(z)} \cdot \left(\frac{\sigma}{1094 \pm 3.7 \text{ km s}^{-1}}\right)^{(0.334\pm0.0014)^{-1}},$$

where the numerical values depend slightly on the physical processes included in the original simulations.

Once M_{200} is determined we derive R_{200} as the radius that encloses M_{200}, assuming spherical symmetry and with a density equals to the critical density of the Universe at the clusters' redshift, $\rho(z)_{crit}$, as follows:

[6]An important caveat that should be mentioned is the difficulty of determining the dynamical mass of a galaxy cluster, and the diversity of the different methods employed to get it (see for instance Old et al. (2014) to a review of methods, problems and uncertainties; or Munari et al. (2013) to see how different implementations of dark matter/baryonic physics can affect the relation between the velocity dispersion and the mass).

Table 4.2: σ-derived M_{200} and R_{200} (see text for details) for each cluster. The third column gives the number of UDGs within R_{200} and the fourth one the number after the background subtraction. The fifth and sixth column are as the fourth and fifth one, but considering only UDGs with circularized effective radius larger than 1.5 kpc.

Cluster	M_{200}	R_{200}	N(UDGs)		N(UDGs,$R_{e,c}$)	
	($10^{13}M_\odot$)	(kpc)	Raw	BS	Raw	BS
A779	4.02	701	24	22	21	20
A1177	3.82	688	14	9	9	8
A1314	7.62	866	36	27	19	(6
A2634	26.60	1314	112	94	60	55
RXCJ1714	0.58	368	8	7	7	7
MKW4S	2.31	583	14	11	5	5
RXCJ1223	1.98	554	17	15	11	11
RXCJ1204	2.88	629	22	21	15	14

$$R_{200} = \left(\frac{3M_{200}}{4\pi\Delta_c\rho(z)_{crit}}\right)^{1/3},$$

but $\rho(z)_{crit} = 3H^2(z)/8\pi G$, thus:

$$R_{200} = \left(\frac{2M_{200}G}{\Delta_c H^2(z)}\right)^{1/3},$$

where by definition we use a density contrast Δ_c = 200. Since the uncertainties in the mass determination are dominated by the errors in the velocity dispersion, we use a conservative approach of assuming an error in the estimated velocity dispersions of ± 20%, and then deriving the upper and lower limits for M_{200} by propagating this error.

All this allows us to get the M_{200} for the x-axis of the relation, and the R_{200} to count the number of UDGs within it. Table 4.2 gives the derived M_{200} and R_{200} for each cluster.

As N we consider the number of UDGs within each R_{200} after subtracting our statistical background decontamination (this is, the total number of UDGs within R_{200} minus the expected number of background sources in the area subtended by R_{200}). These numbers can be found also in Table 4.2.

Using only our data, we plot in Figure 4.9 the N(UDGs)–M_{200} relation. We fit the points using a Orthogonal Distance Regression (ODR) routine that takes into account the x-

and y-errors, so it is more trustworthy that a normal linear regression. We find a slope slightly shallower than 1, with N(UDGs) $\propto$ $M_{200}^{0.81\pm0.17}$. The ODR fit finds a slope steeper than a linear regression (N(UDGs) $\propto$ $M_{200}^{0.66\pm0.13}$), and for illustration we also show this fit (thin line) in Figure 4.9.

The slope found here is lees steep that the slope by van der Burg et al. (2016) (0.93 $\pm$ 0.16), but still in agreement considering both uncertainties; and the same for Román & Trujillo (2017b). It is in tension with van der Burg et al. (2017), notwithstanding (note however that the slopes in the mentioned works are not determined for exactly the same definition of galaxies). What we can also see from there is that there is some intrinsic scatter in the relation even for UDGs with the same definition, and curiously the uncertainty in the slope is basically the same as in van der Burg et al. (2016), so it seems as if at high and intermediate masses the relation has an intrinsic scatter of that order of magnitude, or that that is the scatter introduced by our similar methodologies. The plan, however is to study a broader range in mass; and therefore this plot is illustrative but not the final version we are mainly interested it.

To study the relation in a larger mass range for the reasons above discussed, we complement our sample with the eight clusters studied in van der Burg et al. (2016), and the 3 groups from Román & Trujillo (2017a), both datasets kindly provided by the respective authors, to whom we are thankful. Since these two works together with ours, fill well 3 orders of magnitude in mass, are at nearby redshifts, and are complete under the same definition of UDG (see below), we do not add more clusters to our analysis. Most of the works on UDGs in the literature focus in studying one system, so apart from van der Burg et al. (2016) and this work, there are not studies of large samples of UDGs in clusters studied exactly in the same way. Particularly interesting would be to include the high-mass clusters by Lee et al. (2017), but they are at higher redshifts (so we could not decontaminate in the same way as we do below), and the final number of UDGs reported there is an estimation based on assumptions and corrections and not directly measured; so we prefer to not using them for the sake of congruity. To ensure that our analysis is homogeneous for the datasets studied (and we saw in Chapter 3 that the three studies have basically the same depth), we do as follows:

Regarding van der Burg's data they used the same criteria in surface brightness as we did, but opted for using a circularized effective radius when setting the size criteria. Apart from that, these authors followed the same strategy of detecting UDGs with `SExtractor` and fitting them with `GALFIT`, but they constrained the Sérsic index to be between 0.5

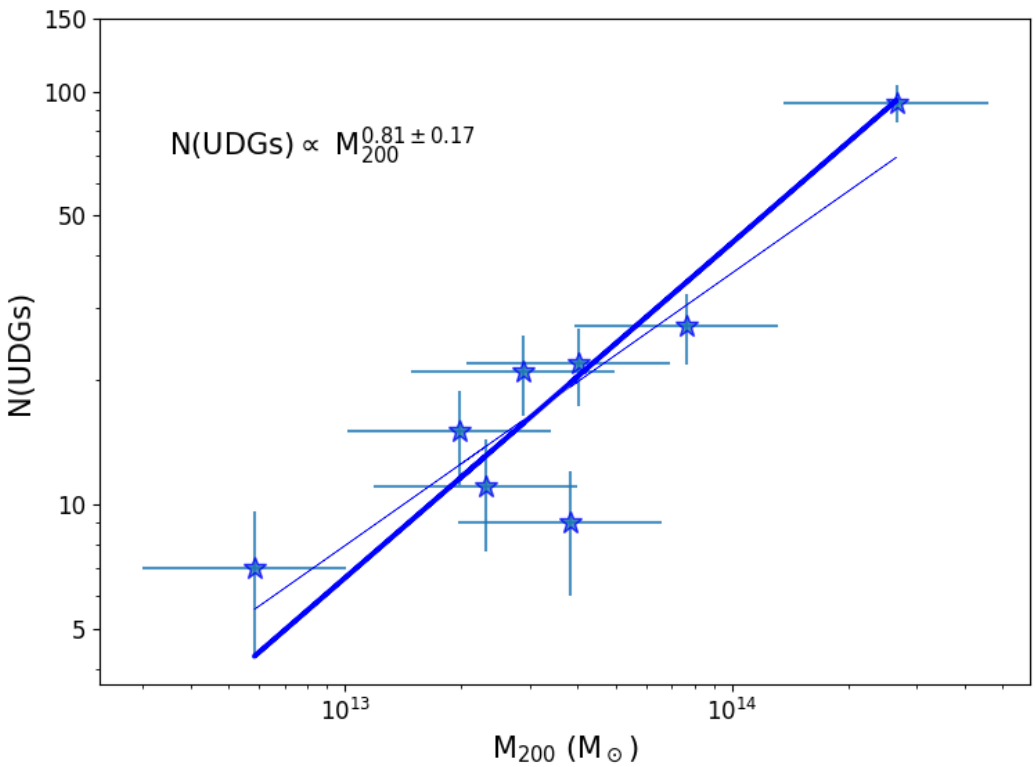

Figure 4.9: Abundance of UDGs in our intermediate-mass clusters. The think blue line shows the best fit of the ODR routine. The thin line is the best fit from a simple linear regression, just shown with illustration purposes. See the text for details.

and 8, while in our models it is totally free. The original MegaCam magnitudes are converted to SDSS magnitudes[7] and we apply K- and cosmological dimming corrections as described in Chapter 3. From their whole dataset, we select the galaxies with -1 $\leq g-r \leq 1.2$ and axis ratio ≥ 0.1, and finally we keep those within 1 R_{200} of each cluster. We decide to using the cluster dynamical masses and radius reported by the authors.

About the UDGs in the groups by Román & Trujillo (2017b), the authors selected all the LSB in the groups with $\mu(g,0) \geq 23.5$ mag arcsec^{-2} and $R_e > 1.3$ kpc. Assuming a color $g-r = 0.6$ and a Sérsic profile n=1, this corresponds to $\langle\mu(r,R_e)\rangle \geq 24.03$ mag arcsec^{-2}. Therefore we assume that this sample (its selection criteria) is also complete under our UDG definition. We then take the parameters from the Sérsic fit ($r-$ band derived), and characterize the UDGs applying also K-corrections and surface brightness dimming. Regarding the M_{200} and R_{200}, we take the values of the velocity dispersion of the three groups (Tovmassian et al. 2006), taking the mean of the cluster and cluster+environment

[7]Using the relations given in http://www1.cadc-ccda.hia-iha.nrc-cnrc.gc.ca/community/CFHTLS-SG/docs/extra/filters.html

velocity dispersion (assuming again an error of 20%), and we use again the relation by Munari et al. (2013). Of the 11 galaxies studied in Román & Trujillo (2017b), 4 fulfill the criteria of having $\langle\mu(r,R_e)\rangle \geq 24$ mag arcsec^{-2}, circularized effective radius $R_{e,c} \geq 1.5$ kpc and a projected clustercentric distance (dproj) < 1 R_{200}; so we include them for our analysis.

Regarding our own data, we circularize all our effective radii and keep those with $R_{e,c} \geq 1.5$ kpc. Since we originally use the effective radius as the radius containing 50% of the galaxy luminosity, along the semi-major axis, it means that our selection criteria selects a wider sample than van der Burg et al. (2016); and the sizes of their sample around 1.5 kpc would be slightly systematically larger[8]. Because our original sample is less restrictive, we can circularize our effective radius being still complete. The last two columns of Table 4.2 give the number of UDGs within R_{200} with $R_{e,c} \geq 1.5$ kpc, and in parenthesis the expected number once the background subtraction is done. This time, we decontaminate with the same routine, but using only the galaxies in our blank field (Figure 4.8) with $R_{e,c} \geq 1.5$ kpc. For the rest of this thesis, whenever we are comparing with the UDGs by van der Burg et al. (2016) and Román & Trujillo (2017b), we are using our data considering circularized effective radii.

To statistically decontaminate the sample of van der Burg et al. (2016), we use our same blank field, using exactly the same strategy as we did with our own data, looking at the number of objects that would have been classified as field-UDGs at the redshift of each cluster. While this is not a perfect procedure, we assume it is a valid approach since our blank field is complete for a background decontamination up to redshift 0.07 (given the size of the galaxies that we analyzed with `GALFIT`, and the furthermost cluster of that sample lies at z = 0.063); and its depth is similar to van der Burg's data.

In the case of the UDGs in Román & Trujillo (2017b), the authors did a very complete search of possible interlopers, but did not find any other LSB galaxy except for those reported in their paper. Additionally, their galaxies have 2 colors ($g-r$ and $r-i$), and they have both colors consistent with colors of spectroscopically confirmed members. Furthermore, the groups are nearby (z = 0.0141–0.0266, by itself this implies that not many interlopers would be expected) Hickson Compact Groups (HCGs, Hickson 1982) that by definition are isolated structures, and the galaxies are at relatively small projected distances of the center of the groups. Finally, the association of several blue galaxies in

[8]For instance, a galaxy with semi-major axis = 1.5 kpc and axis ratio = 0.9 would be selected with our criteria, but the circularized effective radius is 1.42, so it would have not been selected by van der Burg et al. (2016).

Román & Trujillo (2017b) with their HCG has been confirmed by spectroscopic observations (Spekkens & Karunakaran 2018). Based on all this, we decide not to apply extra background decontamination to this dataset.

With all these steps, we can say that this is the best comparison in terms of homogeneity done so far in studying the abundance of UDGs. The result of our analysis is plotted in Figure 4.10. Under this homogeneous analysis, we firstly find $N \propto M_{200}^{0.73\pm0.04}$. Nevertheless, according to van der Burg et al. (2017) most groups with $M \sim 10^{12}$ $M_{\odot}$ could be hosting no UDGs, and in that case the groups of Román & Trujillo (2017b) would not be fully representative; and therefore be biasing the sample. Because of that, we also fitted our data without considering the two groups with lowest mass, and we find $N \propto M_{200}^{0.82\pm0.07}$ (statistically equal to the relation considering the lowest-mass groups). This is the slope that we adopt as the final, and as can be seen is well beyond 1. It is perfectly in agreement with the slope reported here before (Figure 4.9); in Román & Trujillo (2017b), as well as very similar to the estimation by Lee et al. (2017), and also consistent with van der Burg et al. (2016) considering their relatively large error-bars; but it is not consistent with the slope by van der Burg et al. (2017). And overall, we remind the reader that this is the first work that uses a homogeneous analysis to study the relation along all the range in mass available until today.

As discussed by Román & Trujillo (2017b), a slope smaller than 1 disfavors the idea of UDGs being preferably formed in very massive clusters (van der Burg et al. 2017); and it has two main interpretations: either that UDGs preferably form in low-mass systems, or that they are more easily destroyed in high-mass systems. In principle without more information one cannot distinguish between both scenarios (but see next Chapter), but we can conclude that the slope in the relation is shallower than 1 and UDGs are more abundant, per unit host cluster mass, in low-mass systems. There is, however, the possibility that the solution to this observation is not as simple.

Amorisco (2018) explains that a linear regression is a consequence of two conditions: i) the mechanism shaping the properties of UDGs is independent of their environment and ii) most of the UDGs have low-mass halos; so presumably at least one of these two conditions is not fulfilled.

So, apart from UDGs being formed/destroyed in groups/clusters, it could also be that, assuming the halo mass function is approximately universal (Jenkins et al. 2001), the subhalo mass distribution of UDGs is different for host clusters of different mass. This

could be explained, for instance, considering that in different environments the stellar component of the DM halos develops different; therefore a subhalo that in one cluster could host a UDG, in another cluster could be hosting another galaxy that does not accomplish the definition of UDG. A more detailed analysis is still needed and of big interest. It would be very interesting to see if the whole analysis by Amorisco (2018) changes considering this slope.

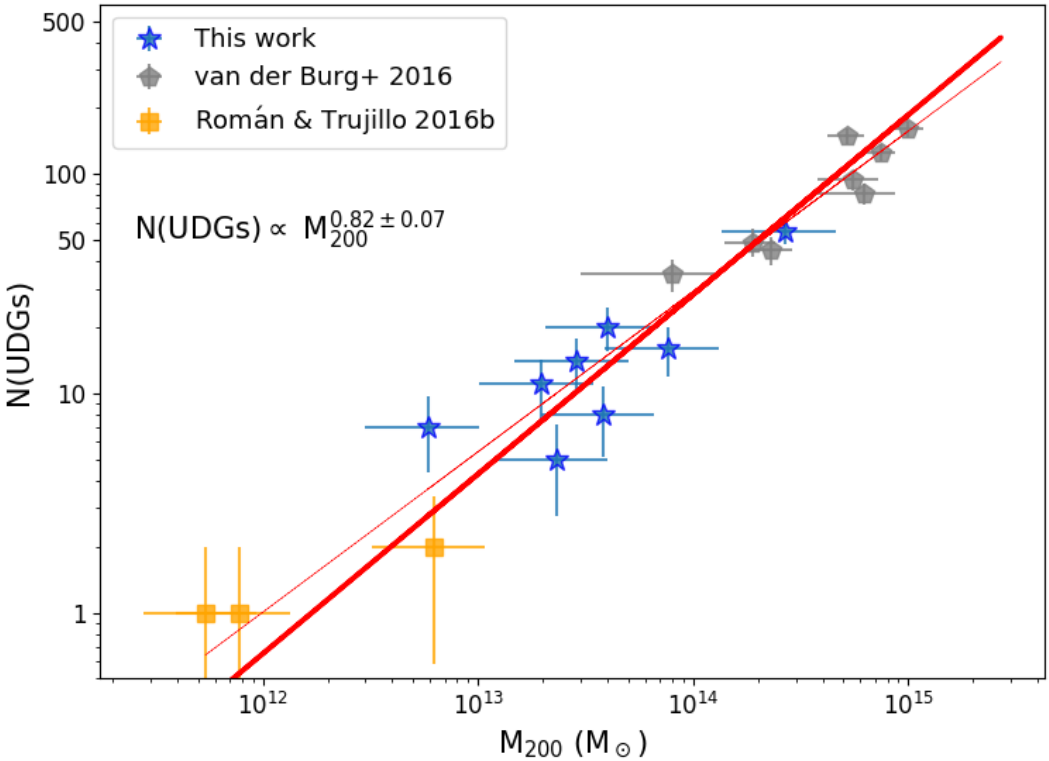

Figure 4.10: Abundance of UDGs in different nearby galaxy clusters, under a homogeneous analysis. The thin red line shows the preliminary fit considering the 19 points, while the think line corresponds to our final relation, without considering the two lowest-mass groups. See the text for more details.

Figure 4.11 shows the mass density (number per unit cluster mass) of the UDGs. As expected from the slope of the abundance as a function of M_{200}, it can be graphically seen that UDGs are more abundant, per unit cluster mass, in groups than in clusters. For this figure we repeat the routine of fitting with and without the two lowest-mass groups.

To complement this, we also study the abundance of UDGs per unit volume, using each R_{200} and assuming spherical symmetry. This is plotted in Figure 4.12. The relation is not very tight and looks noisy, but in general it seems to be a shallow progression

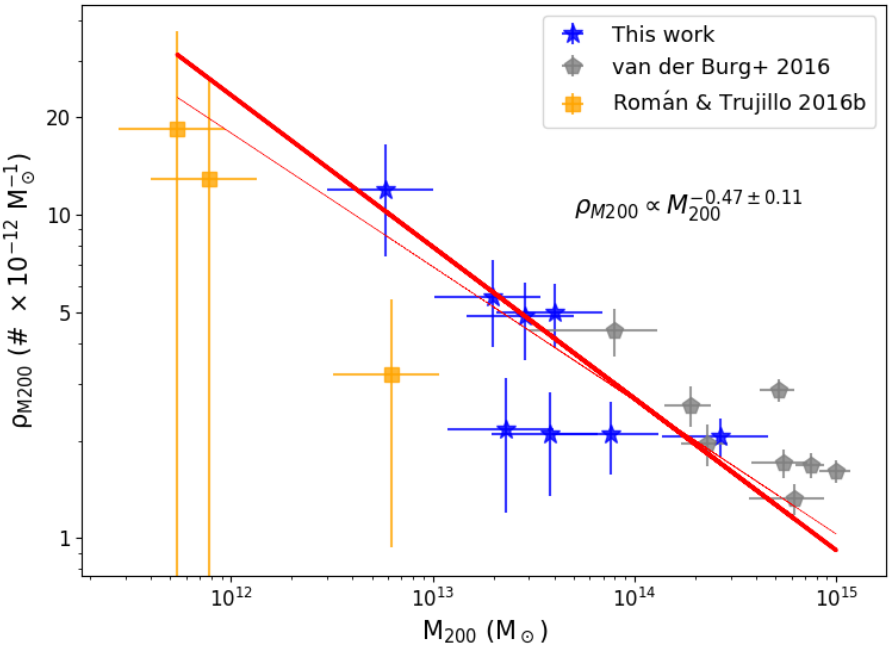

Figure 4.11: Abundance of UDGs per unit host cluster mass. Symbols are as in Figure 4.10.

of this volume density increasing with the mass: staying very linear between, roughly, 10^{12-14} $M_\odot$, and increasing afterwards. Nevertheless, there are groups (e.g. HCG25) with a volume density as high as the 10^{15} $M_\odot$ clusters.

Finally, as some papers have done (e.g. van der Burg et al. 2016; Venhola et al. 2017), we study the N-M_{200} relation but this time distinguishing those UDGs with $R_{e,c} \geq 2.5$ kpc. As we saw (Figure 4.1 and Table 4.1), small UDGs dominate the number of UDGs in clusters, and large ones are not that common. For instance, in MKW4S no larger UDGs than $R_{e,c}$ = 2.5 kpc were detected, neither in the groups by Román & Trujillo (2017b) (but in this last case this could be driven by small number statistics rather than by physical reasons). As shown in Figure 4.13[9], large UDGs follow a shallower relation than the whole population of UDGs, qualitatively in agreement with the previous literature. The slope of the large UDGs is actually very similar as the determined by van der Burg et al. (2016), being 0.59 ± 0.09 for us, and 0.63 ± 0.21 for them.

If large UDGs follow a different relation than small UDGs, this could be an indication that the environment may be important for them. However, while the relations here

[9]For this figure we perform again the same background decontamination but now considering only galaxies with $R_{e,c} \geq 2.5$ kpc.

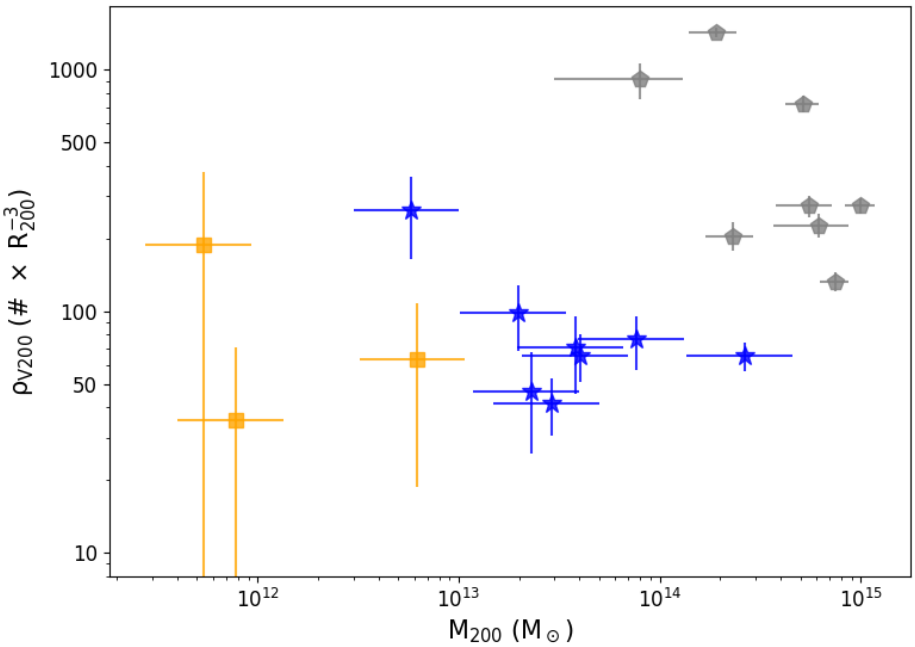

Figure 4.12: Abundance of UDGs per unit host cluster volume. Symbols as in previous figures.

derived for all the UDGs and for the large ones, are statistically different, the difference is marginal if one considers both error-bars at their maximum amplitude.

Under the same context than Figure 4.10, the shallower slope of large UDGs compared with all the UDGs, could be interpreted as large UDGs being even more deficient in high-mass systems. This again can have two interpretations, either that large UDGs get destroyed easier in high-mass systems, or that they preferably form in low-mass systems. While we do not have evidence against the former idea, the second one is also theoretically motivated since low-mass systems experience stronger galaxy-galaxy interactions, than could lead to tidal disruptions, and finally to larger UDGs.

So, while we have (marginal) evidence of differences between the larger UDGs and the bulk of the population, supported also by theory of galaxy interactions, more data is needed to establish in a more conclusive way whether or not the large UDGs behave differently from the others; and the fact that few statistics could dominate the low-mass end of the relation should be taken into account. In next Chapter we will delve more into studying the effects that the environment may have on the UDGs.

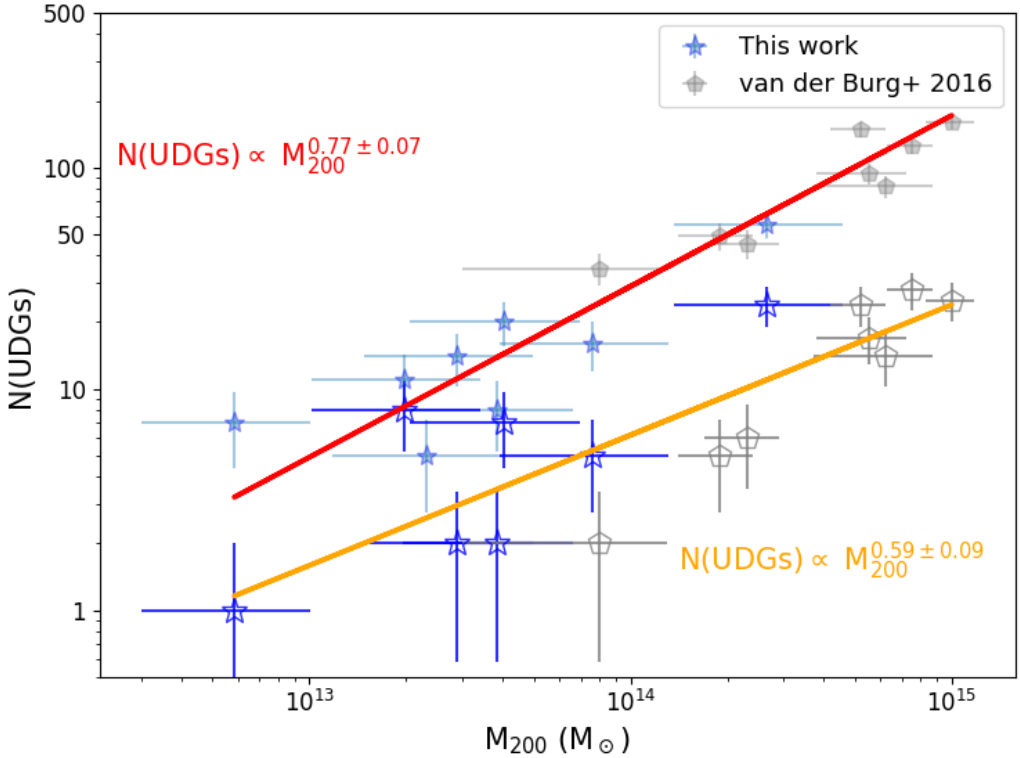

Figure 4.13: Abundance of large UDGs compared with the whole population of UDGs. Open symbols denote the UDGs with $R_{e,c} \geq 2.5$ kpc.

CHAPTER 5

THE EFFECT OF THE ENVIRONMENT ON UDGS

In this Chapter we study the spatial location of UDGs within clusters, as well as the structural parameters as a function of the local (projected clustercentric distance) and the global (cluster mass) environment with the ultimate goal of understanding more about their evolution. For UDG we mean our original definition of $R_e \geq 1.5$ kpc and $\langle \mu(r, R_e) \rangle \geq 24$ mag arcsec^{-2}, unless comparing with other data, where we use $R_{e,c} \geq 1.5$ kpc.

5.1 Spatial distribution

Our observations of the FOV of each cluster cover different areas, but for all of them we cover the area up to 1 R_{200}, so this allows us to study the spatial distribution of UDGs being complete at least in the inner R_{200}.

We plot in Figure 5.1 the spatial distribution the UDGs in the FOVs and within the clusters. Lee et al. (2017) claim that their UDGs are located in a less homogeneous way than the bright galaxies, which could be a sign of UDGs being recent accretions. However, in our opinion, this is barely visible, if visible at all, in their data. In the same way, our Figure 5.1 shows that UDGs (blue stars) are well mixed with galaxies at the clusters redshifts (red stars), finding no evidence of what Lee et al. (2017) reported.

Yagi et al. (2016), studying UDGs in Coma, reported that UDGs in the cluster tend to have their major axis aligned towards the cluster of the center. However, such behavior

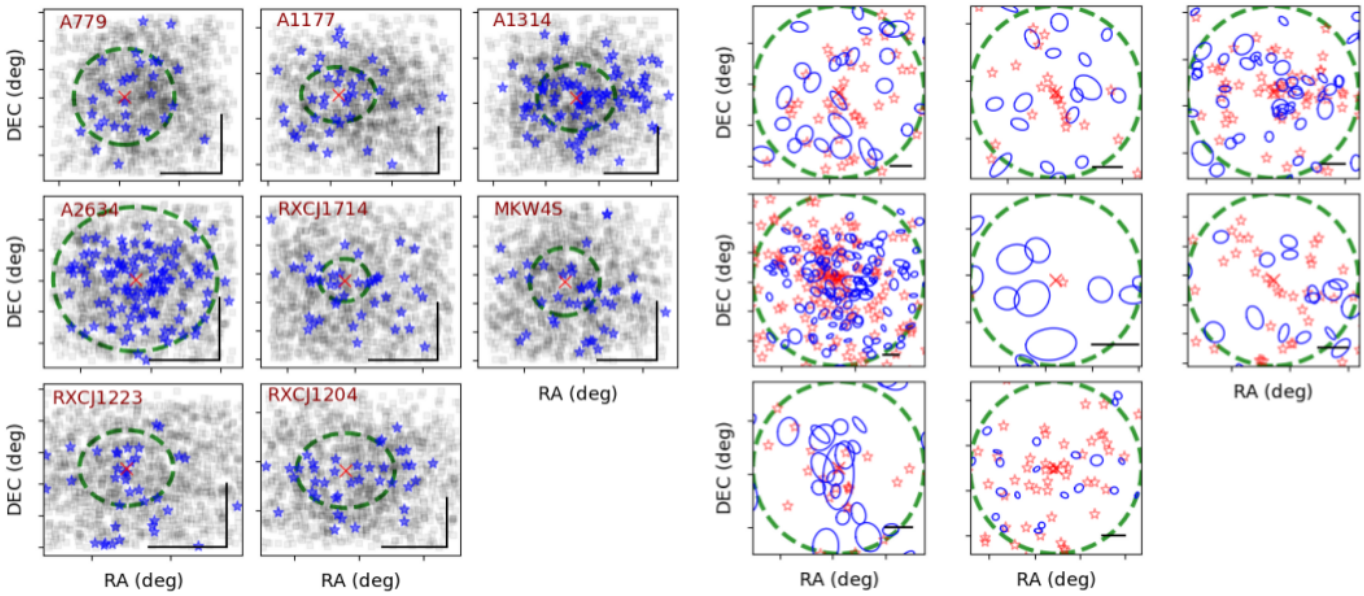

Figure 5.1: Spatial distribution of the UDGs in our sample. The X-ray center is indicated with a red cross, and UDGs with blue stars, while the green circles indicate the projected R_{200}. *Left panel*: our FOVs (demarcated by the gray area) and the UDGs within it; the R_{200} are circular (see right panel), but they look elliptical for the way the figure is plotted. For reference, the black lines indicate the scale of 0.5 deg in RA and DEC. *Right panel*: the inner R_{200} of the clusters; UDGs (blue ellipses) are shown here with their measured position angle and axis ratio, and effective radius have been arbitrarily scaled, but they keep the relative sizes between them. The black scales measure 0.1 deg.

has not been reported in the center of any other cluster, or at least not as clear as Yagi et al. (2016) claim it is in Coma (see for instance Venhola et al. 2017). To study this we now focus on the right hand side of Figure 5.1, where we plot the UDGs in each cluster, showing a representation of their size, axis ratio and position angle. Nevertheless there are also not systematic galaxy alignments visible.

5.1.1 Radial surface density

To describe in more detail the spatial distribution of UDGs, we study the radial surface density profile that they follow within their host clusters. van der Burg et al. (2016) (see their Fig. 8) also studied this in a very careful way, deriving the surface density and applying two corrections to the observed profile: i) background decontamination and ii) radial completeness (that decreases with decreasing projected distance). They found that the surface density increases steeply in the outer parts of the profile, but becomes flat

and decreases in the inner bins.

To compare our results with those in the literature, we also calculate the surface density of our data by counting the number of UDGs within radial bins divided by the area subtended by each radial bin. Since we want to compare with the mentioned authors, we work with the galaxies with $R_{e,c} \geq 1.5$ kpc.

The derived observed surface density is shown (light curve) in the top right panel of Figure 5.2. This is a "raw" profile because it has not been decontaminated, so the next step is decontaminated it. For doing this, we take the individual profiles, and we estimate the expected surface density of background UDGs for each cluster (in #/deg^2) using our blank field, and we subtract the expected contribution of this background in each bin. We do not apply radial completeness corrections: our clusters are not ass massive as the van der Burg ones, and most of them are not strongly dominated by a bright cluster galaxy that could be hiding several UDGs, so for our clusters this correction is less relevant and we do not take it into account (see also the points from Venhola et al. 2017). Then, by stacking the individual decontaminated cluster profiles (bottom right panel of the same figure) we build-up the general profile of our sample.

Figure 5.2 shows this decontaminated total profile (dark curve, top panels). The error-bars come from considering both the errors in the surface density plus the errors associated with the background subtraction; both Poissonian. For comparison, we also show the equivalent plots from van der Burg's data, derived in the same way as ours (so they slightly differ from the profile used in van der Burg et al. 2016 because the background subtraction is different and also since the completeness corrections were not applied).

As can be seen from the figure, both datasets have a similar behavior, with van der Burg's data having a few UDGs at closer projected distances than ours, something that we will review in the next Section. The exact shapes of the curves are of course dependent on the size and distribution of the bins, but overall both datasets are in good agreement. Also the individual profiles have similarities (although of course our clusters are less massive and with less UDGs) with some clusters showing a peak in the inner bins, and others having a core.

Of course just by stacking the data we (and van der Burg et al. 2016) are biasing the profile in favor of the individual cluster profiles with more UDGs. However we keep this approach because weighting the data (in such a way that all clusters contribute the same) introduces even more uncertainty in the inner regions of the clusters with few UDGs. As a sanity check we also build the median-combined general profiles of both

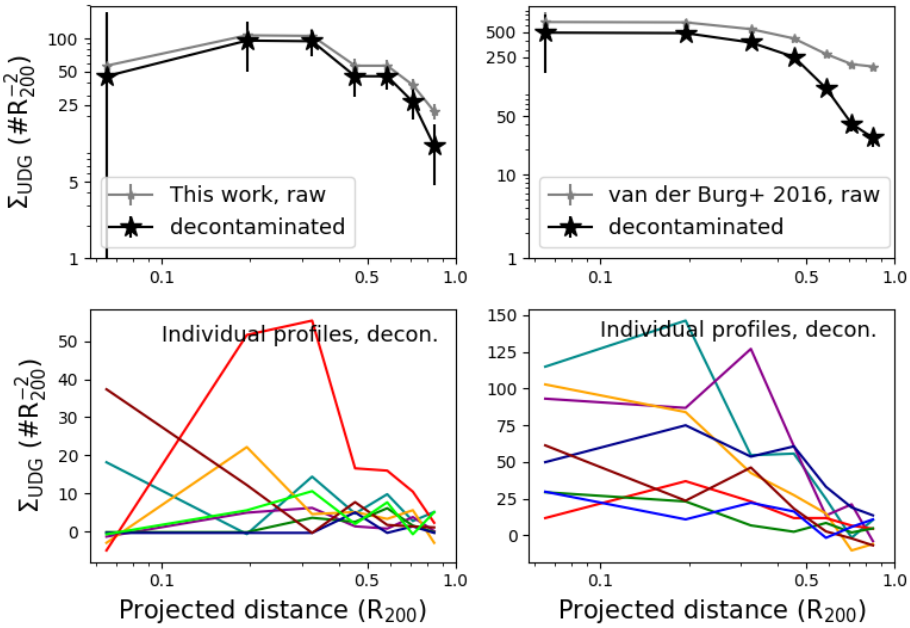

Figure 5.2: Radial surface density profile of UDGs. The left-hand side panels show our data, while the right-hand side ones shows the data from van der Burg et al. (2016). Top panels show in light and dark the raw and decontaminated profiles, respectively. Bottom panels show the individual decontaminated profile for each of the clusters. Stacking these decontaminated profiles we build the general radial surface density profile, shown in dark in the top panels. For the bottom right panel, the color of the individual clusters are as in Figure 4.6.

datasets (where every cluster is given the same weight), and realize that, while more noisy, they follow the same general trend as the stacked general profiles.

Therefore, from here we conclude that the behavior of the radial surface density profile in our clusters is qualitatively in agreement with van der Burg et al. (2016). Regarding the individual profiles, independently on their mass, some clusters have a peak in the inner regions, and some of them a core. However, the general profile rises steeply around 1 R_{200} towards the inner parts, becoming flat or developing a shallow core in the inner bins. Our analysis does not correct for radial completeness as van der Burg et al. (2016), but, as mentioned, our results are consistent with them; confirming that the distribution of UDGs in clusters is not random but follow a radial surface density profile as shown in Figure 5.2. The main difference we appreciate is that the more massive clusters have more UDGs in the very inner regions, something that we investigate in more detail below.

5.1.2 The absence of UDGs in the center of clusters

As mentioned in the Introduction, several works reported a depletion of the number of UDGs in the inner regions of clusters (e.g. van Dokkum et al. 2015a; van der Burg et al. 2016; Wittmann et al. 2017; Merritt et al. 2016; Venhola et al. 2017). This is also consistent with the radial surface density profiles derived above.

This lack of UDGs is believed to be because UDGs are not able to survive the strong disruption forces in the dense center of the potential well, unless they are very big (e.g. Penny et al. 2010); rather than this being an apparent effect due to blending and light excess near the cluster center avoiding the detection of UDGs (see discussion in Venhola et al. 2017); that however might be playing some role (van der Burg et al. 2016; Lee et al. 2017).

To analyze this phenomena in a homogeneous set, we study, for the first time (as far as we know), the relation between the nearest UDG to the center of its host cluster and the mass of the cluster (again, considering UDGs with $R_{e,c} \geq 1.5$ kpc).

The first thing we do is plotting the projected distance from the center of each system to the nearest UDG, for our data and van der Burg's data[1]. The result of this is shown in Figure 5.3. As starking visible, it seems to be a very clear correlation with high-mass clusters having their nearest UDG closer than less massive systems.

A first conclusion that could be drawn is that somehow low-mass clusters destroy the UDGs near the center (for instance via galaxy-galaxy interactions that are more efficient than in high-mass clusters) in a more efficient way than high-mass clusters. However, this could be also only a statistical effect: more massive clusters have more UDGs; so just because of that the chances of finding a UDG near the center (and at any position) is higher than for low mass systems. To test this idea, we perform simulations where we take clusters with different values of M_{200}, and we inject the expected number of UDGs according with the N-M_{200} relation (Figure 4.10), in totally random positions; and we then find the distance to the closest UDG. We repeat this a few hundreds of thousands of times, and we take the mean of the distance to this closest UDG, for each cluster.

As we see in Figure 5.3, the ODR fit to the points generated with the totally random positions, is not very different (although it deviates more towards high-masses). Nevertheless, the slope of the empirical relation between the projected distance to nearest UDG (d_{first}) is $d_{first} \propto M_{200}^{-0.56\pm0.11}$, while the fit for the totally random positions is $d_{first} \propto$

[1]We do not include the groups by Román & Trujillo (2017b) since they have very few UDGs that could be not statistically representative.

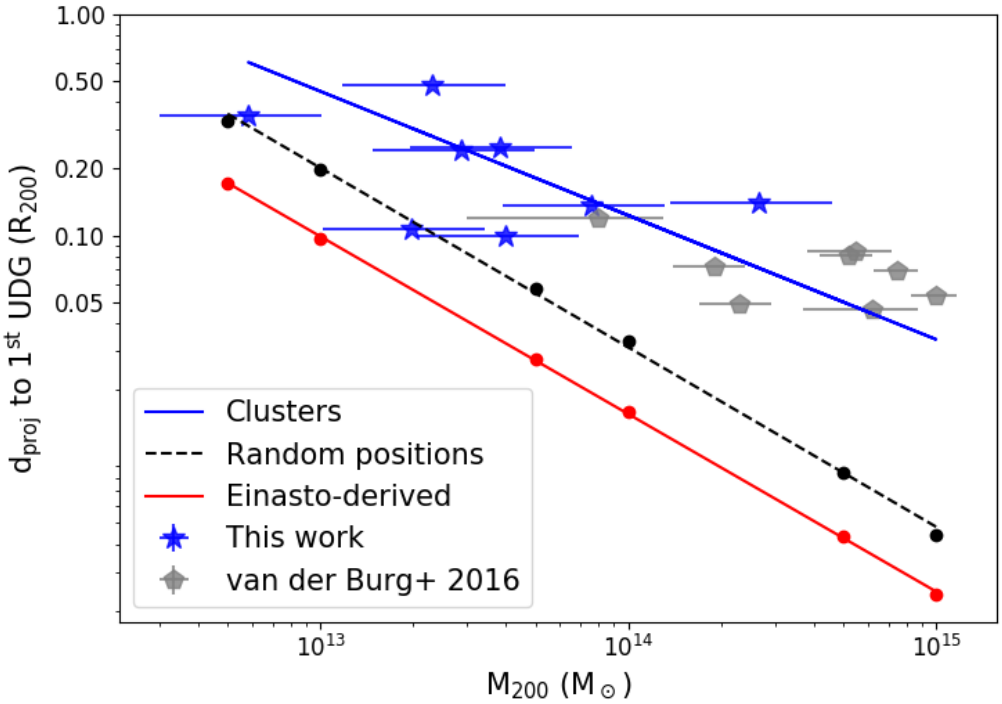

Figure 5.3: Distance to the innermost UDG in each cluster, as a function of the cluster M_{200}. The fit to the observed points (blue stars and gray pentagons) is shown with a blue line. The fit to random points is indicated with the dashed blank line. The red line is the fit to the Einasto-derived points. See the text for details.

$M_{200}^{-0.81\pm0.02}$; so they are actually statistically different.

Notwithstanding, we previously concluded that the spatial distribution of UDGs is not random, but follows a general surface density profile, so it would be more accurate to do the same kind of simulations, but using the surface density profile. For this we do as follows:

In van der Burg et al. (2016), the authors characterized their radial profile with an Einasto profile:

$$\Sigma(r) = A \exp\left\{\left(\frac{-r}{r_0}\right)^{\alpha}\right\},$$

with A, r_0 and α three free parameters to be fitted. Following them, we also fit an Einasto profile. Both datasets are well fitted with profiles that are equivalent (after normalizing) within the uncertainties; so we combine both to make a single general surface density profile. Figure 5.4 shows the individual and general profiles.

The best parameters for the final Einasto fit are $c = 1.15 \pm 0.03$, $r_0 = 0.53 \pm 0.002$, and $\alpha = 2.04 \pm 0.13$; and as can be seen they fit the data reasonable well. The general

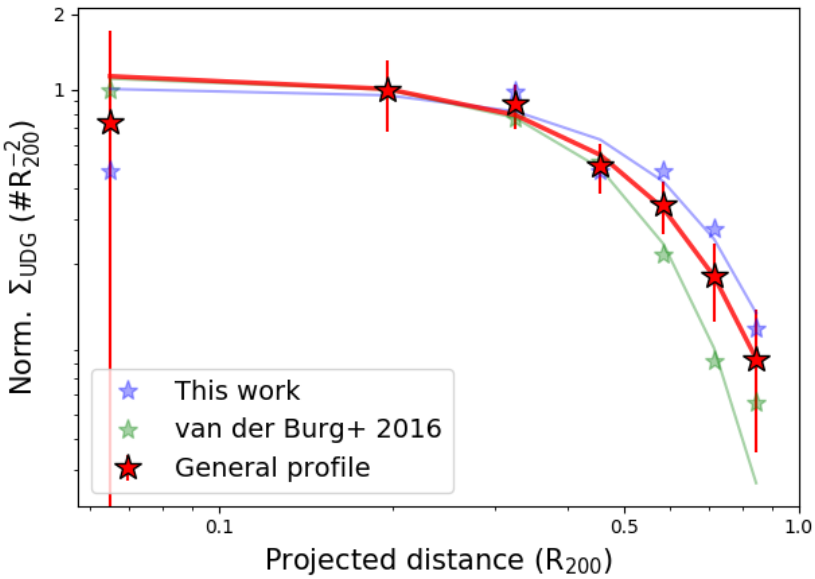

Figure 5.4: Einasto fit to the surface density profile. The blue stars show the points derived from our data, and the blue line is the corresponding Einasto profile. Green stars and line indicate the same, but are derived from the dataset of van der Burg et al. (2016). The red stars show the general (combined) profile, and the red thick line the final derived Einasto fit.

fit (red symbols in Figure 5.4) starts (at large R_{200}) in between the individual profiles; and in the inner bin it resembles more the fit to van der Burg's data, once the errors have been taken into account (otherwise the fit becomes slightly flatter). To explore if the profile is better fit by another function, we also try with a beta function, but the fit is basically exactly the same, so we keep the Einasto fit for consistency with the literature.

Once we have the profile to describe the distribution of UDGs, we convert the profile to a probability function, in such a way that we are now able to generate random positions that follow the radial surface density profile. We incorporate this to our simulations, and we do the same, running the simulation a few hundreds of thousands of times and taking the mean of all the runs. The fit to the generated (red) points is the red line in Figure 5.3.

It is immediately obvious that these points and fit deviate more from the observed points. The slope found for this Einasto profile- generated relation is $d_{first} \propto M_{200}^{-0.80\pm0.01}$, not very different than the totally random slope; but most importantly, is statistically different than the observational slope.

This is an important result, because it means that there should be closer UDGs to the center than what we actually observe. Under the assumption that this trend is *not*

only due to problems detecting UDGs in the inner regions of clusters, is evidence of UDGs being destroyed in the inner regions of their host structures. After correcting for observational biases, the expected distance to the closest UDGs in a 10^{15} $M_\odot$ cluster would be a factor ~40 larger (closer) than in a 10^{13} $M_\odot$ group.

As mentioned in this Chapter and in the Introduction, several works have suggested that idea, and here we show that, under a homogeneous analysis, it is possible, and we quantity the behavior of the relation; showing that the effect is stronger towards the most massive galaxy clusters, with the slope above derived.

Therefore, we have shown that there is observational evidence of UDGs being systematically destroyed in the center of the clusters. This adds to the slope < 1 in the N(UDGs)-M_{200} relation to support a picture of UDGs being destroyed more efficiently in high-mass systems. The final test for this relation would be to increase the sample, but especially make sure than there are not many missing UDGs in the innermost regions of clusters, that are hidden by their bright surroundings.

5.2 Projected clustercentric distance

The projected clustercentric distance is often used as a proxy for the density of the environment, and it is in particular valid for virialized systems. Since the proximity of one UDG to another (density) depends on its location (they are closer to each other in dense regions, thus near the center), the projected distance is often seen as a proxy of the local environment.

In a environment–driven evolutionary scenario, in principle one would expect to see the effect observed by Román & Trujillo (2017b) of UDGs becoming redder, smaller, likely roundish and less massive towards the center of the cluster; although as we discuss in the Introduction, the reported trends in that work were not very strong. On the other hand, with a scenario of evolution dominated by internal processes, the dependence on the projected distance would probably vanish.

To study this, we investigate the behavior of the structural parameters of UDGs as a function of the projected distance. Our first approach is studying if there is any systematic difference in the properties of the inner UDGs (projected distance < 0.5 R_{200}) and the outer ones (projected distance > 1 R_{200}); we excluded the group in between for increasing the contrast between the other two groups. For this, we build histograms of color, effective radius, Sérsic index and axis ratio as in the last chapter, but now splitting

the data in the inner and outer UDGs using this definition. The number of UDGs has been normalized for each group for a better visualization.

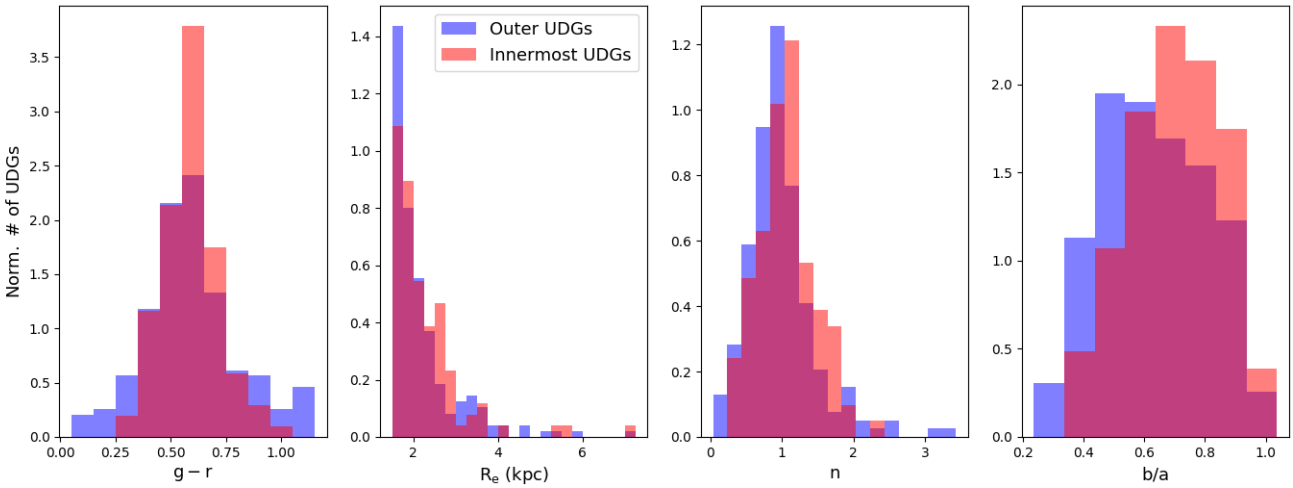

Figure 5.5: Histograms of color, effective radius, Sérsic index and axis ratio of UDGs. The galaxies have been split in those near the center of their host clusters and those in the outer regions. Counts are normalized for a better visualization.

As shown in Figure 5.5, there are no considerable strong differences between both groups of galaxies, at least for the color, the effective radius and the Sérsic index. For the axis ratio we see again a small offset in the peak of the distributions with the innermost UDGs being more round that the outer ones, that looks more disky. This observation takes more relevance when complemented with the latest results on the axis ratio distribution of dwarf galaxies in the Fornax cluster by Venhola et al. (2018b, in prep.) (see their Figure 8). The authors found very clear distributions showing that the late-type dwarfs have a flatter axis ratio distribution than (non-nucleated) dEs; having the last ones a shift towards rounder shapes. Therefore, making the connection with our observations of the axis ratio distribution, it seems like the outer UDGs resemble the late-type dwarfs in Fornax, while our innermost UDGs would be more like the dEs; in a clear picture of the cluster environment changing the morphology of UDGs as it does for smaller dwarf galaxies.

Something else we notice is that the standard deviation of the color, Sérsic index and axis ratio is smaller for the UDGs in the inner regions of clusters. This could be an indication of the cluster environment homogenizing the properties of the nearest UDGs.

Then, to further study this, we plot in Figures 5.6 -5.9 the dependence on the projected

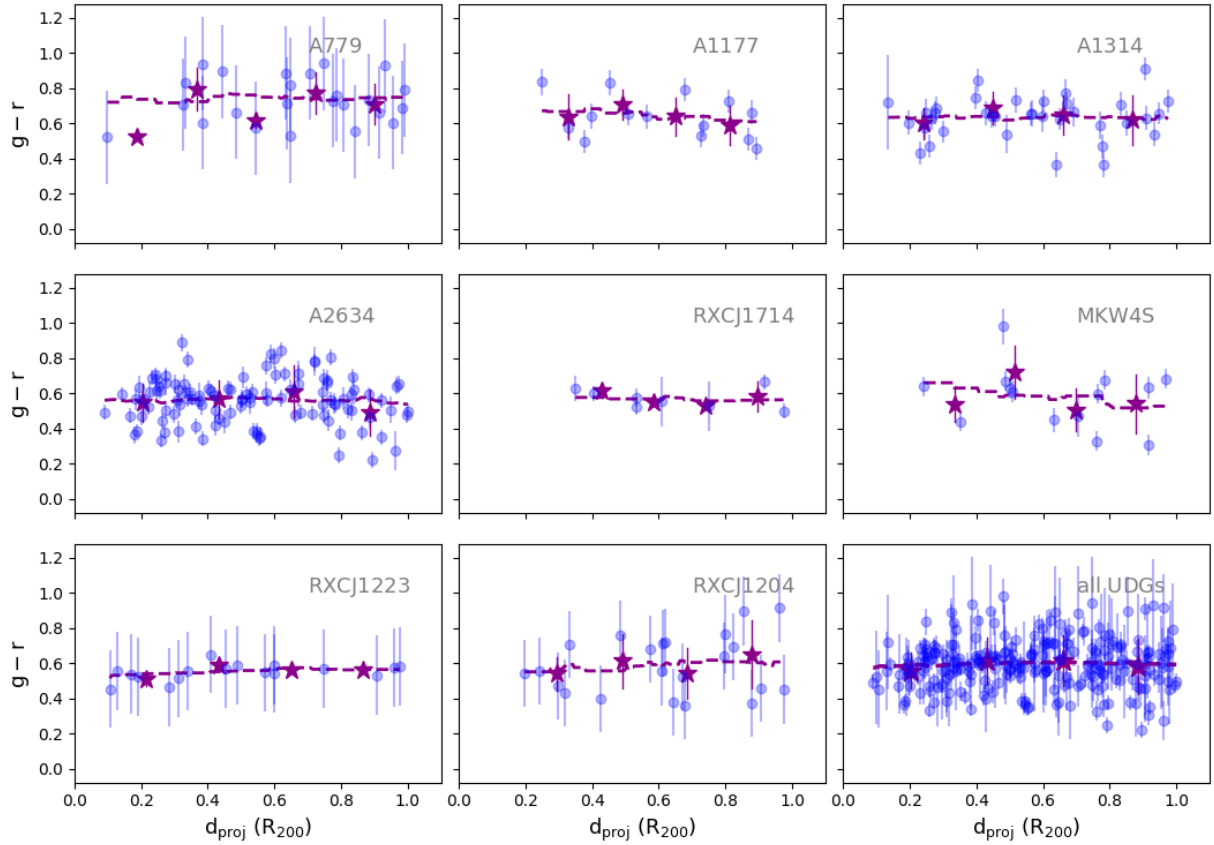

Figure 5.6: Color of UDGs as a function of the projected clustercentric distance, for each cluster and for all the UDGs (last panel). UDGs are shown with blue points. Magenta stars are the value of the binned mean with the errorbars showing the standard deviation of the bin. Finally, the magenta dashed lines show the running mean of the relations.

distance of the structural parameters. Since we fully cover all the clusters only up to 1 R_{200} we limit our analysis to this region.

As can be seen, there are no signs that the structural parameters change in a significant way as a function of the projected clustercentric distance. Perhaps in a few clusters some trends could be present (like larger UDGs being closer to the center, as in A2634; or UDGs having higher Sérsic index and axis ratio towards the center, as with RXCJ1714), but we do not think this effect is 100% real given the dispersion of the data, and for sure not something systematic in all the UDGs as a population.

The fact that we do not find more significant trends of properties as a function of the local environment is a bit disappointing but probably not surprising. For instance, regarding the color, while Román & Trujillo (2017a) and Alabi et al. (2018) reported UDGs being redder in denser regions, other observations have shown (e.g. Sánchez-Janssen

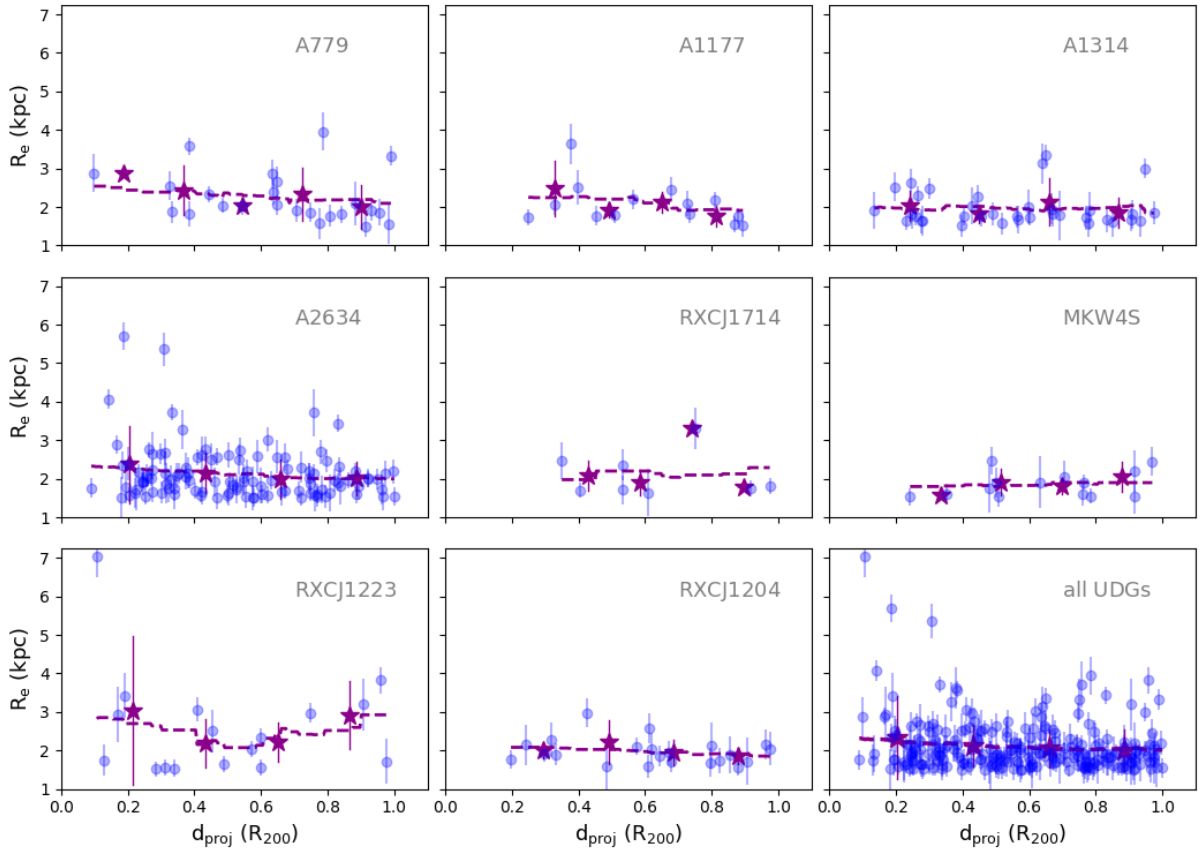

Figure 5.7: Sérsic index of UDGs as a function of the projected clustercentric distance, for each cluster and for all the UDGs (last panel). Symbols are as in Figure 5.6.

et al. 2008, see their Figure 3) that within cluster environments, the red population of dwarf galaxies does not significantly change their color, as opposite to their bluer counterparts, that become redder with decreasing clustercentric distance, as expected due to the interactions with the cluster environment. Moreover, very recently, using the hydrodynamical simulation of a galaxy cluster with the highest resolution available up-to-date, Tremmel et al. (2018) showed that for dwarf galaxies (as most of the UDGs are) the fraction of quenched galaxies is constant (thus independent) as a function of the projected distance, up to 1.5-2 R_{200}. As the authors report, this supports the idea that the processes than quench galaxies are much more efficient in clusters than in the field, specially for low-mass galaxies. Therefore, our observations of the colors are in good agreement with the observations and simulations of dwarf galaxies.

Regarding the rest of the parameters, perhaps the efficient transformation processes in clusters have the same effect and wash out any dependence on the projected distance. Venhola et al. (2017) and Venhola et al. (2018b, in prep.) also reported no variations in

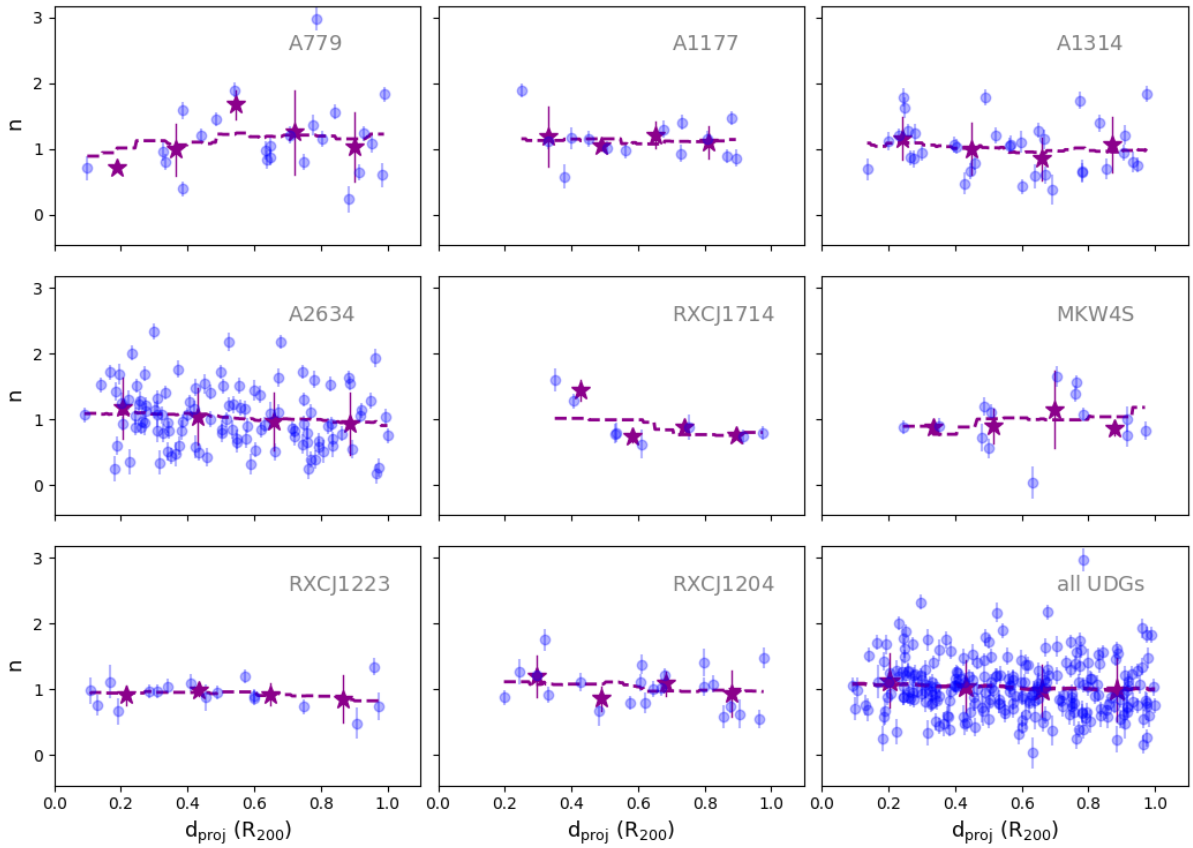

Figure 5.8: Effective radius of UDGs as a function of the projected clustercentric distance, for each cluster and for all the UDGs (last panel). Symbols are as in Figure 5.6.

the general properties of Fornax dwarfs (unless divided in early or late type) with the projected distance. Something else that could remove the trends in our work (if they exist) are interlopers, that look as if they are UDGs within the clusters but they are only projected and therefore not under the cluster environment effects; so, even one was to be careful when possible dealing with projection effects.

5.3 Mass dependencies

With the total mass being the most important physical parameter to characterize clusters, it is interesting to explore if this global parameter affects the properties of UDGs.

For instance, galaxies inhabiting clusters with a lower σ (i.e. which are less massive) are expected to have undergone stronger galaxy-galaxy interactions than galaxies in clusters with a higher σ, since the interactions are stronger in low-velocity collisions. This because lower velocities increase the cross section for mergers; and therefore galaxy-

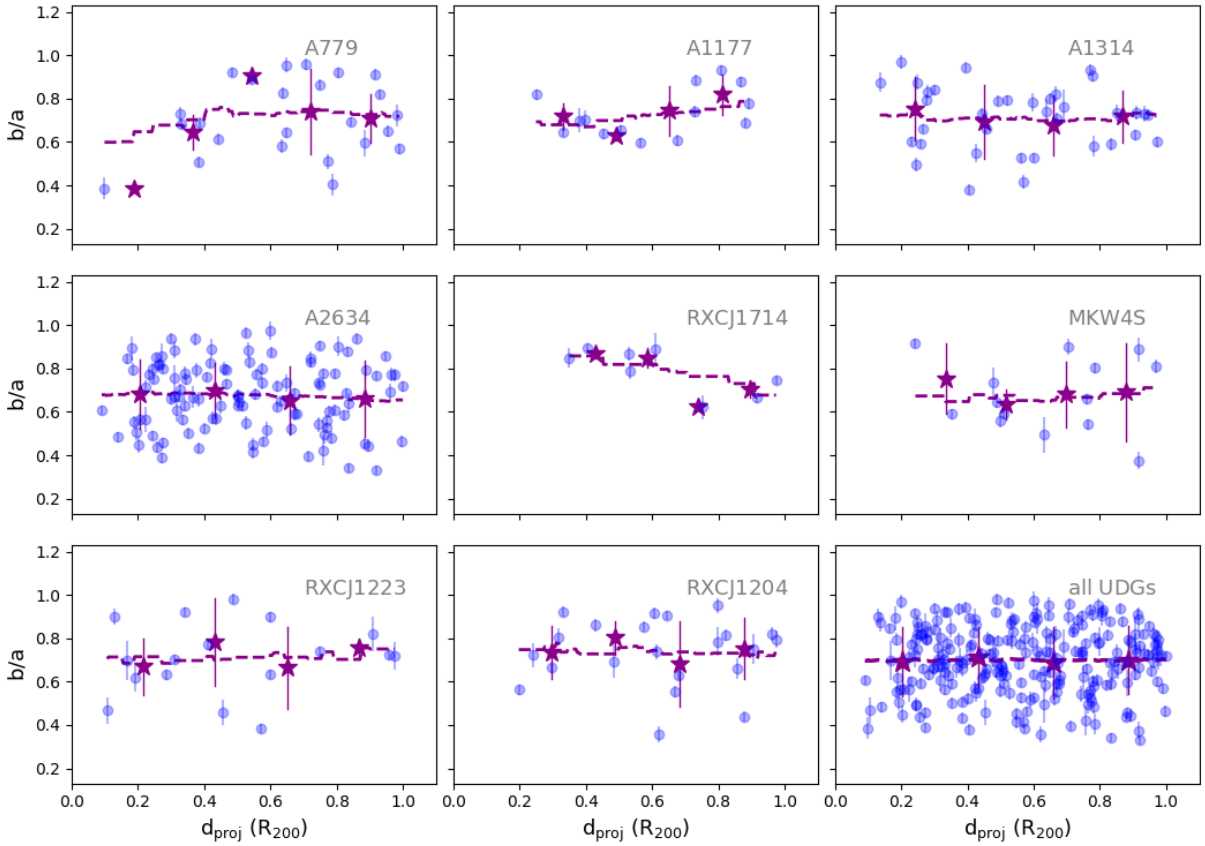

Figure 5.9: Axis ratio of UDGs as a function of the projected clustercentric distance, for each cluster and for all the UDGs (last panel). Symbols are as in Figure 5.6.

galaxy interactions dominate low-mass systems (e.g. Le Févre et al. 2000).

On the other hand, more massive clusters have stronger potentials, and this could also affect the properties of galaxies inhabiting them (like we saw with the projected distance to the first UDG). But the most efficient process for transforming galaxies in massive systems is ram-pressure striping, that goes as σ^2 (so it is more important for high-mass clusters; see for instance Gunn & Gott 1972).

To investigate if any dependence is present, we look at the mean and median values of the structural parameters as a function of M_{200}. For covering a wider range in mass we include the clusters of van der Burg et al. (2016), but not the groups of Román & Trujillo (2017b) since contain too few UDGs. Although when looking separately at our clusters or at the van der Burg's ones no clear trends appear, when combined the picture changes. While there are still no trends in the color or the effective radius, a clear trend appears for the Sérsic index and the axis ratio, with UDGs in more massive systems being more

concentrated and more elongated. However, while these trends could have a physical origin, we believe something else is going on here.

First, regarding the Sérsic index, in principle processes like galaxy harassment (e.g. Moore et al. 1996) can increase the Sérsic index in disky galaxies, such as these dwarf galaxies. And for the axis ratio, stripping would make galaxies in high-mass systems become more disrupted and have lower axis ratios. However how would this work keeping the effective radii unchanged, it is not very clear.

The trends, however, could be explained without any physical motivation, if the sample by van der Burg et al. (2016) (that is slightly less deep and at somewhat larger redshifts) is more contaminated. If that sample has background galaxies, for instance galaxies with bulges at higher redshifts, then this sample would be biased to more concentrated Sérsic profiles. Furthermore, van der Burg's analysis with `GALFIT` constrained the fits to have $n \leq 0.5$, but several LSB have very flat profiles with $n < 0.5$, so this effect should be also biasing the mean and median values of van der Burg's sample. And this also explains the trend in the axis ratio distribution, because if the contamination is strong, and is expected to have an important contribution of background spirals (disks), more galaxies with lower axis ratios would be included in the sample, lowering the mean/median values of the distribution. Moreover, the fact that the trends are not clear in the individual datasets, but only visible once both are combined, is suspicious.

We do not claim that the observed trends are not physical, but in principle could be explained by a contaminated sample, so more homogeneous observations would be needed to make a stronger conclusion.

As a conclusion of this Chapter, we do not find any significant dependence of the color, Sérsic index and effective radius of UDGs as a function of the local (projected cluster-centric distance) environment. This is in agreement with observations and simulations of cluster dwarfs, with the conclusion that the cluster environment is that highly efficient in quenching and transforming galaxies that trends as a function of the density or projected distance, if any, are not visible with our data.

Nevertheless, UDGs in the inner 0.5 R_{200} seem to be more elongated that the outer (outside R_{200}) UDGs, which also have a slightly flatter distribution. As discussed, this is a hint that the cluster environment can be transforming late-type-like UDGs to more spheroidal systems, as in Venhola et al. (2018b, in prep.).

On the other hand, when looking at the dependence of the UDGs' properties as a

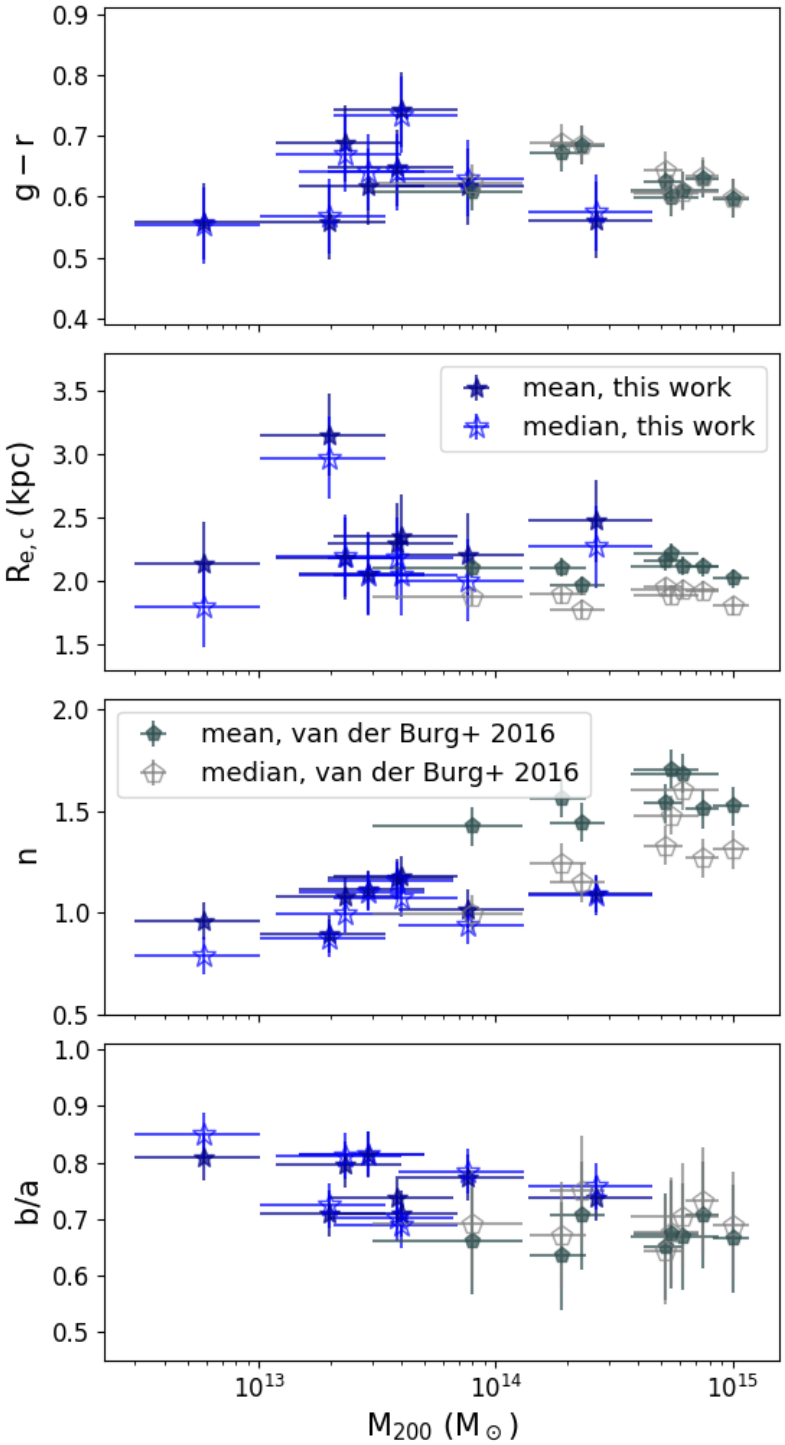

Figure 5.10: Host cluster mass-dependence of the color, effective radius, Sérsic index and axis ratio of UDGs. Solid symbols show the mean values for each cluster, while open symbols show the median. The errors associated with these values correspond to their standard deviation.

function of the M_{200} of the host cluster, we find what seems to be signs of the global environment playing here a role. Apparently, as M_{200} increases, the guest UDGs are found to have higher Sérsic index, and lower axis ratio. As discussed here, while physical mechanisms could be behind this, the same trends can be explained if the sample of van der Burg et al. (2016) is contaminated.

Most importantly, we find evidence that the lack of UDGs in the inner regions of clusters increases with the cluster mass. Together with the results of last Chapter this reflects the role of the global environment in the evolution of UDGs, and contributes to the idea of UDGs being destroyed more efficiently in high-mass systems.

CHAPTER 6

CONCLUSIONS

In this Thesis we assessed the study of UDGs in a set of eight nearby ($z < 0.035$), intermediate-mass ($M \sim 10^{13-14}$ $M_\odot$), galaxy clusters from the WEAVE-Clusters sample with the aim of understanding more about that galaxy population and its evolution in cluster environments. The observations were performed with the 2.5-m Isaac Newton Telescope, and using a combination of software like `SExtractor`, `GALFIT` and self-made programs, we detected the 442 UDGs (247 inside R_{200}) and investigated the properties of their light, looking at the cluster-to-cluster variations and the dependence of the parameters on the environment.

The main conclusions of this thesis are as follows:

Regarding the formation mechanisms of UDGs, our observations support that a good fraction of UDGs are formed according to the model by Amorisco & Loeb (2016); based on the change in the axis ratio distribution between relatively isolated UDGs (flatter distribution) and those in the regions near the center of the clusters. On the other hand, we find that large and small UDGs have basically the same stellar populations, so different sizes in UDGs are not a consequence of different SFHs, as could be expected from the model by Di Cintio et al. (2017) (that however was originally proposed for field galaxies). There is however a tail of large UDGs with bluer colors than the bulk of the UDGs, whose origin is perhaps related with that formation scenario. More statistics from homogeneous studies are crucial to make stronger conclusions.

The evolution of UDGs is affected by the cluster environment, and the effects of

the environment are visible in different ways. First of all, the abundance of UDGs as a function of the M_{200} of their host cluster, after being studied in a more consistent way than usually in the literature, scales as N(UDGs) $\propto$ $M_{200}^{0.82\pm0.07}$. This result, in disagreement with van der Burg et al. (2017), implies that UDGs are more abundant, per unit host cluster mass, in low-mass systems. The cause of this could be that UDGs are preferably formed (or survive the easier) in galaxy groups, or that high-mass systems destroy UDGs in a more efficient way, or that the subhalo mass distribution for UDGs is different in clusters of different mass (or a combination of the three options). In the same direction, we find that large UDGs follow a, statistically different, shallower relation, meaning that the contribution of large UDGs to the whole population decrees with the host cluster mass. The reasons for this are as above, but here galaxy-galaxy interactions may also be playing a role creating large UDGs in low-mass clusters/groups, as proposed by Venhola et al. (2017). Finally, we found evidence that clusters destroy the UDGs near their centers; the higher the mass of the cluster the stronger the effect.

When looking at dependencies of the structural parameters as a function of the projected clustercentric distance up to 1 R_{200}, we did not find any systematic trend in the structural parameters of UDGs. This is in agreement with observations and simulations of dwarf galaxies (e.g. Sánchez-Janssen et al. 2008; Venhola et al. 2017; Tremmel et al. 2018; Venhola et al. 2018b, in prep.), but in disagreement with at least two observational works on UDGs (that have less statistics though; Román & Trujillo 2017b; Alabi et al. 2018).

Notwithstanding, when comparing the axis ratio distribution of the innermost (inside 0.5 R_{200}) and the outermost (outside R_{200}) UDGs, we found that they are slightly different, resembling the trend found by Venhola et al. (2018b, in prep.) between dEs and late-type dwarfs. This adds to a scenario of UDGs being processed by the cluster environment, with their morphologies changing from disk-like to dE-like.

Apparently there could be some extra evidence of the global environment (host cluster mass) playing a role in shaping UDGs. When combining our sample with the sample by van der Burg et al. (2016), a trend of UDGs in more massive clusters having higher Sérsic indices and lower axis ratios appears. While there could be physical reasons causing this, we warn the reader that it is also possible that systematic effects are playing a role, if the sample by van der Burg et al. (2016) is contaminated. More and better data would be needed to test whether or not the effect is real.

About the structural parameters we found that they are in agreement with the picture of UDGs being galaxies with exponential-like light profiles and red stellar populations,

although some of them show also slightly bluer colors. UDGs occupy the same regions as other dwarfs in different scaling relations, confirming that most of them should be large dwarfs. Regarding their spatial location, they are well mixed with the bright cluster galaxies in all clusters, and we did not find systematic galaxy alignments. Their spatial distribution is, however, not random, but follows reasonably well an Einasto profile as suggested by van der Burg et al. (2016). The individual clusters, regardless of the mass, can have shallow cores or cusps, though.

Bibliography

Abolfathi et al. 2018; ApJS, 235, 42A

Abraham, R.G., & van Dokkum, P. G. 2014, PASP, 126, 55

Aguerri, J. A. L., Iglesias-Páramo, J., Vílchez, J. M., Muñoz-Tuñón, C., & Sánchez-Janssen, R. 2005, AJ, 130, 47

Agulli, I., Aguerri, J. A. L., Sánchez-Janssen, R., et al. 2014, MNRAS, 444, L34

Alabi, A., et al. 2018, submitted to MNRAS, arXiv:1801.09686

Amorín, R., Aguerri, J. A. L., Muñoz-Tuñón, C., & Cairós, L. M. 2009, A&A, 501, 7

Amorisco, N. C. 2018, MNRAS, 475, L116

Amorisco, N.C., & Loeb, A. 2016, MNRAS, 459, 51

Amorisco, N. C., Monachesi, A., & White, S. D., 2018, MNRAS, 475, 4235

Astropy Collaboration, Robitaille, T. P., Tollerud, E. J., et al. 2013, A&A, 558, A33

Baushev, A. N., 2018, NewA, 60, 69B

Beasley, M. A., Romanowsky, A. J., Pota, V., et al. 2016, ApJ, 819, L20

Beasley, Michael A.; Trujillo, Ignacio; ApJ, 830, 26

Behroozi, P. S., Wechsler, R. H., Conroy, C., 2013, ApJ, 762, 31

Bellazzini et al., 2017, MNRAS, 467, 3751.

Benn C. R., Ellison S. L., 1998, New Astron. Rev., 42, 5

Bertin, E., Automatic Astrometric and Photometric Calibration with SCAMP, ASP Conference Series, Vol. 351, 2006, C. Gabriel, C. Arviset, D. Ponz, and E. Solano, eds., p. 112

Bertin, E., SWarp: Resampling and Co-adding FITS Images Together, Astrophysics Source Code Library

Bertin, E., & Arnouts, S. 1996, A&AS, 117, 393

Bilir S., Karaali S., Tunçel(2005) S., 2005, Astron. Nachr., 326, 321

Chabrier, G. 2003, PASP, 115, 763

Chilingarian, I., Zolotukhin, I., 2012, MNRAS, 419, 1727

Ciotti, L., & Bertin, G. 1999, A&A,352, 447

Cutri, R. M., Skrutskie, M. F., van Dyk, S., et al. 2003, VizieR Online Data Catalog, 2246

Di Cintio, A., Brook, C. B., Dutton, A. A., et al. 2017, MNRAS, 466, L1

Fasano et al. 2006, A&A, 445, 805

Ferré-Mateu, A., et al. 2018, submitted to MNRAS, arXiv:1801.09695

Giles, P. A., Maughan, B. J., Hamana, T., Miyazaki, S., Birkinshaw, M., Ellis, R. S., & Massey, R. 2015, MNRAS, 447, 304

Graham A. W., Driver S. P., 2005, PASA, 22, 118

Gu, M., et al., 2017; submitted to ApJ, arXiv:1709.07003

Gunn, J. E., & Gott, J. R., III. 1972, ApJ, 176, 1

Hammer, D., Verdoes Kleijn, G., Hoyos, C., et al. 2010, ApJS, 191, 143

Hickson, P. 1982, ApJ, 255, 382

Hoekstra H., Donahue M., Conselice C. J., McNamara B. R., Voit G. M., 2011, ApJ, 726, 48

Impey C., Bothun G., Malin D., 1988, ApJ, 330, 634

Jenkins, A., et al. 2001, MNRAS, 321, 372

Jones, C., & Forman, W. 1999, ApJ, 511, 6

Koda, J., Yagi, M., Yamanoi, H., & Komiyama, Y., 2015, ApJL, 807, L2

Laporte, C. F. P., Agnello, A., & Navarro, J. F., 2018, submitted to MNRAS, arXiv:1804.04139

Le Févre, O., et al. 2000, MNRAS, 311, 565

Lee, M. G., Kang, J., Lee, J. H., & Jang, I. S. 2017, ApJ, 844, 157

Leisman L., et al., 2017, ApJ, 842, 13

MacArthur, L. A., Courteau, S., & Holtzman, J. A. 2003, ApJ, 582, 689

Makarov et al. 2015, A&A, 581, 82M

Martin, N. F. et al., 2018, submitted to ApJL, arXiv:1804.04136

Martínez-Delgado et al., 2016, AJ, 151, 96

McFarland, J. P., Verdoes-Kleijn, G., Sikkema, G., et al. 2013, Experimental Astronomy, 35, 45

Merritt, A., van Dokkum, P., Danieli, S., et al. 2016, ApJ, 833, 168 ;

Mihos et al. 2015, ApJ, 809, 21

Moore, B., Katz, N., Lake, G., Dressler, A., & Oemler, A. 1996, Nature, 379, 613

Munari E., Biviano A., Borgani S., Murante G., Fabjan D., 2013, MNRAS, 430, 2638

Muñoz, R. P., Eigenthaler, P., Puzia, T. H., et al. 2015, ApJ, 813, L15

Old, L., Skibba, R. A., Pearce, F. R., et al. 2014, MNRAS, 441, 1513

Papastergis, E., Adams, E. A. K., & Romanowsky, A. J. 2017, A&A, 601, L10

Peng, C. Y., Ho, L. C., Impey, C. D., & Rix, H.-W. 2010, AJ, 139, 2

Penny S. J., Conselice C., et al., 2011, MNRAS, 410, 1076

Piffaretti R., Arnaud M., Pratt G. W., Pointecouteau E., Melin J. B., 2011, A&A, 534, A10

Reiprich, .H. & Böhringer, H. 2002, Ap. J. 567, 716–40

Roediger, J. C., & Courteau, S. 2015, MNRAS, 452, 3209

Roediger, J.C., Ferrase, L., Côte, P., et al., 2017, ApJ, 836, 120

Román, J., & Trujillo, I. 2017a, MNRAS, 468, 703

Román, J., & Trujillo, I. 2017b, MNRAS, 468, 4039

Ruiz-Lara, T., et al. 2018, submitted to MNRAS, arXiv:1803.06298v1

Sánchez-Janssen, R., Aguerri, J. A. L., & Muñoz-Tuñón, C. 2008, ApJ, 679, L

Sandage & Binggeli, 1984, AJ, 89, 919

Schlafly, E.F., & Finkbeiner, D.P., 2011, ApJ, 737, 103

Sérsic, J. L. 1963, Boletín de la Asociación Argentina de Astronomía La Plata Argentina, 6, 4

Spekkens K. & Karunakaran A., 2018, ApJ, 855, 28

Taylor, M. B. 2005, Astronomical Data Analysis Software and Systems XIV, 347

Taylor, M. B. 2006, Astronomical Data Analysis Software and Systems XV, 66

Tolman, R. C., 1930, Proceedings of the National Academy of Science, 16, 511

Tolman, R. C., 1934, Relativity, Thermodynamics, and Cosmolo

Toloba et al. 2018, ApJ, 856, 31

Tovmassian, H., Plionis, M., & Torres-Papaqui, J. P. 2006, A&A, 456, 839

Tremmel, M., et al. 2018; submitted to MNRAS, arXiv:1806.01282

Trujillo, I., et al., in prep.

Trujillo, I., Román, J., Filho, M., & Sánchez Almeida, J. 2017, ApJ, 836, 191

van der Burg, R. F. J., Muzzin, A., & Hoekstra, H. 2016, A&A, 590, A20

van der Burg, R. F. J., Hoekstra, H., Muzzin, A., et al. 2017, A&A, 607, A79

van Dokkum, P. G., Abraham, R., Merritt, A., et al. 2015a, ApJL, 798, L45

van Dokkum P. G. et al., 2015b, ApJ, 804, L26

van Dokkum P., et al., 2016, ApJ, 828, L6

van Dokkum, P., et al. 2018, Nature Astronomy, 555, 629

Venhola, A., Peletier, R.F., et al., 2017, A&A, 608, A142

Venhola, A., et al., 2018a, in prep.

Venhola, A., et al., 2018b, in prep.

Wittmann, C., Lisker, T., et al., 2017, MNRAS, 140, 1512

Wright E. L., 2006, PASP, 118, 1711

Yagi, M., Koda, J., Komiyama, Y., & Yamanoi, H. 2016, ApJS, 225, 11